International Institute for Applied Systems Analysis
IIASA www.iiasa.ac.at

A Set of Climate Models for Integrated Modelling of Climate Change Impacts. Part I: Introduction and Overview - A 2-Dimensional Zonal Climate Model. A Projected Application to European Forests

Jonas, M., Ganopolski, A.V., Krabec, J., Olendrzynski, K. and Petoukhov, V.K.

IIASA Working Paper

October 1993

Jonas, M., Ganopolski, A.V., Krabec, J., Olendrzynski, K. and Petoukhov, V.K. (1993) A Set of Climate Models for Integrated Modelling of Climate Change Impacts. Part I: Introduction and Overview - A 2-Dimensional Zonal Climate Model. A Projected Application to European Forests. IIASA Working Paper. Copyright © 1993 by the author(s). http://pure.iiasa.ac.at/3756/

Working Papers on work of the International Institute for Applied Systems Analysis receive only limited review. Views or opinions expressed herein do not necessarily represent those of the Institute, its National Member Organizations, or other organizations supporting the work. All rights reserved. Permission to make digital or hard copies of all or part of this work for personal or classroom use is granted without fee provided that copies are not made or distributed for profit or commercial advantage. All copies must bear this notice and the full citation on the first page. For other purposes, to republish, to post on servers or to redistribute to lists, permission must be sought by contacting repository@iiasa.ac.at

Working Paper

A Set of Climate Models for Integrated Modelling of Climate Change Impacts

Part I:

Introduction and Overview
A 2-Dimensional Zonal Climate Model
A Projected Application to European Forests

Matthias Jonas
Andrey V. Ganopolski
Jaroslav Krabec
Krzysztof Olendrzyński
Vladimir K. Petoukhov

WP-93-58
October 1993

IIASA

International Institute for Applied Systems Analysis ☐ A-2361 Laxenburg Austria

Telephone: +43 2236 715210 ☐ Telex: 079137 iiasa a ☐ Telefax: +43 2236 71313

A SET OF CLIMATE MODELS FOR INTEGRATED MODELLING OF CLIMATE CHANGE IMPACTS

PART I

INTRODUCTION AND OVERVIEW

A 2-DIMENSIONAL ZONAL CLIMATE MODEL

A PROJECTED APPLICATION TO EUROPEAN FORESTS

Matthias Jonas
Andrey V. Ganopolski
Jaroslav Krabec
Krzysztof Olendrzyński
Vladimir K. Petoukhov

October 1993

Working Papers are interim reports on work of the International Institute for Applied Systems Analysis and have received only limited review. Views or opinions expressed herein do not necessarily represent those of the Institute, its National Member Organizations, or other organizations supporting the work.

International Institute for Applied Systems Analysis ☐ A-2361 Laxenburg Austria
Telephone: +43 2236 715210 ☐ Telex: 079137 iiasa a ☐ Telefax: +43 2236 71313

Table of Contents

1. SUMMARY

Projections of changes in climate are valuable in their own right, but they raise another, perhaps more important set of questions: What effects might such changes have on food production, on forests, on insect life, energy demand, and fresh water supply - on dozens of factors that directly and indirectly affect human well-being?

To address these questions, specialists must link ecological models with climate models; to assess policies, the climate models must in turn be driven by accounting frameworks that calculate total emissions and concentrations of greenhouse gases, depending on policy scenarios. This chain - from policy-oriented accounting tool to climate model to ecological impact model, with feedback, possibly supported by a model for socioeconomic analyses - comprises an integrated assessment model or an integrated model of climate change, as it is also called.

In terms of running time a climate model can easily play a dominant role within an integrated model of climate change. General Circulation Models are the state of the art for studying and projecting climate, but for integrated assessments they are impractical: they are not computer-efficient with respect to both running time and hardware. They can take weeks, running on a super computer, to calculate one complete scenario. Many ecologists and policy analysts, however, wish to assess a great number of scenarios and therefore need a suitable climate model that can give results within hours, possibly within a day, using a workstation or a PC.

In fact, the needs of impact modellers and other model users are very often antagonistic to each other, like, e.g., their desire for both a quick turnaround time and climatic information with a high spatial and temporal resolution. Therefore, the choice of a proper climate model is crucial for the entire integrated model. In principle, it is the environmental impact one wishes to assess that determines the degree of sophistication of the climate model and thus its computing time requirements. But environmental impact modellers or assessors, on the other hand, must be prepared to answer questions of great consequence. They might be asked, e.g., whether the environmental impact under discussion could also be studied having less climate variables available as input information, and which spatial and temporal

resolution of these climate variables would still be acceptable.

The Working Paper summarizes the status of two climate models out of a set of four of graded complexity that are available or under development at IIASA, and describes the envisaged position of these climate models in the context of an integrated model of climate change. The climate models mentioned in Part I and II of the Working Paper are a 2-dimensional Zonal Climate Model and a 2.5-dimensional Dynamical-Statistical Climate Model, respectively. They offer different sets of climatic information with different spatial and temporal resolutions and thus allow a choice depending on the environmental impact to be studied in an integrated fashion.

The Working Paper also sheds light on a projected application to integrated modelling of climate change impacts, which forms one of the focal points of IIASA's environmental research until 1996 and involves five collaborating research teams from Australia, Finland and Sweden. This will be an integrated assessment of climate change impacts on European forests. A two-step approach employing both the Zonal Climate Model and the Dynamical-Statistical Climate Model is outlined. An important feature of the integrated assessment is that the ecophysiology of a single plant up to that of aggregated forest ecosystems will be considered. This provides a linkage to the climate models mentioned and thus, in combination with a policy-oriented accounting tool for greenhouse gas emissions and concentrations, an integrated assessment becomes feasible.

2. INTRODUCTION AND OVERVIEW

2.1 Objective

The Working Paper summarizes the status of both the **2-dimensional Zonal Climate Model (2-D ZCM)** and the **2.5-D Dynamical-Statistical Climate Model (2.5-D DSCM)** available at IIASA's Forestry and Climate Change Project[1] and describes the envisaged position of these climate models in the context of an integrated model of climate change. The latter model aims at a holistic approach that helps policy analysts to rapidly assess time-dependent changes in regional ecology resulting from various greenhouse gas emission policies. Such an approach is multidisciplinary and involves linking a policy-oriented emission-concentration accounting model framework for natural and man-made greenhouse gases, to a suitable climate model and both, in turn, to models of ecological and socioeconomic change. We know of about five integrated models for climate change analyses which are in use worldwide[2]. Two of these models are mentioned below.

The 2-D ZCM described in Part I of the Working Paper comprises two modules, one for the atmosphere which follows the principles of energy balance modelling, and one for the ocean which employs advective and diffusive transport descriptions. The atmospheric module is used in IMAGE 2.0, the Integrated Model to Assess the Greenhouse Effect, which is being developed at The Netherlands' National Institute of Public Health and Environmental Protection (RIVM) in collaboration with other research institutions. It is one of the few integrated models of climate change aiming at providing a scientifically-based overview of climate change issues to support the evaluation of policies in regard to their environmental soundness. Its turnaround time is expected to be in the order of several hours on a personal computer or a workstation.

---

[1] Emerged from merging IIASA's Forestry Resources Project and Climate Change Response Project.

[2] Three of the five models are not mentioned in the text. These are AIM (under development) of the Japanese National Institute for Environmental Studies; ASF of the U.S. Environmental Protection Agency; and STUGE of the Climate Research Unit of the University of East Anglia, U.K.

A less sophisticated but nevertheless valuable alternative of an integrated model of climate change with a much shorter turnaround time is IMAGE 1.0, also developed at RIVM. It is a policy-oriented model that allows to calculate the effect of different greenhouse gas emission scenarios on global surface air temperature and sea level rise. The limitation of IMAGE 1.0, a climate model with essentially a global and annual resolution, can be remedied by replacing its climate model by, e.g., the (entire) 2-D ZCM or a climate model with another spatial and temporal resolution, depending on the environmental impact to be studied.

We anticipate that IMAGE 2.0 will be an as important scientific tool for deriving future climate management strategies as IMAGE 1.0, which has been used by the Intergovernmental Panel on Climate Change (IPCC, 1991). The higher degree of complexity of IMAGE 2.0 might be compensated for by the greater flexibility of IMAGE 1.0 in improving or exchanging its modules in dependence on the environmental impact under investigation. As already indicated, the modular structure even allows to use only a subset of modules, say, the emission-concentration accounting model framework of IMAGE 1.0. This part may then be modified and linked to a suitable climate model in view of the environmental impact. It is this line of thinking which we have in mind when we discuss the 2-D ZCM as well as other climate models in the context of an integrated model of climate change. This is extensively done in the remainder of Chapter 2. The ZCM itself and its results are described in Chapters 3 and 4. In Chapter 5 the ZCM is discussed in view of a projected application to integrated modelling of climate change impacts, which forms one of the focal points of IIASA's environmental research until 1996. This will be an integrated assessment of climate change impacts on European forests. The conclusions are given in Chapter 6.

The 2.5-D DSCM and its results are described in Part II of the Working Paper. However, Chapters 2 and 5 of Part I also refer to the DSCM and are therefore not repeated in full length in Part II.

2.2 Potential Questions and Implications for an Integrated Model of Climate Change

Ultimately, an integrated model of climate change should unveil cause-effect relationships, i.e., it should start from policy options and come up with results which are useful to decision makers, fellow scientists and the public. Some of the questions, they might ask, are as follows (P. Weaver, personal communication, 1992; Meadows, 1992):

- Where are current emission trends likely to take us?
- What other climate futures are possible?
- What environmental and socioeconomic risks and opportunities do we see in different plausible futures?
- What are the likely implications/costs of different strategies for averting, postponing or adapting to climate change? For example, how would the dynamics of a carbon tax turn out, and what are the implications of introducing carbon-emission rights and their effects on equity?
- Which climate changes are inevitable, which amenable to influence?
- What is the priority of response measures taking into account responsibilities, costs, environmental and socioeconomic benefits, certainty and equity?
- Are some options now available likely to be foreclosed in the future? What are critical environmental and other thresholds?
- Which changes are potentially synergistic, or likely to exacerbate particular problems?

.
.
.

Already these few questions suggest a number of demands of an integrated model of climate change. For example, the model

- must be capable of suggesting policy options and aim at policy exercises, possibly serve as a negotiating tool;
- must be capable of generating consistent scenarios;
- must be computer-efficient (computing time, hardware);
- must have a transparent and consistent modular structure;

- must be dynamic;
- must be fully controllable;
- should represent climate change as the product of human and social forces as well as of the laws of physics, chemistry, etc.;
- should be invertible for optimization purposes (if that is not possible, this disadvantage can be made up for by a rapid turnaround time which allows many scenario runs);
- must have undergone sensitivity tests;

.

.

.

It goes without saying that the modellers must also be open about the weaknesses of their models.

In the next three sections we will dwell on the demands of the climate model in particular as it is usually one of the crucial modules of an integrated model of climate change in terms of running time.

2.3 Information Required by Environmental Impact Modellers or Assessors

A major concern about anthropogenically induced climate change lies in its potential environmental and subsequent socioeconomic impacts. This immediately raises questions concerning the information needs of those modelling and assessing environmental impacts and the way in which climatologists and other scientists can provide that information.

In their recent paper, Robinson and Finkelstein (1991) examined in consultation with environmental impact modellers, who have experience in using climate change scenarios, the information needed for the assessment of the impacts of climate change. Their first question "Lists and rankings of important climate elements?" helped to establish Table 2.1. It summarizes twenty responses that were available for analysis, each reflecting the views of an individual or a group. The fields of interest represented included agriculture, water supply and quality, forestry, ecology, entomology, sea level, air quality, and climate itself.

Table 2.1. Climate element needs of impact assessors in %.						
Variable	Respondents	Priority				
		Very high	High	Medium	Low	Very[1] low
Of general concern						
Temperature	90	84	11			
Precipitation	81	82	18			
Wind[2]	52	18	27	18	18	18
Radiation	48	10	30	50	10	
Water vapor	48	20	50	10	10	10
Clouds	29	33	33	17	17	
Snow	20	25	25	25	25	
Of importance to a few individuals/groups[3]						
Pressure Mixing depth Evaporation Growing season Storms Glaciation						

1) The terms "Very High", "High", etc. were arbitrary ranking which the respondents were asked to use.

2) Usually scalar speed, sometimes vector velocity, sometimes not clearly indicated.

3) Percentage rankings not given because of small number of responses.

(from Robinson & Finkelstein, 1991)

As it is apparent from this table, a wide variety of elements were of interest as well as a general hierarchy with respect to both the importance of the element and the frequency of need. For the respondents temperature and precipitation seem to be the most important and most frequently needed climate elements. It can also be deduced that the need for a particular element (e.g., clouds) may be infrequent, but is still vital for a specific assessment. Note that the percentages in Table 1 are neither even nor do they add up to 100% because many respondents gave more than one answer and some did not respond to every question.

Robinson and Finkelstein's next series of questions

- The desired time intervals for each of these factors (climatic elements)?
- The spatial resolution for each factor?
- The summarizing statistics for each of these factors?
- The types of individual climatic events of importance?

led to their Table 3. According to their survey results, a time scale of one day and a 100 km grid (which is considerably finer than those of the present General Circulation Model (GCM) resolution) satisfied most user needs. Moreover, the response to questions about the actual climatic elements allowed the division of the information needs into the four broad categories

1. simple descriptive statistics: means or associated statistics (e.g., total rainfall amount); standard deviations or ranges; other descriptors such as rate, duration and intensity (e.g., of precipitation); summaries (like, e.g., interannual variability).
2. climatic anomaly information: about the intensity and persistence of extreme events for longer time periods (e.g., droughts) and about the affected areas.
3. threshold values: for information about the probability of significant events and their duration (e.g., probability of number of days below freezing or probability of cloudless conditions for several consecutive days).
4. synoptic information: about particular weather events on the synoptic scale including the time sequence of events and other relevant climatic elements (e.g., number of storms, severity, frequency and storm tracks; flash flooding; frequency of passage of mid-latitude depressions).

The respondents were asked to draw on their experience, but, unfortunately, to downplay reliance on what information they thought might be available and emphasize instead the information (type, spatial and temporal resolution) that would be most useful for them as impact assessors. It was emphasized that this was likely to constitute a wish-list, with no guarantee that the requested information could ever be provided.

We find Robinson and Finkelstein's survey results very helpful although their questions did not aim at integrated modelling of climate change. For this purpose it would be necessary to rather ask whether a certain environmental impact could also be modelled and assessed having less climate variables available as input information, and which spatial and temporal resolution of these climate variables would still be acceptable (see, e.g., Baskin, 1993). Also unlike Robinson and Finkelstein, it would be necessary to point out the drawbacks of a complex three-dimensional GCM, namely that it is not a very useful climate module within an integrated model framework because of its immense computational time and that it cannot be regarded as the starting point for climate scenarios. However, this also means that the climate module of an integrated model of climate change should not compete with GCMs but be complementary to them and take advantage of the scientific results from them (e.g., using GCM results for comparison or calibration purposes) as they represent the state of the art in climate modelling.

In the next section we will discuss two alternatives how to account for a time-efficient climate module for an integrated model of climate change.

2.4 Design of the Climate Module

In principle, we see two independent possibilities in regard to the design of the climate module (see Fig. 2.1 and Table 2.2). The first possibility is a top-down approach as elaborated by Hasselmann and von Storch (1992) for their concept of a Global-Environment-and-Man (GEM) model at the Max-Planck-Institute (MPI) for Meteorology in Hamburg. This approach requires the availability of a full GCM. The GCM is translated into statistically simplified but nevertheless dynamically consistent climate models which retain those variables important for modelling environmental impacts. Economic and decision-making models are also foreseen to be linked to the climate module. The complete system will be composed of

a combination of deterministic and stochastic subsystems and include feedback components and interactive multi-component decision-making elements.

Clearly, the strength of this top-down approach would be that the simplified climate models can fully exploit the statistical information contained in the GCM and that climate quantities as available from the GCM can be statistically linked even if they do not necessarily reveal a direct dependence between each other. In addition, this approach eventually offers a broad choice of output variables and of their spatial and temporal resolution depending on the impact to be studied. However, it should be expected that the number of climate output parameters will actually be limited (e.g., to those given in Table 2.1) in order to restrict the integrated GEM approach to a first order impact assessment and to make it computer-efficient.

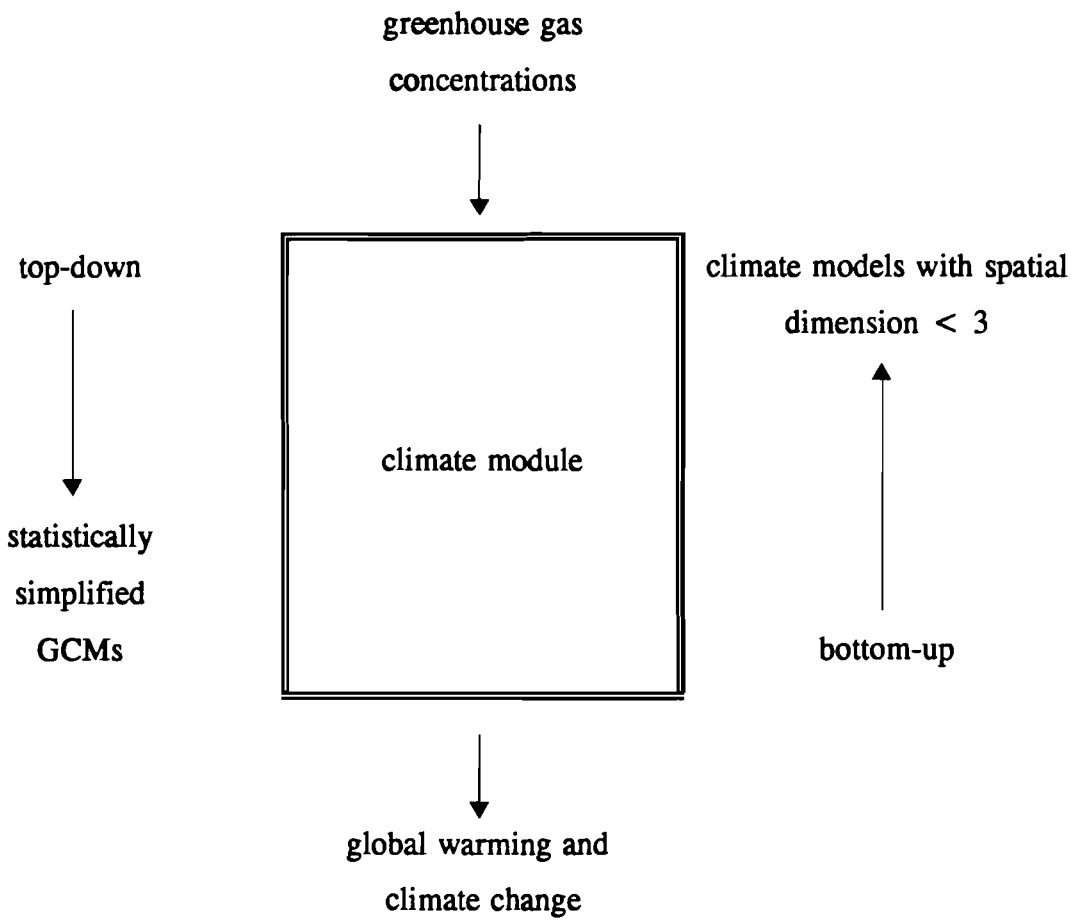

Figure 2.1. Two independent possibilities in regard to the design of the climate module of an integrated model of climate change.

Table 2.2. Some characteristics of top-down and bottom-up climate module design.

Characteristics	Top-down approach	Bottom-up approach
Concept and scientific background	simplify full GCM and derive hierarchy of simplified climate models with fast turnaround times; full GCMs represent state of the art in climate modelling and contain maximum of physical processes	develop hierarchy of fast turnaround climate models, which are not derived from GCMs; number of physical processes and climate variables considered is limited
Basis for climate model construction	relationships based on means and higher statistical moments of the full GCM (depending on its spatial and temporal resolution)	a priori assumptions or parameterizations in connection with climatic means and statistical moments of second order
Availability of GCM	mandatory	not required; GCM results, however, must be used for comparison purposes
Improvements, e.g., introduction of new feedbacks	necessary to improve full GCM first, then derive simplified climate models	can be implemented directly in climate models if appropriate parameterizations exist or can be derived
Study of individual feedbacks	possible if feedback mechanism is preserved by simplification procedure	possible if feedback is explicitly described in climate models
Uncertainties with respect to prescribed parameters, parameterizations, initial conditions (problem of multiple equilibria), etc.	necessary to assure that simplified climate models reveal uncertainties that are consistent with those of full GCM	can be investigated directly in climate models and compared with others
Robustness of climate module to be tested against extreme past climatic events	necessary to investigate full GCM if simplified climate models are not robust	robustness can be secured, if necessary, by adjusting parameters, parameterizations, etc. considering physical reasoning
Cost of climate experiments	full GCM: expensive simplified climate models: inexpensive	inexpensive
Flexibility of approach in regard to requirements of environmental impacts	broad choice with respect to diversity of information (climate elements) and with respect to its spatial and temporal resolution	more restricted choice with respect to diversity of information and with respect to its spatial and temporal resolution
Limitations of usefulness	other scientists can only introduce improvements themselves if they have access to full GCM	other scientists can introduce improvements themselves

The second possibility in regard to the design of the climate module is a bottom-up approach, i.e., to use climate models with spatial dimensions less than three which are not derived from a GCM. We have chosen this approach essentially because neither we nor potential users of an integrated model of climate change normally have a GCM available and to thus limit the dependence on this three-dimensional model. A hierarchical series of four climate models of increasing complexity will eventually be at disposal for selection at IIASA which should be made in dependence of the environmental impact to be studied (see Section 2.5). One of the models has already been completed, while the remaining ones are still under development or under review. The various climate models are

1. Wigley and Raper's (1990) (0+1)-D Energy Balance Model (EBM), as implemented in IMAGE 1.0 (0-D atmosphere, 1-D ocean, annual);
2. the 1-D Energy Balance Model (EBM), as discussed in Jonas et al. (1991) (1-D atmosphere, oceanic mixed layer, annual; 2-D ocean and seasonality envisaged[3]);
3. the 2-D ZCM, as described in Part I of this Working Paper (2-D atmosphere, 2-D ocean, annual; an improved seasonal version under development); and
4. the 2.5-D Dynamical-Statistical Climate Model (DSCM) of the Moscow Institute of Atmospheric Physics, as described in Petoukhov (1991) and in Part II of this Working Paper (spatial resolution $\geq$ (500 km)^2, temporal resolution $\geq$ 10 d; presently under review for necessary improvements).

The running time of these models on a PC or a workstation covers a range of minutes to approximately one day for 100 model years. The final time requirement of the 2-D ZCM is anticipated to be in the order of several hours.

One strength among various others of, e.g., the 2-D ZCM (see Table 2.3) is that it is already sophisticated enough to support analyzing a number of environmental impacts which we are dealing with under a changing climate. On the other hand, the model is still intelligible

[3] The improved EBM should also be termed more correctly a ZCM. However, when mentioning this model in the following we will always call it a (1+2)-D ZCM, i.e., mention it in connection with its dimensions. Otherwise the acronym ZCM always refers to the 2-D ZCM.

enough to provide a physical understanding on how feedbacks work and it easily allows to trace the feedbacks as they influence other processes in the model. If appropriate parameterizations exist or can be derived, especially new processes and feedbacks which are not yet incorporated or thoroughly tested in GCMs, could be implemented and tested to a first order while statistically simplified GCMs are inappropriate for this purpose. They fully depend on the GCM from which they are derived. The original GCM requires the implementation of the new process or feedback mechanism before it can again be statistically simplified.

In our opinion both approaches, the top-down and the bottom-up approach, complement each other and seem to be worthwhile pursuing in parallel. This would be highly desirable because it would offer the possibility to derive climate management strategies independently of different climate model approaches.

In the next section we will discuss the 2-D ZCM in the perspective of environmental impact modellers or assessors. But since we view the ZCM in the context of the climate models mentioned above and others, this section can also serve as a first guide for making use of an appropriate climate model in regard to the environmental impact to be studied.

Table 2.3. Some advantages of climate models available at IIASA and of GCMs.

ZCM[1)] (2-dimensional)	DSCM[2)] (2.5-dimensional)	GCM (3-dimensional)
very rapid	much more rapid than GCMs	state of the art
easy to test and to tune	capable to fairly well describe climatic variations down to a spatial resolution comparable to that of GCMs	highly detailed information on temperature, precipitation, density, pressure, oceanic and atmospheric circulation
useful model to test new feedbacks if appropriate parameterizations exist or can be derived	capable to fairly well describe processes with response times down to ca. 10 days	capable to fairly well describe processes with response times down to ca. 20 minutes
capable to fairly well describe linear processes on an annual and seasonal temporal scale	suitable for integrated models of climatic change	
capable to fairly well describe non-linear processes with long response times		
capable to fairly well describe quasi-zonal, non-linear processes with any response time		
suitable for integrated models of climatic change		

1) 2-D atmosphere, 2-D ocean, annual; under development. Note that the strengths listed for the 2-D ZCM to a varying extent also hold for the other two climate models at IIASA mentioned in the text.

2) Spatial resolution $\geq$ (500 km)^2, temporal resolution $\geq$ 10 d; presently under review.

2.5 The 2-D ZCM in the Perspective of Environmental Impact Modellers or Assessors

Table 2.4 gives an overview over the type of information which the 2-D ZCM and the other climate models available at IIASA are anticipated to pass on to environmental impact modellers or assessors when being fully developed. The classification of the information is in agreement with Robinson and Finkelstein's (1991) classification as described in the previous section.

Of importance is the spatial and temporal resolution of the respective climate model to which the type of information within each column has to be related. For instance, in the case of the 2-D ZCM it is mentioned that this model can pass on i.a. information on temperature which is then zonally (separately for land, ocean and atmosphere) and seasonally (but so far only annually) resolved. Based on this mean, threshold values or exceeding them can be defined or introduced. One can even try to estimate the frequencies and intensities of cyclones in extratropical regions (Mokhov et al., 1992) and also the depth of propagation of storms from tropical to mid-latitude regions (Shuleykin, 1978; Sunders et al., 1980).

In Table 2.5 we tentatively tried to relate some environmental and socioeconomic impacts (which we as climatologists consider to be valuable to study in the context of an integrated model of climate change) to our climate models. Our leitmotif for grouping them was to use the least sophisticated climate model which would enable to study these impacts, to a first approximation, within an integrated model of climate change (assuming that appropriate environmental and socioeconomic impact models are available). Of course, any of these impacts can also be studied by models that are higher in the hierarchy.

In the case of the 2-D ZCM we listed impacts which reveal a more or less zonal dependence or which require more local/regional, but highly uncertain input information, say, from GCMs. In the latter case we felt that taking the zonal means of the respective parameters and superimposing them over regional observations (e.g., the zonal change in precipitation for studying its effect on acidification in Europe) and rather extending the uncertainty ranges of these parameters in sensitivity tests, fully serves the purpose of getting a qualitatively satisfactory picture of the impacts under consideration.

Table 2.4. The type of information (as specified by Robinson and Finkelstein, 1991) which the climate models available at IIASA are anticipated to pass on to environmental impact modellers or assessors.

Type of information / Climate models	(0+1)-D EBM[1]	(1+2)-D ZCM[2]	2-D ZCM[3]	2.5-D DSCM[4]
	O-D A, 1-D_z O annual	1-D_φ A, 2-$D_{\varphi,z}$ O seasonal	2-$D_{\varphi,z}$ A and O seasonal	2.5-$D_{\lambda,\varphi,L}$ A and O seasonal
	few minutes ← running time for 100 model years on a PC/workstation → ca. 24 h			
Climate elements	T	T, Sn, MD, GS(T), G	T, Prec, W, R, WV, C, Sn, MD, MH, E, GS (T, Prec), G	T, Prec, W, R, WV, C, Sn, P, MD, MH, E, GS (T, WA), St (in terms of their statistics), G
Category I (Simple descriptive statistics)	mean of temperature	means of above climate elements	means of above climate elements	means, standard deviations and interannual variability of above climate elements
Category II (Climatic anomaly information)	--	--	--	frequency (probability), intensity, spatial occurrence and persistence of droughts (relative to present climate)
Category III (Threshold values)	--	definition of thresholds (and beyond them) based on means	definition of thresholds (and beyond them) based on means	definition of the probability of thresholds (and beyond them) based on the first two statistical moments
Category IV (Synoptic information)	--	--	frequencies of extratropical cyclones and their intensities	spatial occurrence (in terms of track statistics) and intensities of extratropical cyclones

A atmosphere; O ocean; λ longitude; φ latitude; z height/depth; L parameter of integrative structure describing the large-scale atmosphere and oceanic layers (boundary layer, free troposphere, stratosphere, oceanic mixed layer, seasonal thermocline, main thermocline, bottom layer).

T temperature; Prec precipitation; W wind; R solar and terrestrial radiation; WV water vapor; C clouds; Sn snow; P pressure; MD oceanic mixed layer depth; MH mixing height in the planetary boundary layer; E evaporation; GS growing season; WA water availability; St storms; G glaciation.

1) Wigley and Raper (1990).
2) Envisaged by improving the 1-D EBM of Jonas et al. (1991) by a 2-D ocean and by introducing seasonality.
3) The envisaged version of the 2-D ZCM described in Part I of this Working Paper.
4) Petoukhov (1991); model presently under review for necessary improvements.

Table 2.5. Environmental and socioeconomic impacts related to climate models available at IIASA.

(0 + 1)-D EBM[1)]	(1+2)-D ZCM[2)]	2-D ZCM[3)]	2.5-D DSCM[4)]
global surface temperature change due to anthropogenic greenhouse gas and SO_2 emissions • • •	shift of snow/sea-ice line change in growing season based on degree-days change in ice caps and sea level rise • • •	ozone holes in connection with UV radiation reaching the surface and its effect on health shift of permafrost boundary shift of tundra/taiga and other ecoclines change of productivity of oceanic biota in connection with the geochemical cycle influence of changes in precipitation on acidification (using IIASA's RAINS model) • • •	droughts and associated consequences for food production and water management shift of climatic zones and the potential threat of associated diseases occurrence of forest fires change of natural vegetation patterns incl. deforestation influence of change in wind velocity field and mixing height on transport patterns climatic information for energy demand and production • • •

[1)] Wigley and Raper (1990).
[2)] Envisaged by improving the 1-D EBM of Jonas et al. (1991) by a 2-D ocean and by introducing seasonality.
[3)] The envisaged version of the 2-D ZCM described in Part I of this Working Paper.
[4)] Petoukhov (1991); model presently under review for necessary improvements.

However, we think that environmental impact modellers or assessors should be provided with additional knowledge about the climate module of the integrated system (e.g., with respect to its capabilities or weaknesses. So far, we identified the following questions which might be of interest for environmental scientists:

1. Which feedbacks are explicitly or implicitly included in the climate model chosen?
2. What is, for the simulation of present climate, the increase of uncertainty of a climate variable when the spatial and/or temporal resolution of the climate model is increased?
3. What are the sensitivity ranges of climate variables in different climate models with regard to standard experiments, say, a relative change in the solar constant or a doubling of CO_2? And
4. what are the stability ranges of the different climate models?

The first question aims at providing environmental scientists with a short technical description of the capabilities of the four climate models mentioned above. On the one hand we restricted this description to temperature-related feedbacks (see Table 2.6), on the other hand, however, we attempted to also introduce representatives of other climate model classes into this description. IIASA's climate models (as we might shortly call the climate models which are available at IIASA) are again assumed to be fully developed.

By terming a feedback explicit we mean that the respective climate quantity is explicitly described by, e.g., some differential equation or parameterized by some algebraic formula, which links this quantity directly or indirectly to the main variables (e.g., temperature) of the climate model. We call the feedback implicit if the respective climate quantity is implicitly included, e.g., in some climatological data used or in some model parameters. If the feedback is neither explicitly nor implicitly described by the climate model, we indicate this by no.

From these definitions it is clear that only in the case of an explicit description or parameterization a feedback process can be studied individually. Therefore, Table 2.6 advises environmental scientists which least sophisticated climate model to choose if they are

Table 2.6. Comparison of climate models in regard to temperature-related feedbacks.

Atmosphere	0-D[1]	Boxes[2]	0-D[3]	1-D_z[4]	1-D_φ[1),5)]	2-$D_{\varphi,z}$[6),7)]	2-$D_{\lambda,\varphi}$[8)]	2.5-$D_{\lambda,\varphi,LA}$[9)]
Ocean			1-D_z	ML	1-D_φ[1),6)]		2-$D_{\lambda,\varphi}$	2.5-$D_{\lambda,\varphi,LO}$
					2-$D_{\varphi,z}$[5),7)]			
Atmosphere:								
Water vapor	i	i	i	e	e[12)]	e	i	e
Snow albedo	e	e	i	e[10)]	e	e	e	e
Cloudiness	i	i	i	e[11)]	i	e[13)]	i	e
Lapse rate	i	i	i	e	i	e	i	e
Horizontal transport processes	no	e	no	no	e	e	e	e
Vertical transport processes	i	i	i	i	i	e	i	e
Vegetation-soil moisture	no	no	no	no	no	e[14)]	no	e[14)]
Ocean:								
Ice albedo	e	e	i	e[10)]	e	e	e	e
Meridional heat transport	no	e	no	no	e	e	e	e
Vertical heat transport	no	e	e	no	no/e	no/e	no	e

λ longitude; φ latitude; z height/depth; ML mixed layer; L_A,L_O parameters of integrative structure describing the large-scale atmospheric and oceanic layers (boundary layer, free troposphere, stratosphere, oceanic mixed layer, seasonal thermocline, main thermocline, bottom layer).

e explicit, i.e. respective climate quantity explicitly described by, e.g., some differential equation or parameterized by some algebraic formula which links this quanity directly or indirectly to the main variables of the climate model;
i implicit, i.e. respective climate quanity implicitly included, e.g., in some climatological data used or in some model parameters;
no neither explicit nor implicit.

1) North et al. (1981); 2) Saltzman and Vernekar (1971); 3) Wigley and Raper (1990); 4) MacKay and Khalil (1991); 5) envisaged by improving the 1-D EBM of Jonas et al. (1991) by a 2-D ocean and by introducing seasonality; 6) Peng et al. (1982); 7) the envisaged version of the 2-D ZCM described in Part I of this Working Paper; 8) North et al. (1983); 9) Petoukhov (1991); model presently under review for necessary improvements; 10) Wang and Stone (1980); 11) Karol and Frolkis (1984); 12) Flannery et al. (1984); 13) Smagorinsky (1960); 14) e.g., Dickinson et al. (1986).

interested in investigating a particular feedback process for their purposes. In addition, of course, they must also keep an eye on the spatial and temporal resolution of the climate model. However, it was not our aim to discuss the quality of the various explicit parameterizations or descriptions. This would have been a task in itself.

All climate model classes are identified by a literature source in which a typical representative of each class or, in the case of an IIASA climate model, the model itself is described. The table also gives additional references which are noteworthy, e.g., if a particular feedback process has been investigated outside the given background literature or to simply indicate from where some of the major improvements of IIASA's climate models originate.

The next two questions we would like to answer provisionally with the help of Figures 2.2 and 2.3. The purpose is to look at a common climate variable (e.g., temperature[4]) at the characteristic spatial and temporal resolution of a number of climate models, and to put some quantitative perspective on the uncertainty and sensitivity problem. However, we do not wish to have our quantitative results interpreted too literally, for the number of models available or surveyed is too small for solid statistical statements. In particular with respect to the limited number of GCMs this situation will eventually change upon completion of the Atmospheric Model Intercomparison Project (AMIP) (Gates, 1992). In this Project up to 29 atmospheric GCMs are presently undergoing a systematic intercomparison and validation of their performance on seasonal and interannual time scales to support the in-depth diagnosis and interpretation of the model results.

Figure 2.2 shows the temperature uncertainty (standard deviation) of various climate models involved when simulating present climate. For simplicity the climate models are grouped according to their spatial (atmospheric) dimensions which admittedly leaves some room for discussions, in particular with respect to the 1-D and 2-D climate model classes. E.g., Sellers' (1973) zonal model also accounts for two layers in the atmosphere. However, their

[4] Here we do not distinguish between surface, surface air or sea level temperatures since we are only interested in temperature differences to observations or simulated present climate.

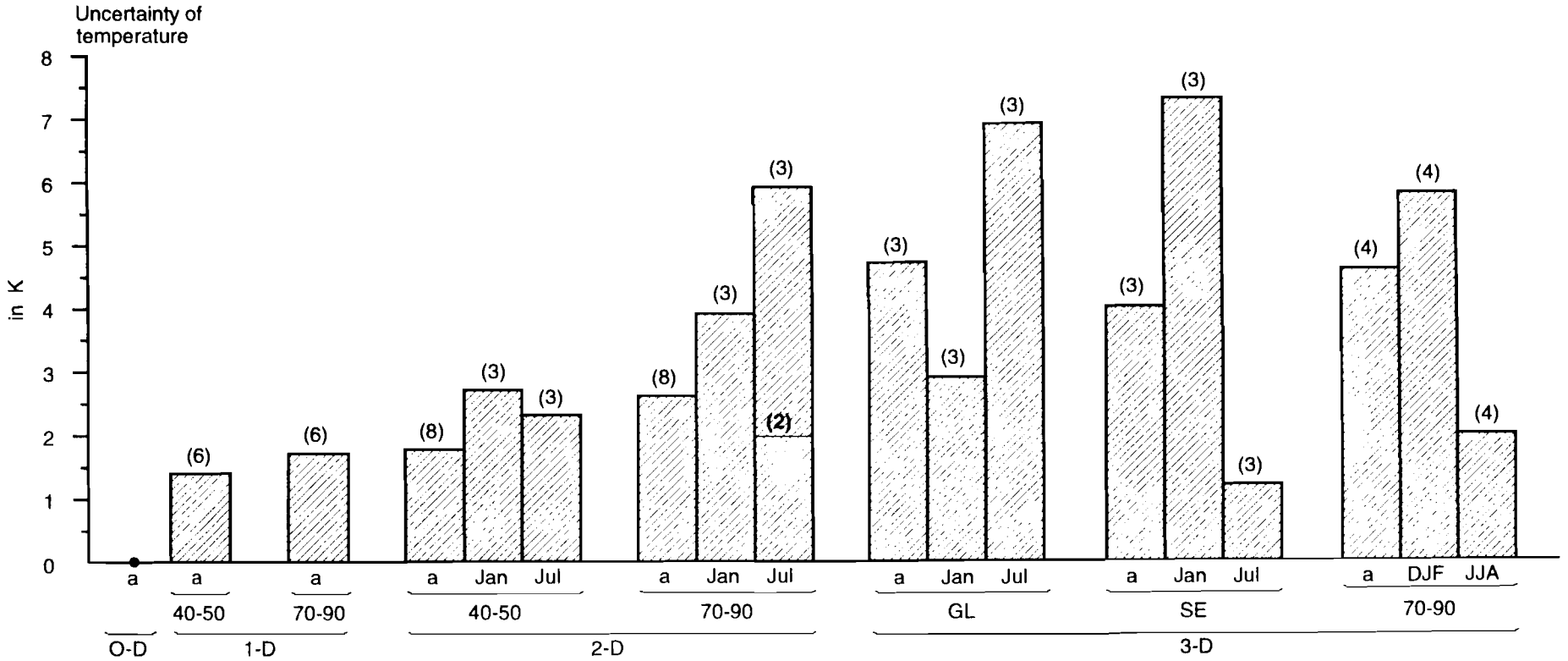

Figure 2.2. Temperature uncertainty (standard deviation) of climate models simulating present climate at different spatial and temporal resolutions. The climate models are grouped according to their spatial (atmospheric) dimensions. The standard deviation is defined as $\left\{\sum_{i=1}^{n} (T_i - T_{obs})^2 / n\right\}^{1/2}$ where the computed (T_i) and observed temperatures (T_{obs}) are referring to the same spatial and temporal resolution; n is the amount of models surveyed (indicated by the number in parentheses above each bar).

Temporal resolutions: a annual; DFJ, JJA seasons; Jan, Jul months.
Spatial resolutions: 40-50, 70-90 latitude belts in the northern hemisphere; GL, SE grid boxes (4.5° latitude by 7.5° longitude) in the Great Lakes region and in the southeast of the U.S.

1-D class: Budyko (1969); Sellers (1969); Sellers (1973); Oerlemans and van den Dool (1978); North and Coakley (1979); Thompson and Schneider (1979).
2-D class: Petoukhov (1976); Sellers (1976); Ohring and Adler (1978); Robock (1978); Peng et al. (1982, 1987); Harvey (1988); IIASA's 2-D ZCM as described in Part I of this Working Paper.
3-D class: Mearns et al. (1990); Walsh and Crane (1992).

temperatures are expressed as functions of the respective latitudinal surface temperature, which we used as a guideline for grouping such borderline cases. If these functional relationships are employed by the climate model, we put it into the 1-D class, otherwise not.

As can be seen, the uncertainty of simulating present climate in general increases with increasing spatial or temporal resolution. For example, the annual temperature uncertainty increases by about a factor of 3 when going from latitude belt 40-50°N in the 1-D class (1.4°C) up to the gridbox GL (Great Lakes region in the U.S.) in the 3-D class (4.7°C). This grid box is located in the same belt. The comparison with the gridbox SE (southeast of the U.S., i.e. latitude belt 30-40°N) seems to suggest that the uncertainty derived for the gridbox GL is not extreme.

For completeness the following remarks should be added:

- The high July temperature uncertainty of latitude belt 70-90°N in the 2-D class (5.9°C) is caused by Robock's (1978) climate model. Without his model the uncertainty is only about 1.8°C. Both values seem to indicate the borders of a possible range.
- The relatively high temperature uncertainty found in the Arctic region in GCMs seems to result from a bias of not correctly simulating winter months.
- The observational data sets behind the climate models are not necessarily consistent. Virtually all models employ different observational data sets to which they are either tuned or against which they are compared. However, we consider this to be fully admissible.
- An uncertainty of zero is assigned to 0-D climate models. Here we simply assumed that these models can always be perfectly tuned to observations.

Figure 2.3 shows the uncertainty of temperature sensitivity (standard deviation) of almost the same selection of climate models as for Figure 2.2 in regard to two standard experiments: a decrease of the solar constant by 1% and CO_2 doubling. We would have rather preferred a 2% increase in the solar constant as it is often cited in literature as being somewhat similar to CO_2 doubling. However, this selection criteria would have seriously reduced the number

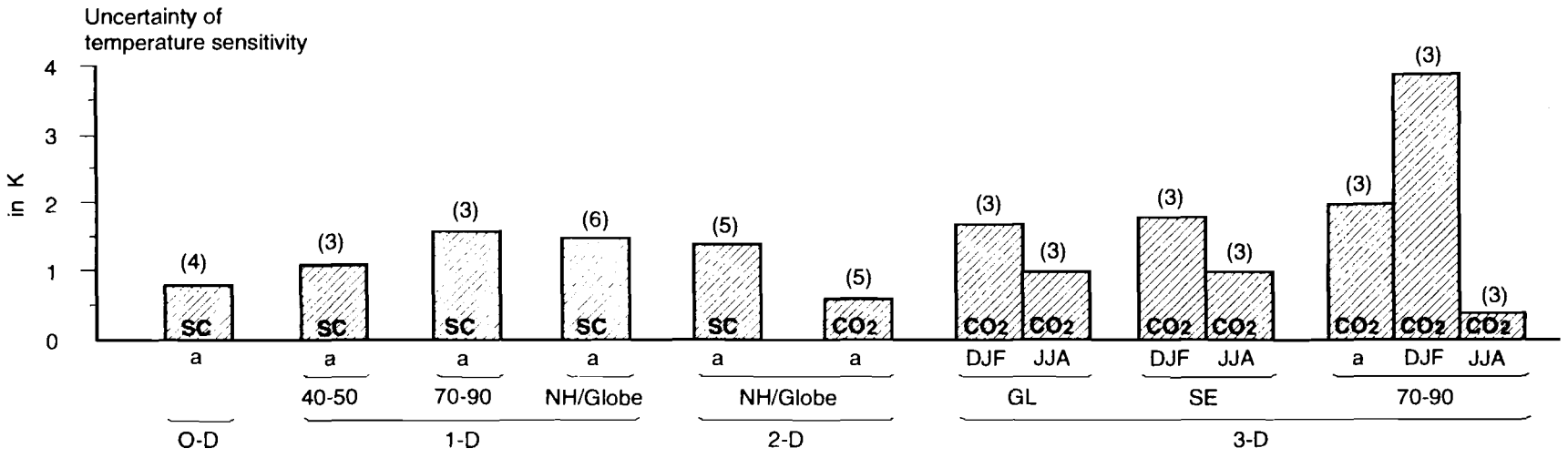

Figure 2.3. Uncertainty of temperature sensitivity (standard deviation) of climate models with regard to standard experiments (SC: decrease of solar constant by 1%; CO_2: doubling of CO_2) and to different spatial and temporal resolutions. The climate models are grouped according to their spatial (atmospheric) dimensions. The standard deviation is defined as $\left\{\sum_{i=1}^{n}\left(\Delta T_i - \overline{\Delta T}\right)^2/n\right\}^{1/2}$ where the computed temperature changes (ΔT_i) and their arithmetic means are referring to the same spatial and temporal resolution; n is the amount of models surveyed (indicated by the number in parentheses above each bar).

Temporal resolutions: a annual; DJF, JJA seasons.
Spatial resolutions: 40-50, 70-90 latitude belts in the northern hemisphere (NH); GL, SE grid boxes (4.5° latitude by 7.5° longitude) in the Great Lakes region and in the southeast of the U.S.

0-D class: Crafoord and Källén (1978), Fraedrich (1978), North et al. (1981).
1-D class: Budyko (1969); Sellers (1969); Sellers (1973); Oerlemans and van den Dool (1978); North and Coakley (1979); Thompson and Schneider (1979).
2-D class: Ohring and Adler (1978); Robock (1978); Peng et al. (1982, 1987); Petoukhov and Manuilova (1984); IIASA's 2-D ZCM as described in Part I of this Working Paper.
3-D class: Gutowski et al. (1988), pp. 82, 91, 98; IPCC (1990), pp. 165, 166.

of available 1-D climate models. A more extensive literature review in the future might possibly remedy this shortcoming and bring to light more climate models.

While hardly any sensitivity experiments for the 1-D climate models (which were popular in the seventies) are available in regard to CO_2 doubling, the same seems to hold for GCMs in regard to changes in the solar constant. The more expensive they become to run the less frequent they take a changing solar constant into consideration but CO_2 related experiments only.

When looking at CO_2, Figure 2.3 seems to suggest that the uncertainty of temperature sensitivity is increasing with increasing spatial and temporal resolution. This would mean that the greater the temperature uncertainty of a climate model the greater also the uncertainty of its temperature sensitivity to CO_2 doubling. However, more models would definitely have to be surveyed to consolidate our first conjecture.

The fourth question, finally, aims at a careful and thorough testing of climate models by utilizing i.a. the knowledge of extreme climatic events in the Earth's past. Although we raised this question, we feel that we can answer this question only in regard to the models which we have developed or have in use ourselves. It is anticipated that a complete answer will be given for each of the climate models which are available at IIASA.

2.6 The Integrated Model of Climate Change in the Perspective of Environmental Impact Modellers or Assessors

This section we would like to briefly sketch out now and to elaborate in the future. Questions similar to those which have been put forward in the previous section are also of relevance with respect to the entire integrated model of climate change. By all means, an environmental scientist wanting to use such an integrated model must be particularly informed on

- the various feedbacks that are realized between the respective modules of the model;
- the uncertainty of the integrated model that is involved in reproducing (past and)

present conditions;

- those model parameters to which the model is most sensitive; and
- on the stability (or the tested) ranges of the most important model parameters.

3. DESCRIPTION OF THE 2-D ZCM

3.1 Status of the 2-D ZCM

As it became clear from Table 2.4 of the previous chapter, the 2-D ZCM takes a place somewhere in the middle of the hierarchy of climate models that are available or under development at IIASA and reveal a graded complexity. The idea is to allow for making a choice among the climate models depending on the needs of the environmental impact to be studied. Table 3.1 gives a short overview of the present status of the ZCM. A more detailed description of the model is given in the forthcoming sections of this chapter.

3.2 Atmospheric Component

The 2-D ZCM represents a coupled system comprising an atmospheric and an oceanic component. In this section we will describe the atmospheric component, while the oceanic component is described in Section 3.3 and the linkage of both components in Section 3.4.

3.2.1 Model structure

The atmospheric component is based on energy balance considerations. In comparison with classical 1-D EBMs (e.g., Budyko, 1969; Sellers, 1969) in which latitude is the only independent variable, height is an additional model coordinate. Such a model then resolves latitude (in our case 18 latitude belts of 10° width each for the entire globe) and height (deducted from a pressure related sigma-coordinate system in our model). Thus, the model belongs to the category of Multilayer Energy Balance Models as termed by Peng et al. (1982). Typical of this category is that its models combine models which describe the radiative transfer - so called 1-D Radiative Convective Models (1-D RCMs) - with 1-D EBMs as described by Henderson-Sellers and McGuffie (1987).

The atmosphere is divided vertically into eight basic model layers for which all processes mentioned below are parameterized. These layers are distributed as follows: the lowest layer extending up to 875 hPa represents the planetary boundary layer, three (two) layers are in

Table 3.1. Main features of the 2-D ZCM.

spatial resolution[1]	18 latitudinal belts of 10°width, 8 vertical layers in the atmosphere (18 layers for radiative transfer calculations); 11 vertical layers in the ocean
temporal resolution[1]	annual (seasonality envisaged)
governing equations	energy balance equations for atmospheric, land and sea ice surface temperatures; advection-diffusion equation for oceanic temperatures; diagnostic equation for vertical overturning stream function
prescribed characteristics	relative humidity, clouds (height, cover, optical depth), mixed layer depth, surface albedos of free land and free ocean, water availability
computed climate elements[1]	T, Prec, WV, R, H[2], E, Sn, SI[2]
main processes	radiation transfer, diffusive horizontal and vertical heat and moisture transport in the atmosphere, convection by means of convective adjustment, latent heat release, horizontal and vertical heat transport in the ocean by means of large scale circulation, diffusion and convection
explicit feedbacks related to temperature[3]	water vapor, snow-albedo, sea ice-albedo, horizontal and vertical transport of heat and moisture
surface types	four with respect to surface albedo: free land, land covered by snow, free ocean and sea ice
orography	none (envisaged)
greenhouse gases	LW calculations: H_2O, CO_2, CH_4, N_2O, O_3, CFC-11, CFC-12 SW calculations: H_2O, O_3, CO_2, O_2
running time	ca. 5 minutes on a SUN SPARC 2 workstation for one model year

[1] See also Table 2.4.
[2] H sensible heat flux at the surface; SI sea ice.
[3] See also Table 2.6.

the lower (upper) troposphere (below and above 500 hPa, respectively) and the remaining two layers are above 100 hPa representing the stratosphere. The upper stratospheric layer is centered at about 17 hPa. Orography is not taken into account with the model surface corresponding to 1000 hPa.

While the air temperature is computed as a latitudinal average, the temperature of the surface in each latitude belt is further subdivided into temperature of land, free ocean and sea ice (if the fraction of sea ice in a given latitude belt is not zero). Thus, the spatial resolution of the model output concerning the surface is more detailed than just the latitudinal average. On the other hand, this approach, which was also used by Peng et al. (1987), can be regarded as a drawback because the air temperature above the surface types is not computed individually. As mentioned in Peng et al. (1987), it is equivalent to assuming an instantaneous coupling between the atmospheres of the three surface sectors. However, to reduce possible errors in computing the surface sensible heat flux, the vertical temperature gradient near the surface is parameterized above the individual surfaces.

The current version of the 2-D ZCM simulates mean annual thermodynamic conditions. The schematic structure of one latitude belt is shown in Figure 3.1.

3.2.2 Governing equation for the atmosphere

The equation used for the atmosphere is

$$\frac{\partial T}{\partial t} = A + Q_S + Q_I + Q_L \,, \tag{3.1}$$

where Q_S ,Q_I and Q_L are heating rates (K/day) due to solar radiation, infrared radiation and latent heat release, and the A term represents the net effect of the redistribution of thermal energy by dynamical mechanisms (Peng et al., 1982). In the following we briefly discuss the individual components of Equation (3.1).

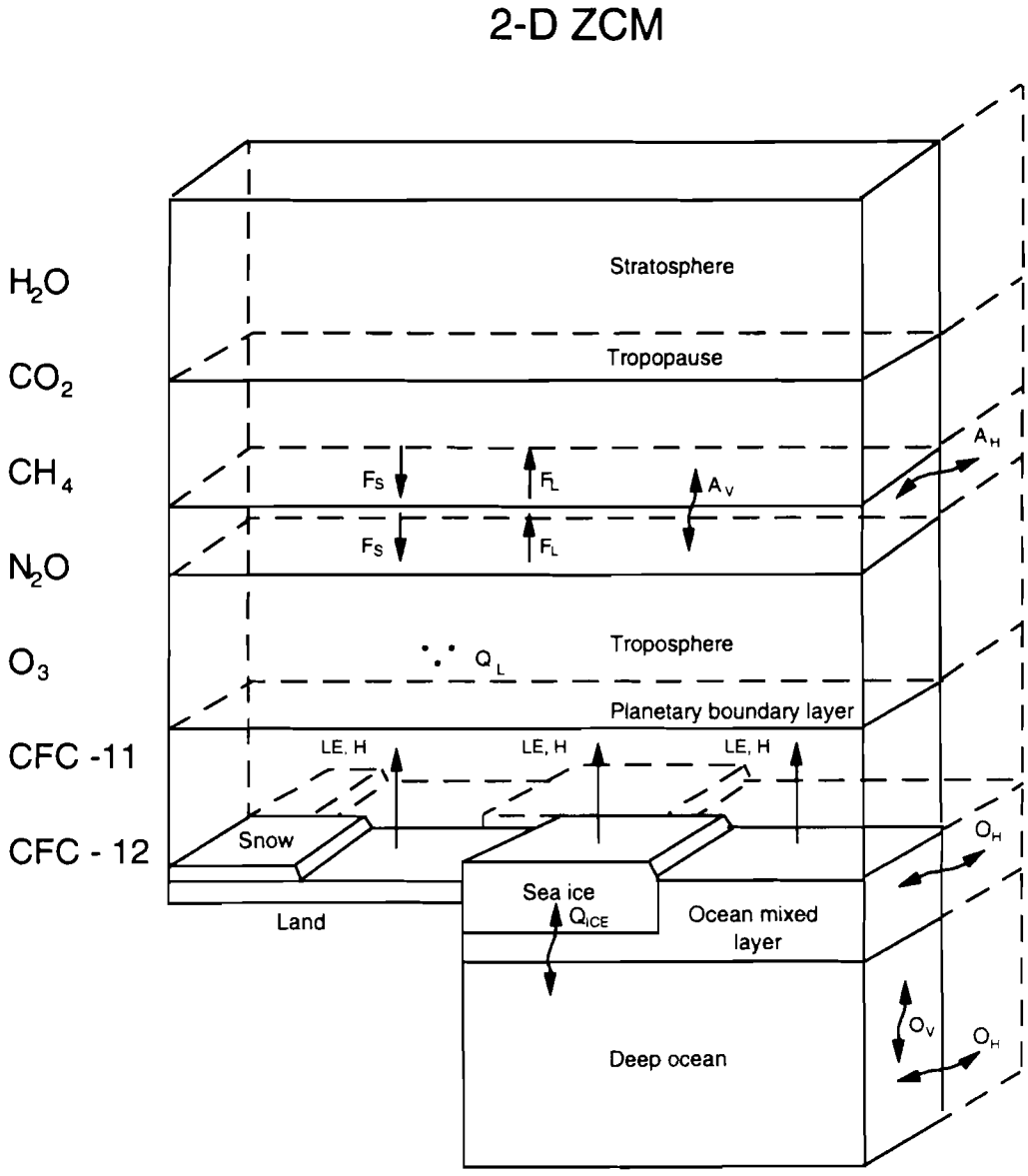

Figure 3.1. Schematic illustration of one latitude belt of the 2-D Zonal Climate model. F_S, F_L denote short-and long-wave radiation, A_V and A_H vertical and horizontal heat transport; Q_L latent heat release; Q_{ice} heat flux through the sea ice; LE and H latent and sensible heat fluxes for land (with and without snow), sea ice and ocean; O_V and O_H vertical and horizontal heat transport in the ocean.

a) Redistribution of heat due to dynamics

The term A can be subdivided into horizontal and vertical components:

$$A = A_H + A_V \quad . \tag{3.2}$$

With respect to the horizontal component, A_H, we do not distinguish between tropical and extratropical regions. Peng et al. (1982) used Stone's parameterization for large-scale eddies in the extratropics (Stone, 1978) and a simplified parameterization of the Hadley cell in the tropics. Instead, we parameterize the horizontal heat transport by means of a simple horizontal diffusion. There is no doubt that such an approach is less sophisticated than the attempt made by, e.g., Peng et al. (1982). On the other hand, even using a parameterization of Stone's type is not free of problems and it does not necessarily lead to better results in comparison with the simpler diffusion approach. When the diffusion approach is used, one can derive the diffusion coefficients for present climate (at least for the troposphere) depending on latitude and height, which should then result in a more or less correct meridional heat transport in the model. However, such a horizontal and vertical tuning of the diffusion coefficient does not have to give the appropriate heat transport under a changed temperature distribution in the atmosphere. In this study we use a single prescribed value for the diffusion coefficient D. For the experiments described in Chapter 4 we use $D = 0.15*10^7$ m^2/s everywhere for both heat and moisture transport which is also parameterized in terms of diffusion. The term A_H is thus given by:

$$A_H = \frac{1}{R^2 \cos\varphi} \frac{\partial}{\partial \varphi} \left(\cos\varphi \, D \frac{\partial T}{\partial \varphi} \right), \tag{3.3}$$

where R is the Earth's radius and φ the latitude.

With respect to the vertical component, A_V, we distinguish between the planetary boundary layer and the free atmosphere. The vertical heat flux $T\omega$ (positive downward) at the top of the model boundary layer (875 hPa) is expressed by

$$T\omega = -\frac{gH}{2c_p}, \tag{3.4}$$

where H is the surface sensible heat flux, c_p the specific heat of dry air, and g the acceleration due to gravity.

In the free atmosphere the flux is computed by means of

$$T\omega = -\rho g K_z \left(\rho g \frac{\partial T}{\partial p} - (\Gamma_d - \Gamma_c) \right) . \tag{3.5}$$

In the equation ρ is the air density, Γ_d is the dry adiabatic lapse rate and Γ_c the countergradient factor, which is (as in Peng et al., 1982) taken to be equal to the product of the relative humidity and the difference between the dry and moist adiabatic lapse rates. The vertical diffusion coefficient K_Z decreases linearly with pressure from 1 m^2/s at the top of the boundary layer to zero at the tropopause. The vertical component A_V then reads:

$$A_V = -\frac{\partial (T\omega)}{\partial p} . \tag{3.6}$$

b) Radiative heating and cooling rates

A radiative transfer scheme developed by MacKay and Khalil (1991) is integrated into the 2-D ZCM. In their scheme, a vertical resolution of 18 vertical layers (of which 6 layers are above 250 hPa) is used for the evaluation of the radiative fluxes. Once the fluxes are known at the top and bottom of each of the eight basic model layers, the radiative heating and cooling rates are computed (see Eqs. (3.7) below).

The radiative transfer scheme is described in detail in MacKay and Khalil's (1991) paper. Therefore, only a brief description is given. As far as the absorption and emission of the longwave (terrestrial) radiation is concerned, the contributions of the following atmospheric

gases are taken into account: water vapor (H_2O), carbon dioxide (CO_2), ozone (O_3), nitrous oxide (N_2O), methane (CH_4), and chlorofluorocarbons (CFC-11 and CFC-12). With respect to H_2O the absorption of terrestrial radiation is confined to three spectral bands: the vibration-rotational band (centered at 6.3 μm), the pure rotational band (for wavelengths greater than 12 μm), and the continuum band (extending from 8.3 to 20.8 μm). The emissivity formula given by Ramanathan (1976) is used for the first two spectral bands, while the transmissivity parameters given by Roberts et al. (1976) are used to calculate the emissivities of the water vapor continuum band. Concerning carbon dioxide, the integrated band absorptance for the 15 μm band is computed according to Cess and Ramanathan (1972). The overlap with water vapor in the 15 μm region is also taken into account. With respect to O_3, CH_4, N_2O and CFCs, not only their absorptances are computed but also the respective overlaps are taken into account.

Solar absorption due to H_2O, O_3, CO_2 and oxygen (O_2) is parameterized. The principal absorbers are H_2O in the troposphere and O_3 in the stratosphere; H_2O absorbs primarily in the near-infrared region ($0.7 \leq \lambda \leq 4$ μm) while O_3 is the main absorber at shorter wavelengths (ultraviolet and visual regions). CO_2 and O_2 are minor absorbers of the shortwave radiation; they together contribute about 9% to the total atmospheric absorption of the solar radiation. The method developed by Lacis and Hansen (1974) is used to calculate the solar absorption due to H_2O and O_3 for both clear and cloudy sky conditions, while the treatment of Sasamori et al. (1972) is used to calculate the absorption of solar radiation by CO_2 and O_2.

Clouds are treated in the scheme as a single effective cloud layer with prescribed cloud cover, height and cloud optical thickness (see Section 3.2.4). The height of the effective cloud layer depends on latitude with its maximum in the tropics and its minimum in high latitudes, while the effective cloud optical depth is kept constant.

The radiative heating rates in Equation (3.1) are computed according to

$$Q_S = \frac{g}{c_p}\frac{A_S}{\Delta p}$$

$$Q_I = \frac{g}{c_p}\frac{\Delta F}{\Delta p}\ , \qquad (3.7)$$

where A_S is the net flux of solar energy (W/m^2) absorbed by the respective layer, Δp its pressure thickness and F the net upward flux of infrared radiation.

c) Heating rate due to latent heat release

To obtain heating rates due to latent heat release in individual atmospheric layers, the precipitation rate reaching the surface is computed first. In each latitude belt, we require that the precipitation rate and the vertically integrated horizontal divergence of water vapor (sinks of moisture in a vertical atmospheric column) balance the surface evaporation rate (source of water vapor) . This balance is given by

$$P = E - \frac{1}{g}\int_{p_t}^{p_s} D_{q_H}\, dp\ , \qquad (3.8)$$

where the horizontal divergence of water vapor D_{qH} is computed by means of a diffusive approach, and p_s and p_t are pressures at the surface and tropopause, respectively. For the region from 30°N to 30°S we follow Peng et al. (1982). Equation (3.8) is not applied to each latitude belt separately but to the entire region. The total amount of precipitation is then redistributed according to present climatology (Jaeger, 1976).

Once the total precipitation rate P at the surface is known, a question arises how to compute the amount of latent heat released in individual vertical layers. We use an approach similar to that of Peng et al. (1982) when we define a dimensionless relative distribution function $\eta(p)$

$$\eta(p) = \begin{cases} \dfrac{c(p)\ \Delta p(p)}{\sum_{p_t}^{p_b} c(p)\,\Delta p(p)} & \text{for } p_b > p > p_t \\ 0 & \text{elsewhere} \end{cases} \qquad (3.9)$$

where

$$c(p) = \max(-D_q(p),\ 0)\ , \qquad (3.10)$$

$\Delta p(p)$ is the pressure thickness of a layer centered at p, p_b is the pressure at the top of the boundary layer, and D_q the divergence of water vapor.
The heating rate due to latent heat release can finally be computed by

$$Q_L(p) = \frac{g}{c_p \Delta p(p)}\, L\eta(p) P\ , \qquad (3.11)$$

where L is the latent heat of condensation.

We use this approach directly in the extratropical region where the large-scale convergence of the water vapor plays the dominant role (processes which lead to the origin of stratiform clouds). In the tropical region, however, convective processes are more important. In Peng et al. (1982), an attempt was made to account for this fact by expressing the relative distribution function by means of the difference between temperature of the model atmosphere and temperature of a convective cloud. The vertical temperature profile within the convective cloud was parameterized by means of Kuo's scheme (Kuo, 1965). However, it leads to a discontinuity in the vertical distribution of latent heat release at the boundary between the extratropical and tropical regions (outside the tropics, the maximum of the latent heat release is in the lower troposphere; while the maximum lies between the middle and upper troposphere in the tropics). Therefore we use some extratropical average of the relative distribution function also for the tropical region in the current model version.

3.2.3 Governing equations for the individual surface types

At the surface, three surface types are distinguished with respect to surface temperature computations: land (which is subdivided into free land and land covered with snow with respect to surface albedo), sea ice, and open ocean. Energy balance equations applied to land and sea ice read:

$$C_L \frac{\partial T_L}{\partial t} = S_L - I_L - H_L - LE_L$$
$$C_I \frac{\partial T_I}{\partial t} = S_I - I_I - H_I - LE_I + q_I \,, \tag{3.12}$$

where S is the shortwave radiative flux (W/m^2) absorbed by the surface, I the net surface flux of thermal radiation (positive upward), and H and LE are sensible and latent heat fluxes, respectively. Indices L and I refer to land and sea ice. On the left hand side, C stands for the effective heat capacity of the surface for which a small value that does not disturb the numerical stability of the model is used. The term q_I refers to the heat flux through sea ice; its computation is described in Section 3.3.

a) Shortwave radiation absorbed by the surface

The method developed by Lacis and Hansen (1974) serves as a basis for the computation of the absorption of shortwave radiation at the surface. This computation is part of the radiative transfer scheme. Surface albedos of free land and open ocean are taken from Sellers (1965) and Curran et al. (1978), respectively, and so far are held constant with time. Albedos of land covered by snow, α_S, and of sea ice, α_I, are parameterized in terms of snow cover on land and extent of sea ice, respectively:

$$\alpha_S = 0.5 + 0.2 f_S$$
$$\alpha_I = 0.4 + 0.2 f_I , \qquad (3.13)$$

where f_S is the fraction of land covered by snow and f_I the fraction of ocean covered by sea ice. The albedos of free land and land covered by snow are then used to compute the effective albedo of land which is necessary for the evaluation of the term S_L in Equation (3.12). The fraction of land covered by snow is a function of the surface air temperature above land. This functional relationship is based on present mean annual temperatures that are height-corrected to sea level pressure. The fraction of ocean covered by sea ice is a function of mixed layer temperature (see below).

b) Net longwave radiation from the surface

The net longwave radiation from the surface, I, is computed according to

$$I = \sigma T^4 - I^{\downarrow} , \qquad (3.14)$$

where $I^{\downarrow}$ is the downward longwave radiation from the atmosphere as computed in the radiation scheme, T the surface temperature, and σ the Stefan-Boltzmann constant.

c) Surface sensible and latent heat fluxes

For the surface sensible and latent heat fluxes, we use the following parameterizations:

$$H = c_p \rho K(\gamma - \Gamma_d + \Gamma_c)$$
$$LE = -LW\rho K\left(\frac{\partial q}{\partial z}\right) , \qquad (3.15)$$

where γ is the vertical temperature gradient near the surface, K the vertical diffusion

coefficient, W the water availability and q the water vapor mixing ratio. The parameterization is applied separately for land, ocean and sea ice surfaces with vertical diffusion coefficients taken from Peng et al. (1987). The water availability W is 1 for ocean, 0.2 for snow and sea ice surfaces, and 0.7 for free land. Since the air temperature above individual surface types is not computed, the temperature gradient γ has to be parameterized. The parameterization is based on the difference between the latitudinally averaged temperature and the temperature at the same height above individual surfaces. The difference is supposed to be maximal at the surface where the value is given by the model, and it is supposed to decrease exponentially with decreasing pressure. Using such a parameterization, the temperature above individual surface sectors can be assessed. The lapse rate γ is then derived from the surface temperature and the temperature at the top of the boundary layer for each surface type separately.

3.2.4 Prescribed parameters

One of the most important prescribed parameters is relative humidity. Zonally averaged relative humidity as a function of height was kindly provided by the European Centre for Medium-range Weather Forecasts (ECMWF) (E. Klinker, private communication, 1992). The data reflected mean atmospheric conditions over the period 1985 - 1990. Although the relative humidity is kept constant over time, the actual amount of water vapor is allowed to vary due to changes of temperature.

As mentioned in Section 3.2.2, clouds are treated as a single effective cloud layer with prescribed height, optical depth and fractional cover. While the cloud cover is taken from Harvey (1988), the effective height of the cloud layer and the effective cloud optical depth serve as tunable parameters of the model. This is justified because of their uncertainty.

Also prescribed are the surface albedos of free land and open ocean, as mentioned in Section 3.2.3, together with the surface water availability W.

The fractions of land and ocean are specified to present conditions. For the solar constant the value of 1368.3 W/m^2 is used. Latitudinal values of the mean annual solar zenith angle are taken from Ohring and Adler (1978).

3.2.5 Numerical algorithm

Surface temperatures of land and sea ice are updated employing a first order explicit numerical scheme:

$$T^{n+1} = T^n + \Delta t \left(\frac{\partial T}{\partial t}\right)^n , \tag{3.16}$$

where n is the index indicating the time level and Δt the time step of the integration (set to three days).

For updating atmospheric temperatures we currently use a three-level scheme with respect to time following Sellers (1983)

$$T^{n+1} = T^n + 0.5 \left(\left(\frac{\partial T}{\partial t}\right)^n \Delta t + (T^n - T^{n-1}) \right) , \tag{3.17}$$

which removes possible spurious oscillations in the temperature field.

The radiative transfer scheme consumes most of the running time. To speed up the computations, the radiative part of the code is not called every time step but just once per five model steps. In the meantime, the radiative fluxes are held constant. As the model reaches equilibrium, the radiation code is called less frequently. Further improvements of this technique are envisaged.

3.3 Oceanic Component

The development of zonal ocean models is a rather difficult task because large-scale ocean processes are principally three-dimensional, and meridional boundaries which separate the world ocean into a few quite different, but at the same time closely connected ocean basins play an extremely important role in the oceanic circulation. It is one of the reasons, why until recently the oceanic modules of zonal climate models were very simple and physically poor. A new approach developed by Wright and Stocker (1991) and Stocker and Wright (1991) (both of them hereafter WS) seems to support the development of more credible zonal ocean models.

The model described below is similar to WS's model in many respects and, also, it is based on the same main assumptions which receive support from GCM results and observed data:

1. the zonally averaged meridional and vertical circulation (the so-called vertical overturning) plays the major role in the meridional oceanic heat transport; and

2. the vertical overturning can be reproduced as a function of zonal wind stress and meridional density gradients only.

At the same time there are some important differences between our model and that of WS. The main one is that WS's model describes the ocean basins individually, while in our case all oceans are combined into one basin. The separate description of the different oceans is to be preferred from the oceanographic point of view. But since our ocean module was to be coupled with a zonal atmospheric model, we did not consider several ocean basins for reasons of consistency. In addition, we parameterized the vertical overturning in integral form rather than in a differential form as it was done by WS.

3.3.1 Temperature equations

The present version of the zonal advective-diffusive ocean model describes mean annual conditions. Salinity is not considered. The mixed layer (ML) depth is kept constant. The

model describes the world ocean as one basin the longitudinal extent of which is given by the fractional ocean area in each zone. The equation for the zonally averaged ocean temperature can be derived by integrating the three-dimensional temperature equation under the assumption that all nonzonal terms are negligible. It is convenient to write the temperature equations separately for the ML

$$h_1 \frac{\partial T_1}{\partial t} = -\frac{1}{Rl}\left[\frac{\partial}{\partial \varphi}(\Psi_1 T_1) - \frac{\partial \Psi_1}{\partial \varphi} T_h\right] + \frac{A_x h_1}{R^2 l}\frac{\partial}{\partial \varphi}\left[l\frac{\partial T_1}{\partial \varphi}\right] + (q_0 - q_1)(c_p \rho_0)^{-1} , \qquad (3.18)$$

and for the deep ocean

$$\frac{\partial T}{\partial t} = -\frac{1}{Rl}\left[\frac{\partial}{\partial \varphi}\left[\frac{\partial \Psi}{\partial z} T\right] - \frac{\partial}{\partial z}\left[\frac{\partial \Psi}{\partial \varphi} T\right]\right] + \frac{A_x}{R^2 l}\frac{\partial}{\partial \varphi}\left[l\frac{\partial T}{\partial \varphi}\right] + A_z \frac{\partial^2 T}{\partial z^2}, \qquad (3.19)$$

where T_1 is the ML temperature, $T(\varphi,z)$ the mean zonal ocean temperature for $z > h_1$, h_1 = 50 m the ML depth, $l(\varphi)$ the longitudinal extent of the ocean in a latitude belt, and A_x and A_z are the coefficients of horizontal and vertical temperature diffusion, respectively. The vertical overturning stream function (VOSF) Ψ is connected with the horizontal and vertical components of the mean zonal current velocity by the relations

$$u = \frac{1}{l}\frac{\partial \Psi}{\partial z} , \qquad w = -\frac{1}{Rl}\frac{\partial \Psi}{\partial \varphi} . \qquad (3.20)$$

The VOSF takes the value Ψ_1 at the bottom of the ML. The vertical heat fluxes at the ocean surface and through the bottom of the ML are determined by

$$q_0 = S_O - I_O - H_O - LE_O \qquad (3.21)$$

and

$$q_1 = - A_z \, c_p \, \rho_0 \left. \frac{\partial T}{\partial z} \right|_{z=h_1+0} , \tag{3.22}$$

where S_O is the absorbed solar radiation, I_O the infrared flux from the ocean surface, H_O and LE_O are the sensible and latent heat fluxes at the ocean surface, c_p is the specific heat capacity of water, and ρ_0 the water density.

The temperature at the bottom of the ML, T_{h_1}, is determined by

$$T_{h_1} = \begin{cases} T_1 & if \quad w(h_1) > 0 \\ T_2 & if \quad w(h_1) < 0 , \end{cases} \tag{3.23}$$

where T_2 is the temperature of the underlying layer.

The boundary conditions for Eqs. (3.18) and (3.19) at the lateral boundaries (φ = 90°N for the North Pole, φ = 80°S for the Antarctic boundary) and at the ocean bottom ($z = H_b$) are

$$\begin{aligned} \frac{\partial T}{\partial \varphi} &= 0 \quad if \quad \varphi = 80^o S \, , \, 90^o N \\ \left. \frac{\partial T}{\partial z} \right|_{z=H_b} &= 0 \end{aligned} \tag{3.24}$$

If the temperature of the upper layer is lower than that of the underlying layer (i.e. the density of the upper layer is greater than the density of the underlying layer) the vertical stratification is unstable, and convective mixing must occur. In this case the procedure of convective adjustment, similar to the one in the atmosphere, is used

$$if \quad T_{ij+1} > T_{ij} \quad \Rightarrow \quad T^n_{ij+1} = T^n_{ij} = \frac{T_{ij+1}h_{j+1} + T_{ij}h_j}{h_{j+1} + h_j} , \qquad (3.25)$$

where index n denotes the new value of the ocean temperature after convective adjustment, and h_j is the thickness of model layer j. After one full cycle of the convective adjustment instability may appear between other pairs of layers. Therefore, it is necessary to repeat the convective adjustment procedure in form of an iterative process.

Preliminary results show that the model reasonably well reproduces the vertical temperature structure in lower latitudes but significantly overestimates the temperature below the ML in high latitudes. This shortcoming is due to the fact that convective mixing leads to uniform temperatures over the depth of hundreds of meters or more in high latitudes. To avoid determining the temperature of deep mixed layers by mean annual conditions, while in reality this temperature is determined by late winter conditions, a special parameterization of the seasonal surface temperature course was introduced into the model. In this parameterization the temperature of the ocean surface, which forms the boundary condition to the atmosphere, is determined via

$$T_1^* = T_1 + \Delta T_1 , \qquad (3.26)$$

where the amplitude of the seasonal ocean surface temperature course, ΔT_1, was derived from empirical data of Oort (1983). It means that the heat exchange between atmosphere and ocean is determined by the mean annual ocean surface temperature, while the heat exchange between ML and deep ocean layers is controlled by the minimum ocean surface temperature. It should be noted that the amplitude of the seasonal course may change with global climate change, but we suppose that this effect can be neglected to a first approximation.

3.3.2 Description of zonally averaged ocean circulation

The total VOSF is reproduced in the model as the sum of winddriven, baroclinic and interhemispheric exchange components (see also Fig. 3.2):

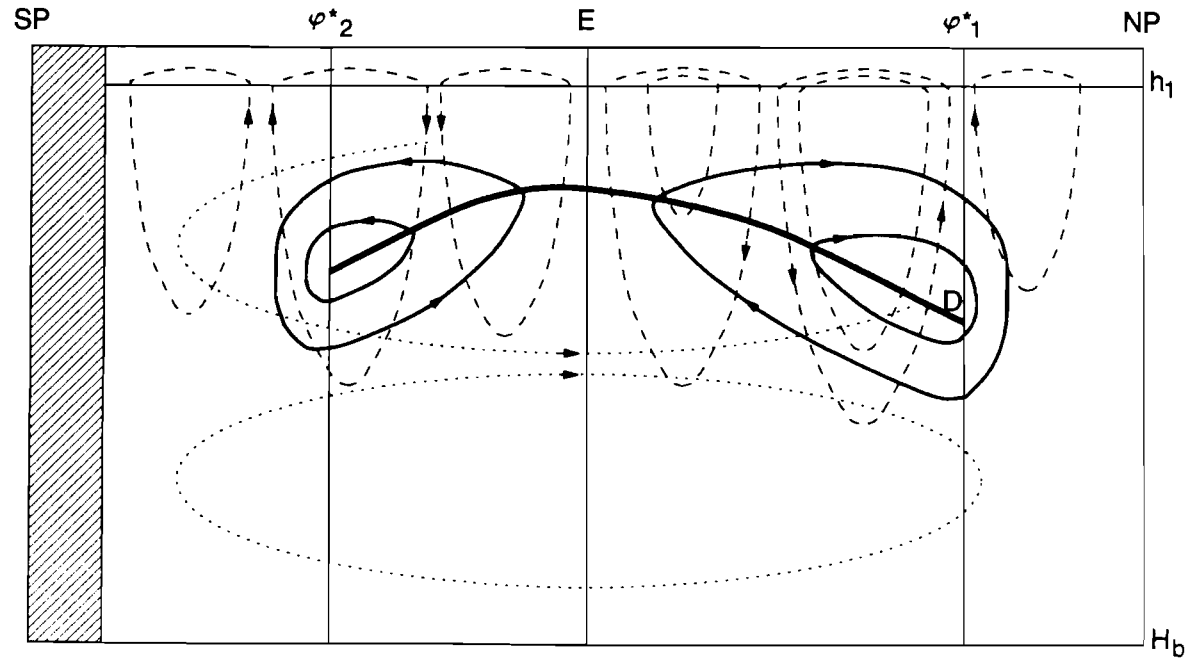

Figure 3.2. Schematic representation of the three components of the vertical overturning stream function: baroclinic (solid line), winddriven (dashed line) and interhemispheric exchange (dotted line) components. The thick line indicates the location of the bottom of the main thermocline.

$$\Psi = \Psi_w + \Psi_b + \Psi_{IH} \quad . \tag{3.27}$$

The winddriven component Ψ_w is determined by using Ekman's meridional mass transport

$$\Psi_w = - \frac{\tau_x \, l}{\rho_0 \, f} \psi_0(z) \quad , \tag{3.28}$$

where τ_x is the zonal component of the zonally averaged wind stress, derived from Han and Lee (1983), f the Coriolis parameter, and

$$\psi_0(z) = \begin{cases} \dfrac{z}{h_1} \quad , & z \le h_1 \\ \dfrac{H_b - z}{H_b - h_1}, & z > h_1 \quad . \end{cases} \tag{3.29}$$

In agreement with GCM results it is assumed that the zonally averaged baroclinic circulation is asymmetric horizontally and vertically with a broad region of weak upwelling in lower and middle latitudes and with a relative narrow region of downwelling near the northern (southern) boundary of the baroclinic cell. In the northern hemisphere the boundary of the baroclinic cell is located at $\varphi_1^*=70^\circ$ N, which is connected with the geography and the topography of the North Atlantic. In the southern hemisphere the boundary of the baroclinic cell is at $\varphi_2^* = 40^\circ$ S because of missing meridional continental boundaries south of this latitude. It is supposed that every baroclinic cell is restricted to one hemisphere and the interhemispheric exchange can be described separately. The VOSF of each hemispheric baroclinic cell is represented by a product of three functions each of which depends only on one variable

$$\Psi_b = \psi_1(\Delta\xi)\ \psi_2(\varphi)\ \psi_3(z) \ . \tag{3.30}$$

These functions are derived from the extensive set of numerical experiments with the Ocean General Circulation Model (OGCM) produced by Weaver and Sarachik (1991) and from unpublished results of numerical experiments with a multilayer ocean circulation model of Ganopolski (1991). The maximum value of the VOSF intensity in a given hemisphere, ψ_1, depends on the meridional difference of surface elevation ξ

$$\psi_1 = \frac{k_\psi\ g}{\bar{f}} \Delta\xi \ , \tag{3.31}$$

where k_Ψ is an empirical coefficient, $\bar{f}$ the Coriolis parameter averaged over the ocean area

occupied by the baroclinic cell, and $\Delta\xi = \xi_{max} - \xi_{min}$ the difference in surface elevation. The maximum and minimum values of surface elevation are determined for latitude belts between 0 and φ_n^* (n=1; northern hemisphere; n=2 southern hemisphere).

In a first approximation the value of the surface elevation can be determined by the vertical integration of the density anomaly

$$\xi(\varphi) = \frac{1}{\rho_0} \int_o^{H_b} (\rho_0 - \rho(z))dz \ . \tag{3.32}$$

The horizontal structure of the overturning cell is described by a linear function depending on latitude between the equator and φ_n^* according to

$$\psi_2 = \begin{cases} \dfrac{\varphi}{\varphi^*} & if \ |\varphi| \leq \varphi_n^* \\ 0 & if \ |\varphi| \geq \varphi_n^* + 10°. \end{cases} \tag{3.33}$$

The vertical structure of the overturning cell, finally, is reproduced by the formula

$$\psi_3 = \frac{z}{D} \exp\left[1 - \frac{z}{D}\right] \ , \tag{3.34}$$

which gives the maximum of the VOSF at $z = D$. The depth D is the thermocline depth which is determined from the temperature condition

$$T(\varphi,D^*) = T(\varphi,H) + [\ T(\varphi,0) - T(\varphi,H_b)\ ]\ e^{-1} \tag{3.35}$$

where D^* is an intermediate value, and

$$D = \min\ (1000\ m,\ D^{*})\ . \tag{3.36}$$

The vertical structure of the interhemispheric mass exchange is described by trigonometrical functions which reasonably reproduce the vertical overturning pattern of GFDL OGCM (Manabe et al., 1991):

$$\Psi_{IH} = \psi_4\ \psi_5(\varphi)\ \psi_6(z)\ , \tag{3.37}$$

where ψ_4 is the maximum value of the interhemispheric mass transport at the equator,

$$\psi_5 = \cos\left[\pi\ \frac{\varphi}{\varphi^{**}}\right]\ , \tag{3.38}$$

where $\varphi^{**} = 140^{\circ}$ is the latitudinal extent of the interhemispheric exchange gyre, and

$$\psi_6 = \sin\left[2\pi\frac{z}{H}\right]\ . \tag{3.39}$$

The density of sea water is determined from the equation of state (Gill, 1985) with constant salinity (S=35 ppt).

3.3.3 Sea ice parameterization

Because our ocean model is meant to describe mean annual conditions we do not follow a traditional thermodynamic approach for modelling sea ice, as such an approach can only produce realistic results if seasonality is taken into consideration. Instead, we parameterize the sea ice fraction. It is assumed that the sea ice fraction f_I depends only on the ocean surface temperature T_1^{*}

$$f_I = a_{ni} - b_{ni}\, T_1^* \ , \tag{3.40}$$

where the empirical parameters a_{ni} and b_{ni} are determined separately for both hemispheres and for three temperature intervals (see Table 3.2) on the basis of empirical data for both annual ocean temperature (Levitus, 1982) and mean annual sea ice fraction (Curran et al., 1978).

The average sea ice thickness h_I is reproduced as a function of local (latitudinal) sea ice fraction and total hemispheric sea ice cover S_n in the form

$$h_I = c_n\, S_n \sqrt{f_I} \ , \tag{3.41}$$

where c_n is an empirical coefficient, and the value of S_n can be determined in a dimensionless form by

$$S_n = \sum_j f_o^j f_I^j \cos \varphi_j \ , \tag{3.42}$$

where f_o^j and f_I^j are the ocean and sea ice fraction, respectively, in latitudinal belt j, with φ_j as its center latitude.

To avoid that sea ice thickness is close to 0, which can cause numerical instabilities, the lower limit for sea ice thickness $h_I = \max(h^*_I, 0.5\ m)$ is used, where h_I^* is the sea ice thickness obtained from (3.41).

The heat flux in a uniform sea ice layer can be described by

$$q_I = \frac{k_I}{h_I} (T_b - T_I) , \tag{3.43}$$

where k_I is the heat conductivity of sea ice, T_I its surface temperature, and T_b the temperature at the sea ice bottom, determined by $T_b = \min(T^*_1, 0^\circ C)$.

To take into consideration the effects of snow cover and nonuniformity of multiannual sea ice (both of them decrease the heat flux through sea ice), the coefficient of the effective sea ice heat conductivity was quantified as follows:

$$k_I = \frac{k_I^o}{\max(h_I , 1\ m)} , \tag{3.44}$$

where k_I^0 is the heat conductivity of uniform ice.

In latitude belts where sea ice exists, the effective oceanic net surface heat flux q_0^* is determined by

$$q_0^* = q_0 (1-f_I) - q_I f_I . \tag{3.45}$$

3.3.4 Numerical algorithm

For solving equations (3.18) and (3.19) numerically the technique of shifted grids is used. The temperature is determined in gridpoints (i,j), the VOSF in gridpoints (i+1/2,j+1/2), the horizontal fluxes in gridpoints (i+1/2,j) and the vertical fluxes in gridpoints (i,j+1/2). The ocean is divided into 11 layers, including the ML. The vertical resolution varies from 50 m at the surface to 1000 m at the bottom. The list of important model parameters is given in Table 3.3.

An ordinary first-order explicit numerical scheme is used in the ocean model. In the present version a time step of up to 30 days can be used.

3.4 Linkage

In this section we briefly describe the procedure of linking the atmospheric to the oceanic module. The ocean surface temperature is used in the atmospheric module for the computation of upward longwave radiation and sensible and latent heat fluxes from the free ocean. The vertical heat flux through sea ice, in turn, is calculated in the ocean module using the atmospheric temperatures of the previous time step. This heat flux is then used in the atmospheric module for updating the sea ice temperature.

Different methods of linking the atmospheric to the oceanic module are used for equilibrium and time dependent experiments. The main reason is the great characteristic time of the ocean-atmosphere system. Indeed, to achieve equilibrium for the deep ocean, at least a 1000 year integration is necessary. Such a long integration is extremely expensive because of the atmospheric module. Therefore, the so-called asynchronous linking method was used for climate equilibrium computations. In this case, ocean and atmosphere are integrated using different time steps: three days for the atmosphere and one month for the ocean. Such a procedure is used in many numerical experiments with mean annual climate models. In the case of time-dependent experiments, the time step for the integration of the ocean model is the same as for the integration of the atmosphere model (three days).

Table 3.2. Coefficients of the sea ice parameterization.

	Northern hemisphere (n=1)		
i	1	2	3
Temperature interval (°C)	-1.8 ... -1.5	-1.5 ... 0	0 ... 7.5
a_{ni}	1	0.75	0.75
b_{ni}	0	0.167	0.10
	Southern hemisphere (n=2)		
Temperature interval (°C)	-1.8 ... -1.5	-1.5 ...-0.5	-0.5 ... 2.5
a_{ni}	1	0.25	0.416
b_{ni}	0	0.50	0.167

Table 3.3. Physical parameters of the model.

Horizontal diffusion	A_x	$= 10^3$ m^2/s
Vertical diffusion	A_z	$= 10^{-4}$ m^2/s
VOSF coefficient	k_ψ	$= 10^2$ m
Interhemispheric mass exchange	ψ_4	$= 5 \times 10^6$ m^3/s
Sea ice heat conductivity	k_I	$= 2$ W· m/K
Sea ice thickness coefficients	c_1, c_2	$= 10$ m
Mixed layer depth	h_1	$= 50$ m
Ocean depth	H_b	$= 5000$ m

4. DESCRIPTION OF MODEL RESULTS

4.1 Overview of Results

In this chapter we discuss the results which we obtained with the 2-D ZCM. Table 4.1 gives an overview of the results and the figures presenting them. The figures are grouped into three parts: simulation of present climate (indicated by "1xCO_2"), equilibrium response to a doubling of CO_2 ("2xCO_2"), and time dependent experiments ("Scenario"). This division corresponds to the sections of Chapter 4.

Table 4.1. Overview of model results.

	1xCO_2
Fig. 4.1	Temperature field.
Fig. 4.2	Difference between simulated and observed temperature fields.
Fig. 4.3	Evaporation and precipitation rates.
Fig. 4.4	Atmospheric and oceanic meridional heat transport.
Fig. 4.5	Outgoing longwave radiation and albedo at the TOA.
Fig. 4.6	Net heat flux at the ocean surface.
Fig. 4.7	Vertical overturning stream function in the ocean.
	2xCO_2
Fig. 4.8	Temperature response to a doubling of CO_2.
Fig. 4.9	Land surface air and mixed layer temperature responses.
Fig.4.10	Precipitation response.
	Scenario
	IPCC Scenarios A and D with CO_2-equivalent (1985-2084)
Fig.4.11	1990 IPCC Scenarios A and D of CO_2-equivalent concentration.
Fig.4.12	Time evolution of global surface air temperature.
Fig.4.13	Transient relative response of surface air temperature.
Fig.4.14	Time evolution of hemispheric surface air temperatures.
Fig.4.15	Latitudinal distribution of surface air temperature change.
Fig.4.16	Profiles of temperature change at the end of Scenario A.
Fig.4.17	Evolution of precipitation changes under Scenarios A and D.
Fig.4.18	Changes of the ocean circulation at the end of Scenario A.
Fig.4.19	Sea level rise at the end of Scenarios A and D.
	Scenario with greenhouse gases treated explicitly (1900-2100)
Fig.4.20	1990 IPCC Scenarios A and D of CO_2 concentration.
Fig.4.21	Evolution of the latitudinal response of surface air temperature.

4.2 Simulation of Present Climate

Before any climate model can be used for the simulation of future climate, it has to be able to reproduce present climate to a reasonably good approximation. Even if there is a belief that a small drift from the present climate is acceptable (how small this drift can be is not clear at all) because this bias will disappear when a climate change is assessed; a good simulation of the current climate is a necessary (but not a sufficient) condition for the correct simulation of climate change (Boer et al., 1992). If the simulation of the present climate is not satisfactory, it can mean that some processes are badly parameterized in a climate model or, even worse, that a process or a feedback is not described at all. Therefore, a considerable effort is devoted to render climate models capable of describing present climate and to an intercomparison of individual climate models among themselves (e.g. Boer et al., 1991; Gates, 1992). At the level of GCMs these intercomparisons usually comprise only the atmosphere, because the oceanic mixed layer temperature and the extent of sea ice are prescribed from present climatology. The atmosphere is then forced to adjust to these boundary conditions. In the case of fully coupled GCMs, such comprehensive intercomparisons do not yet exist because, up to now, there are only four fully coupled atmosphere-ocean GCMs available (see Section 4.3).

Initially we also tested the atmospheric component of the 2-D ZCM in a similar way. We used both a model version with prescribed mixed layer temperatures and a model version with a simple mixed layer model according to Lee and Snell (1977). However, what is more important is to demonstrate how the entire coupled model describes present climate, because this present climate state will then serve as the starting point for time-dependent runs during which greenhouse gas concentrations are increased. Therefore, we limit ourselves to the coupled atmosphere-ocean system when describing the simulation of present climate.

The coupled model is run in an asynchronous way for 1000 oceanic years after which the model climate is already very close to its equilibrium. The asynchronous integration - the atmospheric model is then run with a shorter time step than the oceanic model - is used for speeding up computations. The model is steered by the following greenhouse gas concentrations: 353 ppm CO_2, 1.72 ppm CH_4, 0.31 ppm N_2O, 280 ppt CFC-11 and 484 ppt

CFC-12, which correspond to the estimates for the year 1990 according to the IPCC (IPCC, 1990). The temperature distribution for both the atmosphere and the ocean is shown in Figure 4.1. Orography is not considered in the model and the model surface corresponds to the atmospheric pressure level of 1000 hPa. Therefore, especially in Antarctica, where the real surface pressure is about 700 hPa, an artificial atmospheric mass is treated in the model. It is a typical problem found in all meteorological or climate models which do not take orography into account.

The difference between simulated temperatures and observed values (estimates for the atmosphere are taken from Oort, 1983, and for the ocean from Levitus, 1982) is shown in Figure 4.2. Since Oort does not give the profiles for latitudes 85°S and 85°N (as initial values we use temperatures obtained by horizontal extrapolation), the differences in the atmosphere are shown only for the region from 75°S to 75°N. The present temperature distribution is simulated to a good approximation in the troposphere with the exception of the northern polar region, where the model is substantially cooler, while the remainder does not reveal a difference that exceeds 3 K. However, the difference between simulated and observed temperatures is substantially higher at the tropopause and in the lower stratosphere. This model behavior corresponds to many GCMs results (see, e.g., Boer et al., 1991). As concluded in Boer et al. (1991), the upper troposphere and lower stratosphere of high latitudes represent regions which are systematically cooler in GCM simulations in comparison with present climate with the difference exceeding 20 K in some models. It seems to indicate that even in GCMs, the parameterization of processes in the upper troposphere and lower stratosphere is not complete or not fully correct. If we take into account that there is no special attempt in our model to treat the stratosphere in a more sophisticated manner, this cool bias in the polar lower stratosphere is not surprising.

With respect to the simulation of the oceanic temperature field, the model successfully reproduces some important features, namely the shallowing of the main thermocline near the equator and its deepening in middle latitudes. The absolute difference between model and observed temperatures at the surface layer is, as for most of the ocean interior, less than 1 K. Only in regions of intensive downwelling in both hemispheres the model systematically overestimates the temperature by 1 to 3 K. It is likely that essentially two reasons are

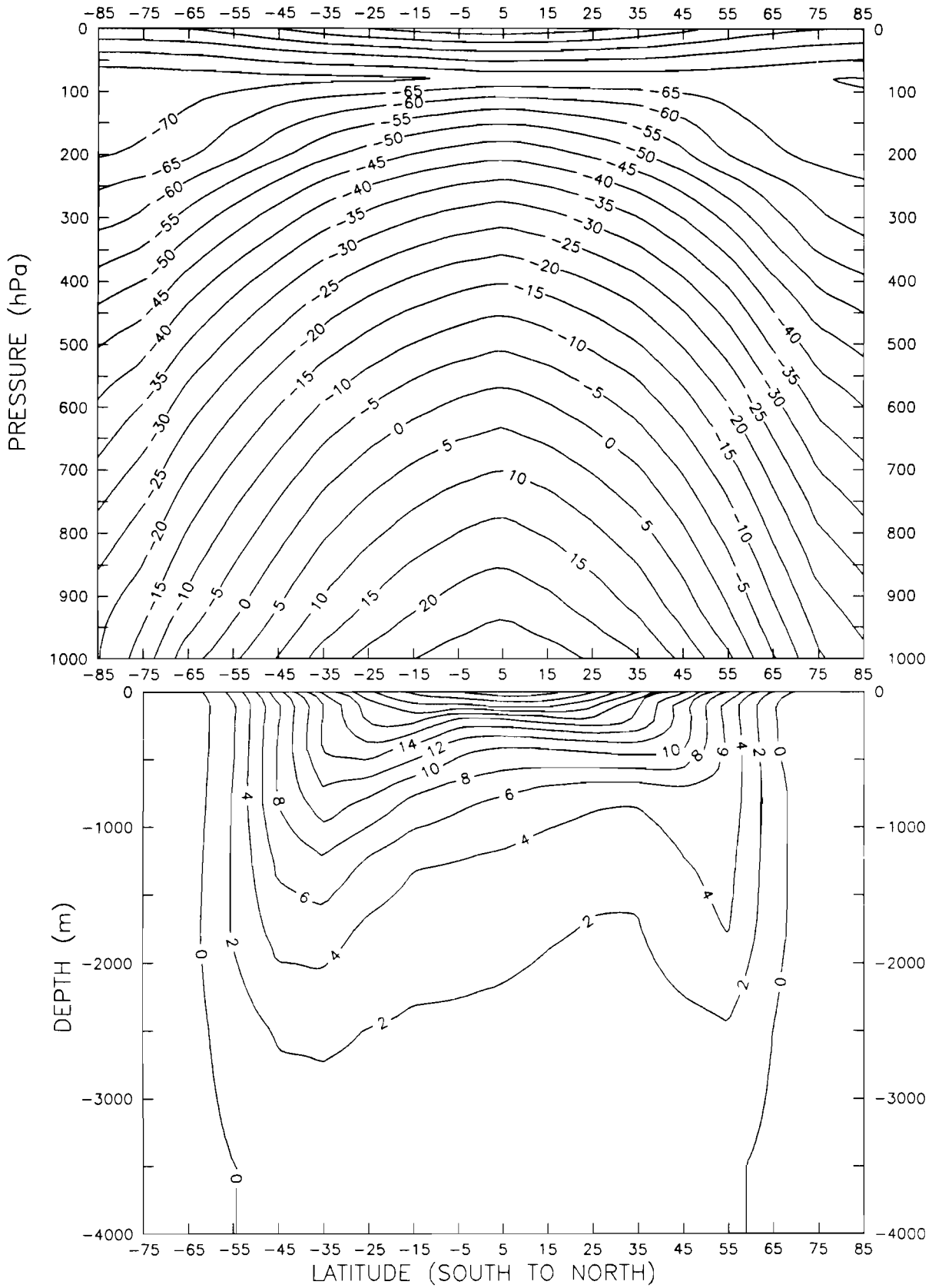

Figure 4.1. Temperature field for $1xCO_2$.

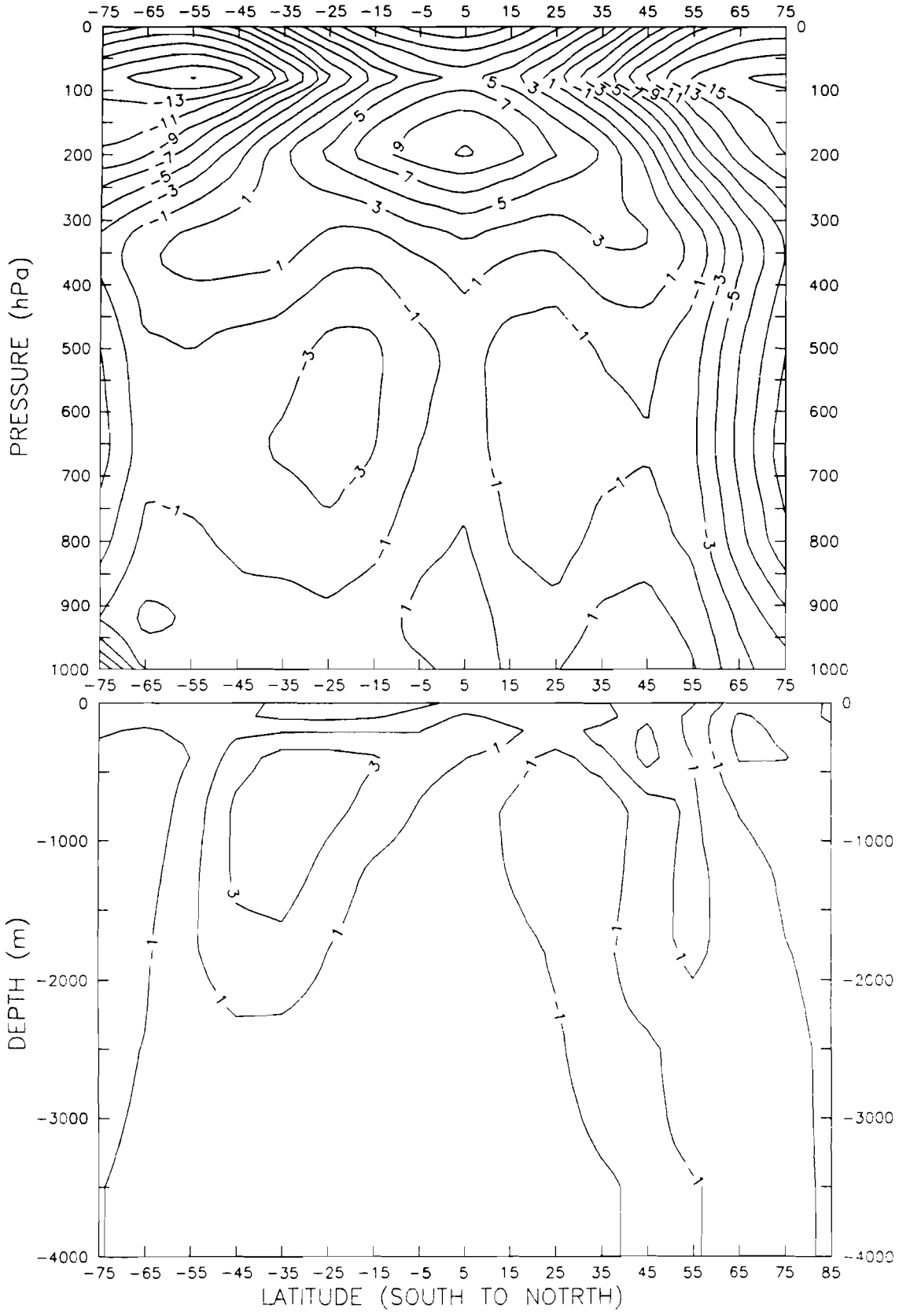

Figure 4.2. Difference between simulated and observed temperatures.

responsible for this model bias. The first one is the overestimated intensity of the vertical overturning in the model (see below) and, as a result, a more effective downward heat transport. The other reason, and maybe more important, is the fact that different oceans are combined into one basin. Indeed, the Atlantic ocean is warmer than the Pacific, especially in mid latitudes because of a more intensive meridional circulation. Our model is more similar to the Atlantic ocean in terms of vertical overturning, while the Pacific ocean has a significant impact on the zonal average temperature because of its larger areal extent.

In Figure 4.3, the surface variables connected with the hydrological cycle are shown, namely evaporation (above) and precipitation (below). Both rates (in mm/day) are compared with the estimates of Baumgartner and Reichel (1975) and Sellers (1965). Evaporation rates are slightly overestimated in the tropical region and agree well with Baumgartner and Reichel's data in middle and high latitudes. Concerning precipitation there is some overestimation in the tropics, probably connected with the overestimation of evaporation in this region. The slight underestimation in middle and high latitudes is caused by some underestimation of horizontal water vapor transport. In general, however, precipitation is computed, at least qualitatively, quite well. The globally averaged precipitation rate, which is equal to the globally averaged evaporation rate, is 2.82 mm/day which is slightly higher than the estimate of 2.73 mm/day given by Jaeger (1976). As far as the hemispherical distribution of precipitation and evaporation is concerned, the precipitation of the northern hemisphere exceeds the precipitation of the southern hemisphere and the opposite is true for evaporation. In the case of evaporation, the difference between both hemispheres is greater than in the case of precipitation. This hemispherical distribution corresponds to observations. In terms of percentages the calculated precipitation rate for the northern hemisphere is 1.8% higher than the global average (0.5% according to observations given by Sellers). The computed evaporation rate of the northern hemisphere, on the other hand, is 5% less than the global average (6% according to Sellers).

In Figure 4.4, the atmospheric (above) and oceanic (below) poleward heat transport in PtW ($1\text{PtW} = 10^{15}$ W) is compared with estimates based on observations. For the atmosphere the model results correspond quite well with the estimates given by Carissimo et al. (1985), even if the model maxima are somewhat lower in absolute terms. In the ocean the estimates are

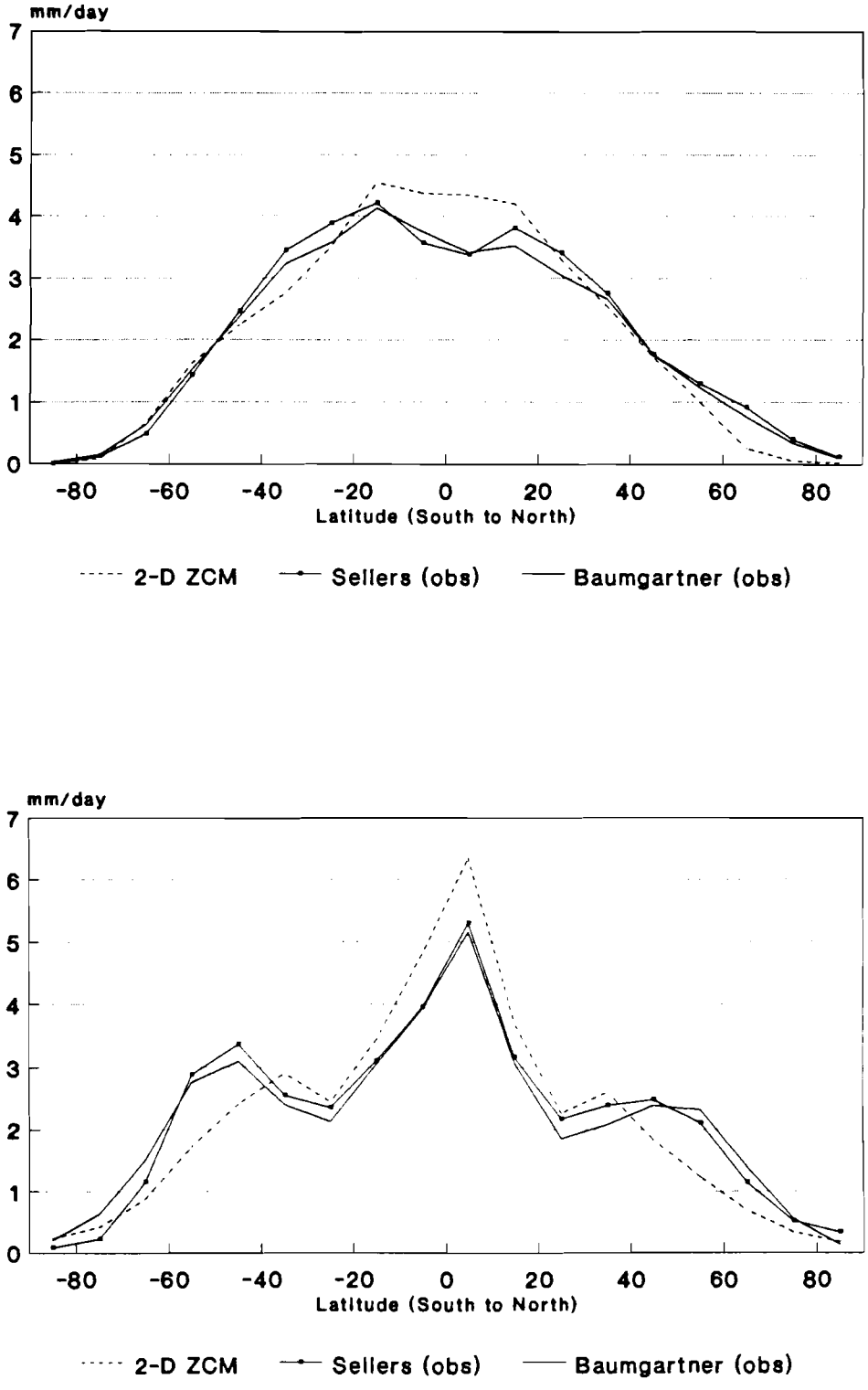

Figure 4.3. Evaporation rates (above) and precipitation rates (below).

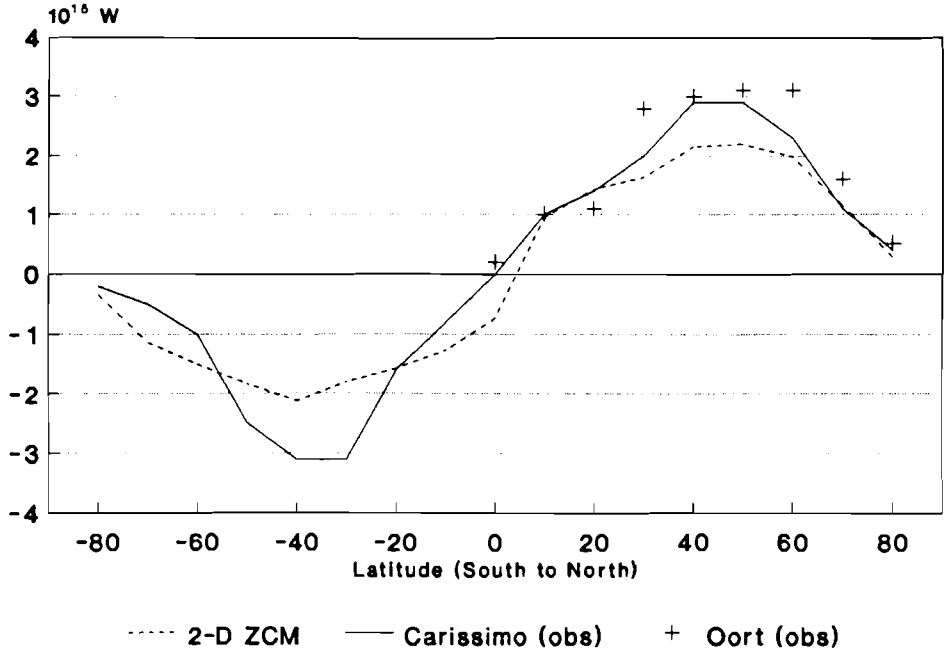

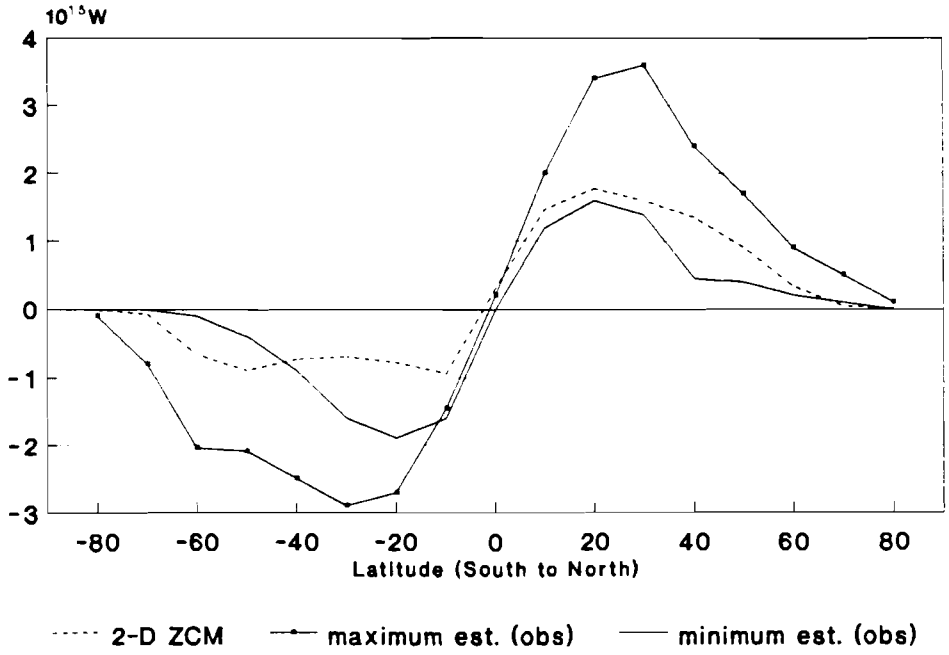

Figure 4.4. Atmospheric (above) and oceanic (below) meridional heat transport.

still highly uncertain, and there are significant systematical differences among different estimation methods. This uncertainty is reflected by a maximum and a minimum estimate of the meridional heat transport. The maximum estimate is derived from satellites measuring the outgoing longwave radiation (Carissimo et al.,1985; Trenberth, 1979), the minimum estimate from the surface heat flux estimations (Hsiung, 1985; Talley, 1984). It is worth mentioning that GCM results, as a rule, are closer to the minimum estimate rather than to the maximum one. Although the model seems to slightly underestimate the meridional heat transport in the southern hemisphere, in general our results lie in line with other models. This also holds for the northward heat transport through the equator (about 0.3 PtW).

An important variable which reflects the atmospheric thermal structure is the outgoing longwave radiation at the top of the atmosphere (TOA). This radiative flux (in W/m^2), positive upward, is shown in Figure 4.5 in comparison with observations of Smith and Smith (1987) and Ellis and Vonder Haar (1976). In the northern hemisphere the calculated flux agrees well with the observations. In the southern hemisphere the agreement is not as good. The calculated flux reveals an underestimation in mid latitudes and an overestimation in high latitudes. In the same figure the albedo of the system is compared with estimates of Ellis and Vonder Haar (1976) and Smith and Smith (1987). The model results agree well with the estimates in low and polar latitudes, whereas they show a pronounced underestimation in mid latitudes.

The net heat flux at the ocean surface in comparison with empirical data of Budyko (1974) and Esbensen and Kushnir (1981) is shown in Figure 4.6. The model reproduces the ocean heat uptake in the tropical region quite well and also the heat loss in the northern hemisphere. In the southern hemisphere the difference is more significant. However, one has to keep in mind that the accuracy in estimating heat fluxes in the southern hemisphere is still very low. More important is the fact that the model correctly reproduces the important hemispheric features. Indeed, the zone between 20°S and 50°S represents a transient zone indicating a weak heat exchange between ocean and atmosphere, contrary to the corresponding zone in the northern hemisphere.

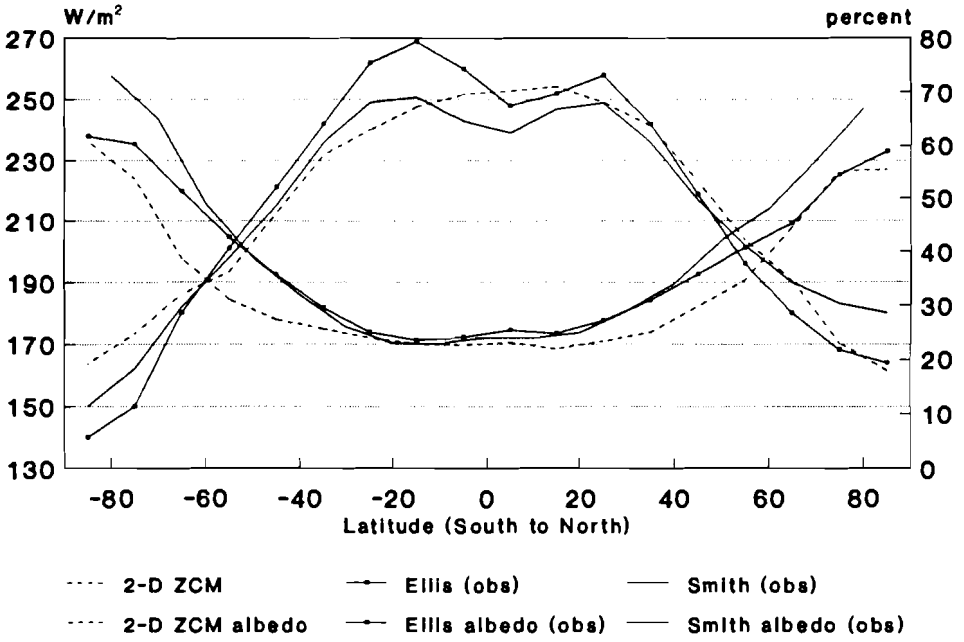

Figure 4.5. Outgoing longwave radiation and albedo at the top of the atmosphere.

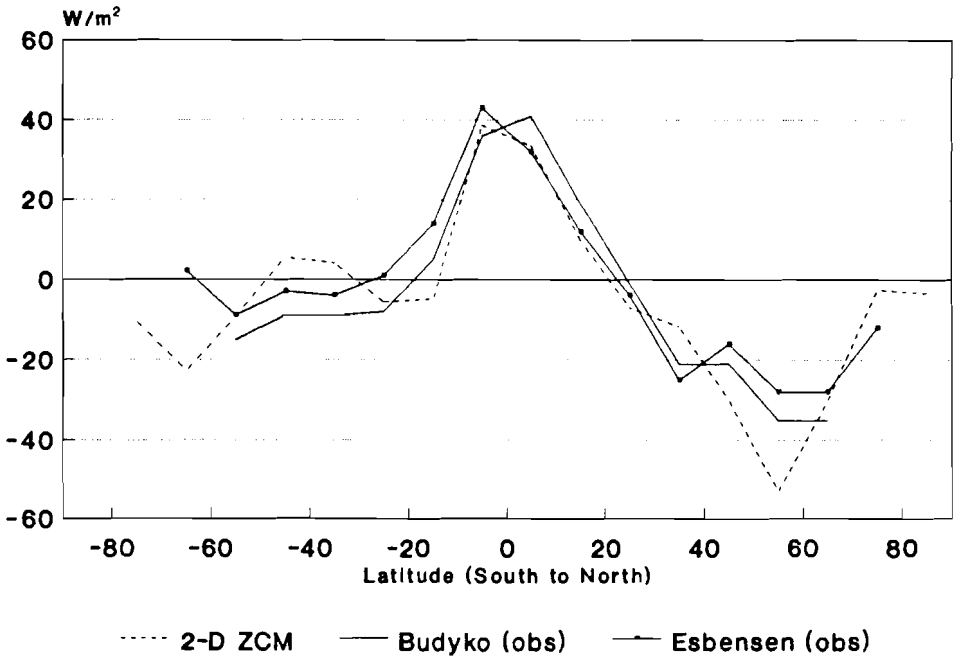

Figure 4.6. Net heat flux at the ocean surface.

As mentioned above, the vertical overturning is the major mechanism of meridional and vertical heat transport in the ocean. Since direct measurements of this characteristic are impossible, only a comparison with oceanic GCM results can be done. Figure 4.7 shows the vertical overturning stream function generated by the model in Sverdrups ($1Sv=10^6$ m^3/s). Obviously, there is a significant difference between the northern and southern hemisphere. In the northern hemisphere a gyre of vertical circulation is dominant with northward motion in the upper layer and southward recirculation below the main thermocline, while winddriven circulation gyres are relatively weakly pronounced. In the southern hemisphere winddriven circulation cells are much more intensive, while the baroclinic circulation is restricted by 40°S. The fact is connected with the absence of meridional boundaries in the Southern ocean, which are responsible for the vertical overturning. The intensity of deep water formation in the northern hemisphere is about 35 Sv which is greater than indirect estimates and GCM results (15-25 Sv). The more intensive overturning is necessary to compensate for the absence of nonzonal mechanisms of the meridional heat transport in the model.

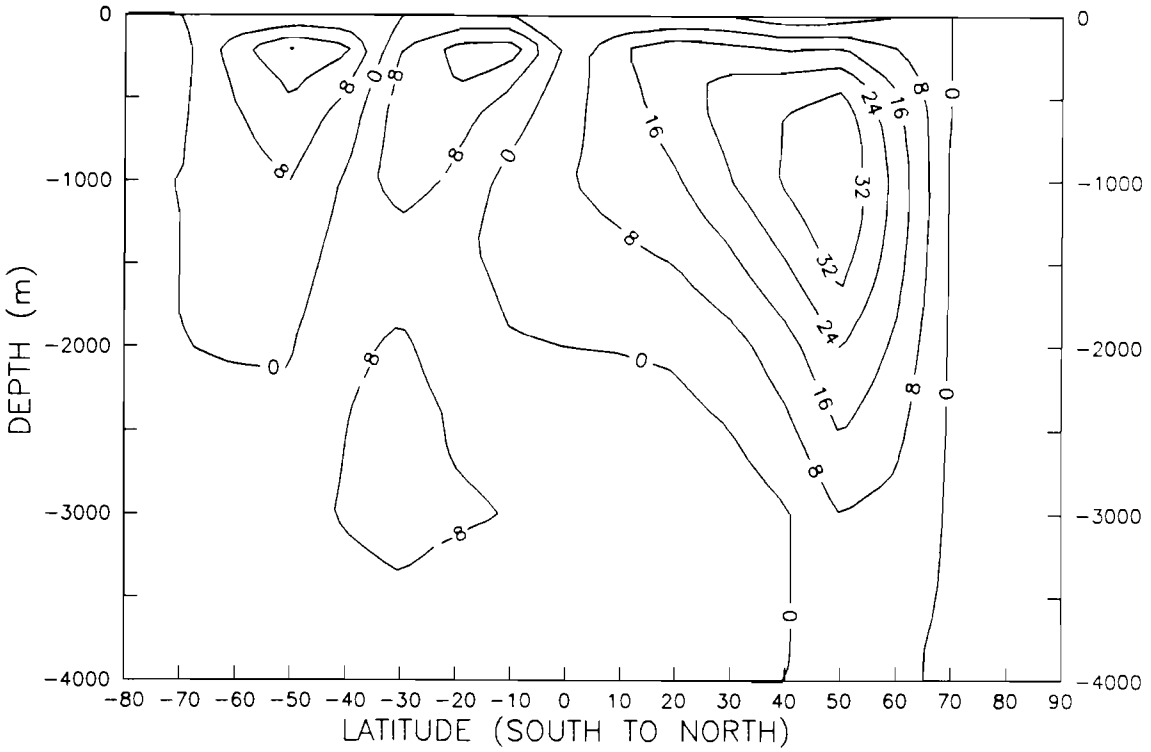

Figure 4.7. Vertical overturning stream function in Sv (1 Sv = 10^6 m^3 s^{-1}).

4.3 Equilibrium Response to a Doubling of CO_2

Equilibrium runs for a doubling of CO_2 have become a benchmark in climate change studies. An instantaneous and significant change in atmospheric CO_2 makes it easier to detect the response of the Earth's climate system to the prescribed forcing, as the response is expected to exceed the amplitude of the natural variability.

Many doubling experiments were made using sophisticated GCMs. In almost all cases these runs were made using a slab or a mixed layer ocean. In this case the computer time needed for the computation of a new equilibrium state can be vastly reduced. On the other hand, potential changes in the thermal structure and circulation of the ocean are not accounted for. The IPCC reports (1990, 1992) discuss the results of such runs in detail.

Recently the Geophysical Fluid Dynamics Laboratory (GFDL) in Princeton, USA (Manabe et al., 1990, 1991, 1992) carried out the doubling experiment using a 3-D ocean and both a synchronous (transient) and an asynchronous coupling to the atmosphere. In the latter case, in order to speed up the computations, the oceanic component was accelerated by a factor of approximately 150. As the 2-D ZCM also includes the deep ocean and a parameterization of the oceanic circulation, it is logical to compare our results with the results of the GFDL GCM.

In the CO_2 doubling experiment with the 2-D ZCM the concentrations of all greenhouse gases except for CO_2 are the same as for current climate. The CO_2 content is increased from 353 ppm to 706 ppm. The model was run for about 1000 oceanic years with the acceleration factor of 10 (the time step in the atmosphere is 3 days and 30 days in the ocean). It corresponds to 100 atmospheric years. The results at the end of the run are then compared with the initial state, i.e. the equilibrium for $1xCO_2$ (present climate).

a) Temperature response

The response of the climate system in terms of temperature to a doubling of CO_2, after the new equilibrium state has been reached, is shown in Figure 4.8. The global surface air

temperature change or climate sensitivity realized in the model is 1.84 K. This value lies in the lower range of the IPCC estimate: 1.5 - 4.5 K. Hemispherically the temperature increase is slightly higher for the northern hemisphere (1.94 K) than for the southern hemisphere (1.74 K). Except for latitudes poleward of 70° the temperature increase in the northern hemisphere exceeds the increase at the respective latitudes in the southern hemisphere. Near the poles the opposite is true and the maximum values are near the South Pole. Generally, for a given latitude the temperature increase reaches its maximum near the surface and then decreases with height up to the tropopause. Only for latitudes close to the equator the maximum temperature increase is realized in the lower troposphere.

GCMs usually predict that the maximum response descends from the upper troposphere at low latitudes to the surface level at high latitudes. Therefore, in comparison with GCMs results, the 2-D ZCM does not catch the secondary maximum near the equatorial tropopause. The reason for this drawback may be the highly simplified circulation in the tropics. In the stratosphere, the cooling is distributed rather evenly and varies between 3.6 K and 4.3 K (not shown in the figure).

The distribution of the warming signal in the ocean is characterized by vertical uniformity. The temperature change increases from 1 K near the equator to 2 K in the subpolar region of the northern hemisphere and to 1.5 K in the southern hemisphere. In high northern latitudes the temperature increase is much smaller. The main reason is that salinity effects are not taken into consideration in the present version of the ocean model. As a result, deep convection develops in the entire Arctic region, impeding ocean warming. In reality, low salinity in the upper ocean layer in high northern latitudes suppresses convection and permits subpolar water masses to warm and penetrate poleward into regions beneath the Arctic upper layer. With this exception our results are qualitatively very similar to those of the GFDL GCM (Manabe et al., 1990) for the same CO_2 doubling experiment.

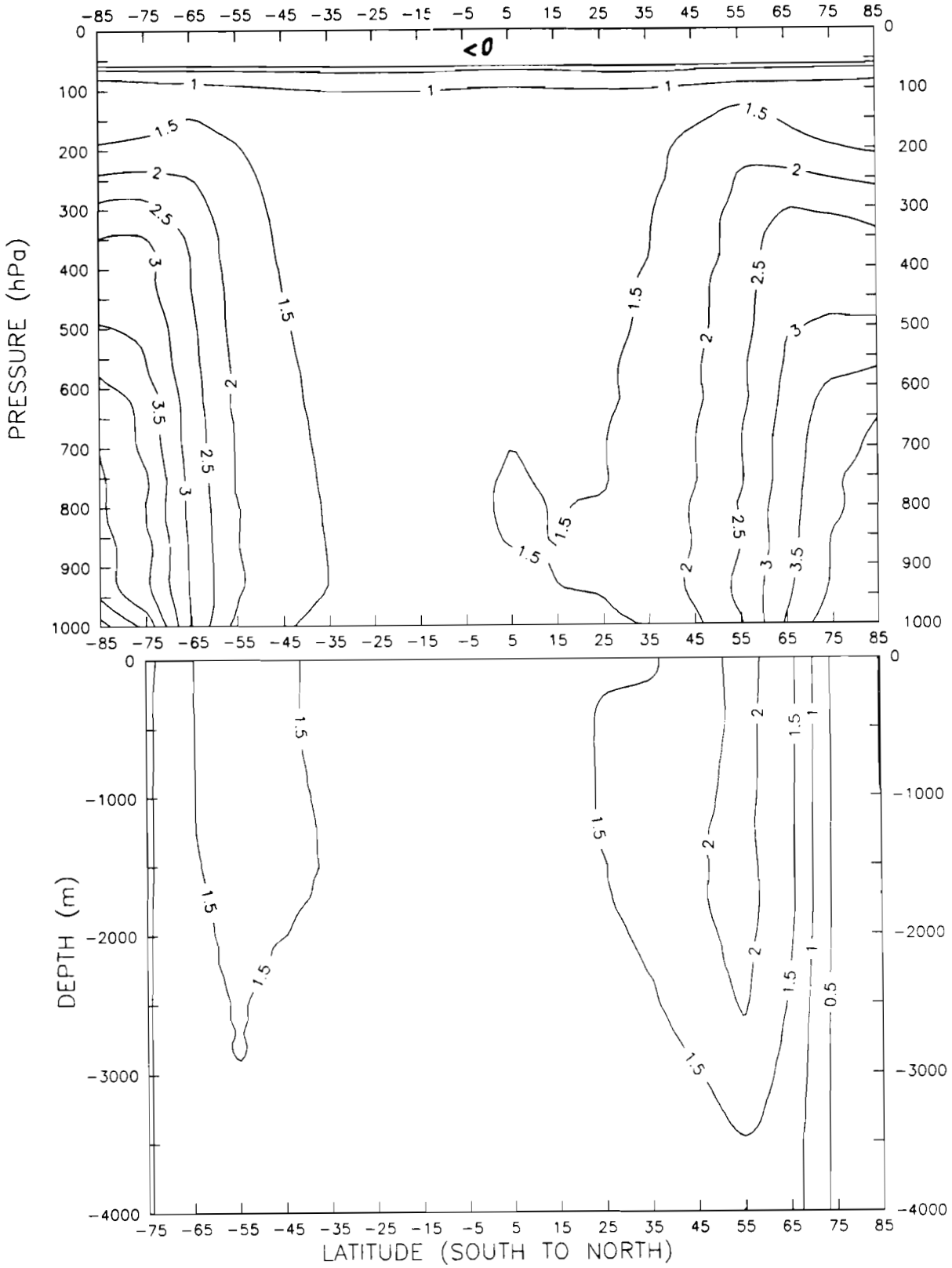

Figure 4.8. Temperature response to a doubling of CO_2.

Figure 4.9 shows the latitudinal distribution of both the change of surface air temperature over continents and the change of the oceanic mixed layer temperature. The temperature change over continents is lowest in the tropics and increases poleward with the polar maximum of the southern hemisphere being slightly higher than that of the northern. Temperature changes in the oceanic mixed layer are lower than over continents. Also shown in the figure are temperature changes over continents for the GFDL model. The GFDL model reveals temperature changes that are similar to the ZCM, but the changes are greater in the GFDL model due its greater climate sensitivity of 4 K compared to 1.8 K for the ZCM.

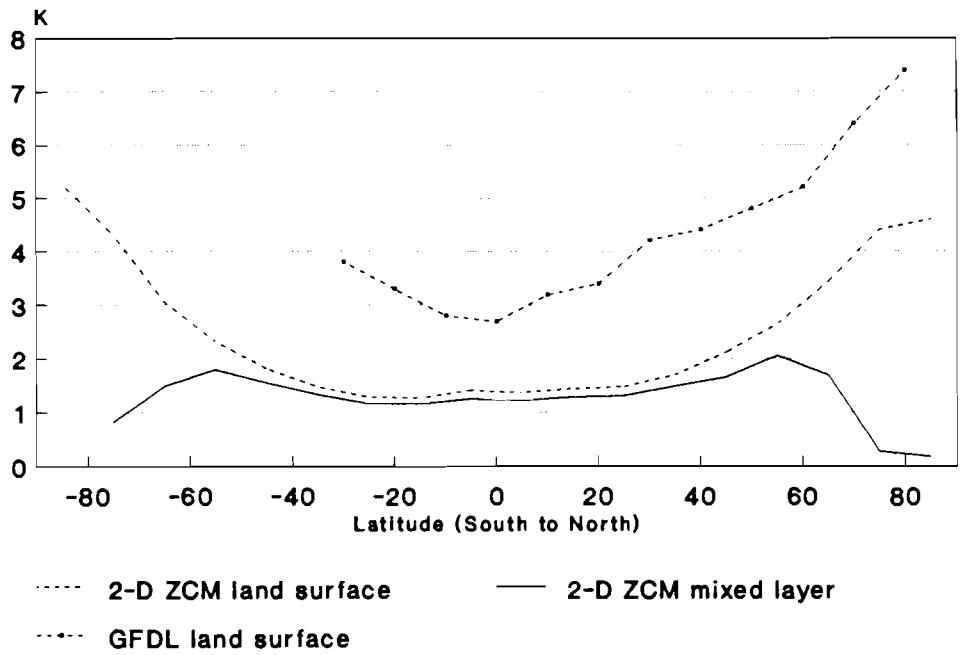

Figure 4.9. Surface air above land and mixed layer temperatures response to a doubling of CO_2.

b) Precipitation response

The change of the precipitation rate is shown in Figure 4.10. It reveals a strong latitudinal dependence for three models presented: the ZCM and the GCMs of the GFDL and of the Max-Planck-Institute (MPI) for Meteorology in Hamburg, Germany. The maximum change for all three models occurs near 65°S. Local maxima are near the equator and in mid northern latitudes. The minima are located at the boundaries of the Hadley cell. The differences in the magnitude of changes can be explained by the differences in the global precipitation increase which is highest for the GFDL GCM (8%) and lower for the other models (5.8% for the MPI GCM and 5% for the ZCM). The considerable differences between the GFDL and MPI results indicate the uncertainty associated with the assessment of precipitation changes on both global and latitudinal (regional) scales. According to the IPCC (1990), the estimations of the globally averaged precipitation response based on GCMs vary from 3% to 15%.

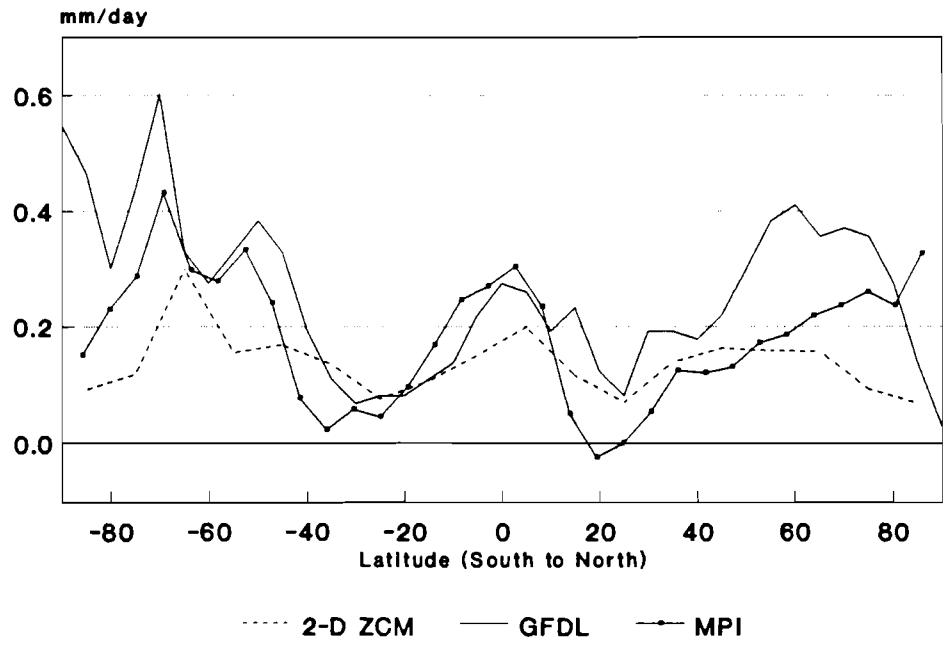

Figure 4.10. Precipitation response to a doubling of CO_2.

4.4 Time-dependent Experiments

The idea of integrated modelling of climate change is to analyze various policy-oriented scenarios beginning with calculating emissions and concentrations of greenhouse gases, after that the resulting climate change and, finally, environmental and socio-economic impacts. For this purpose, coupled atmosphere-ocean climate models, which are run in a synchronous way and take the huge thermal capacity of the oceans into account, are necessary. Only such climate models are capable of simulating the delay of the climate response to an increasing radiative forcing and the redistribution of heat by the oceanic circulation, and thus potential changes of the Earth's climate. Up to date, there is only a very limited number of scenarios available computed by the following four coupled GCMs: GFDL, MPI, NCAR (National Center for Atmospheric Research, Boulder, USA) and UKMO (the Hadley Centre of the United Kingdom Meteorological Office, UK). Due to this fact, it is not yet possible to make a consistent comparison of these results. At the same time, the time-dependent runs of the coupled GCMs are partly connected with severe problems as, for example, the so-called cold start problem and the application of a flux correction, which does not allow the coupled system to significantly drift away from real climate. However, because of the major effort devoted to the development of coupled GCMs, further improvements and updated scenarios are to be expected.

a) Time-dependent experiments based on a CO_2-equivalent concentration scenarios (1985-2084)

In this part we describe the results of the coupled 2-D ZCM, when atmospheric and oceanic components are integrated in a synchronous way using a scenario of increasing CO_2-equivalent concentrations. Even if the radiation code of the 2-D ZCM allows to treat greenhouse gases individually as described in Chapter 3, we use here only CO_2-equivalent concentrations to be able to compare our results with recently published results of the MPI GCM (Cubasch et al., 1992). We also employed the 1990 IPCC Scenarios of CO_2-equivalent concentration A and D, which MPI kindly provided us with. These scenarios, starting in 1985 and extending to one hundred years, are shown in Figure 4.11. They were used for the time-dependent runs described below.

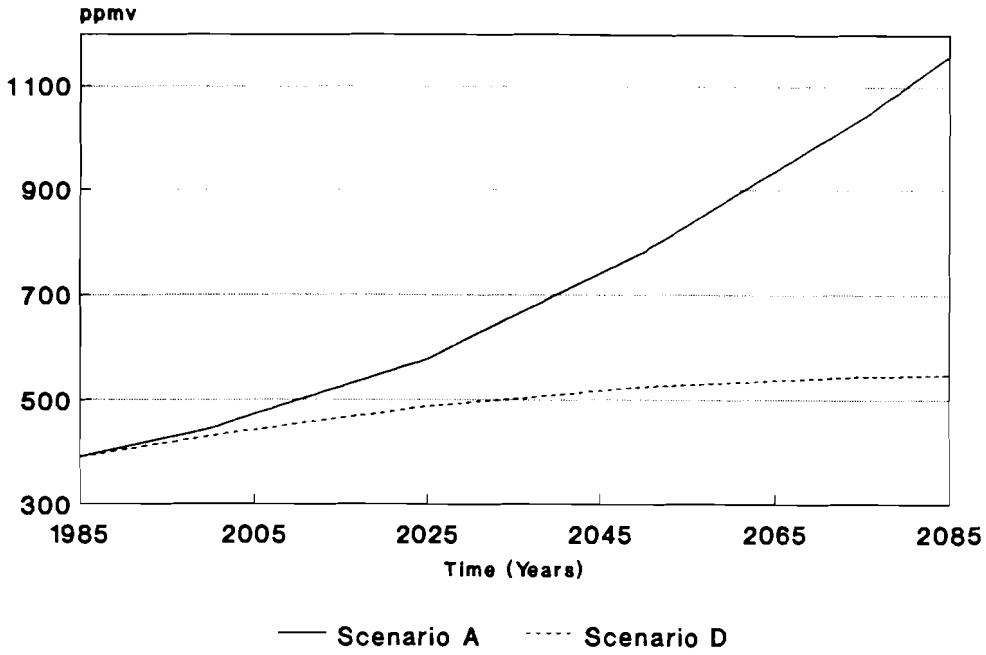

Figure 4.11. 1990 IPCC Scenarios A and D of CO_2-equivalent concentration.

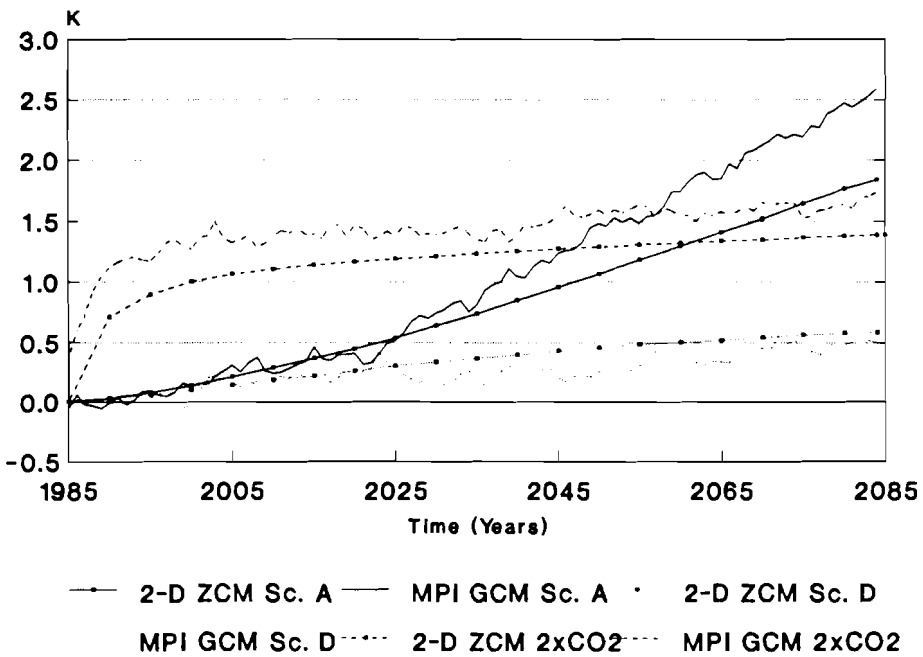

Figure 4.12. Time evolution of global surface air temperature.

Figure 4.12 shows the time evolution of the globally averaged surface air temperature for Scenarios A and D and, also, for the transient experiment, i.e. an instantaneous doubling of the initial CO_2-equivalent concentration. The experiments were carried out in the following way: for a CO_2-equivalent concentration corresponding to the year 1985 the model was initially run for 1000 oceanic years in an asynchronous fashion. The run was then continued for 10 years in a synchronous fashion (with a time-step of three days for the atmosphere and the ocean). Then the three different options mentioned above were used for a 100 year integration up to the year 2084. To be sure that there was no drift from the initial state corresponding to the year 1985, the control run was continued for 1985 conditions as well. The model temperatures did not change within a precision of 0.01 K.

In case of the transient experiment, the temperature change increases very fast during the first years, and then it increases much more slowly but monotonously. As mentioned above, the equilibrium response of the 2-D ZCM to a CO_2 doubling is 1.84 K. The shape of the curve is in agreement with the time evolution of the globally averaged surface air temperature change of the MPI GCM. Because of the higher climate sensitivity of the MPI model (about 2.6 K), the response of the MPI model is slightly higher despite of the fact that the CO_2-equivalent concentration was not really doubled in the MPI transient experiment (only 720 ppm instead of 756 ppm). Comparing the corresponding temperature curves for Scenario A, we can see that after approximately the first 40 years (cold start problem) the curve of the MPI GCM becomes steeper, again due to the greater climate sensitivity of the MPI model. In case of Scenario D, which reveals a very weak temperature signal, the differences between both models are quite small.

In Figure 4.13 the transient run is investigated in more depth by means of a transient response R defined by (see, e.g., Peng et al., 1987):

$$R(\varphi,t) = \frac{T_S(\varphi,t)-T_S(\varphi,0)}{T_S(\varphi,\infty)-T_S(\varphi,0)} \quad . \tag{4.1}$$

The transient response indicates how quickly the zonal surface air temperature T_S approaches equilibrium. One can see that the transient response rapidly increases during the first years after perturbation, but then slows down. If we compare both hemispheres, it is evident that the northern hemisphere as a whole approaches the equilibrium warming faster than the southern hemisphere, due to the greater extent of continents. As in the case of the 2-D Multilayer Energy Balance Model of Peng et al. (1987), there are two local minima of the transient response: in the polar region of the northern hemisphere and around 50° to 75°S, which are the regions of strong albedo feedback, large ocean cover and descending surface water masses. However, the minima in the southern hemisphere in our case are substantially lower than in the case of Peng et al., which seems to be more realistic taking into account the great extent of oceans in this region and the delay of the climate reaction due to the oceanic thermal capacity.

The transient reaction, which reflects an instantaneous doubling of CO_2-equivalent concentration - although important for our understanding of the behavior of the climate system - is still far from reality. In the following, we deal with the reaction of the ZCM to scenarios of increasing CO_2-equivalent as shown in Figure 4.11. In Figure 4.14, the time evolution of the globally and hemispherically averaged surface air temperature is shown using Scenario A. The northern hemisphere evidently warms faster, by about 0.3 K compared to the global mean at the end of the run. The huge thermal capacity of the oceans is again the reason for this effect: 81% of the southern hemisphere is covered by ocean, while this fraction in the northern hemisphere is only about 61%.

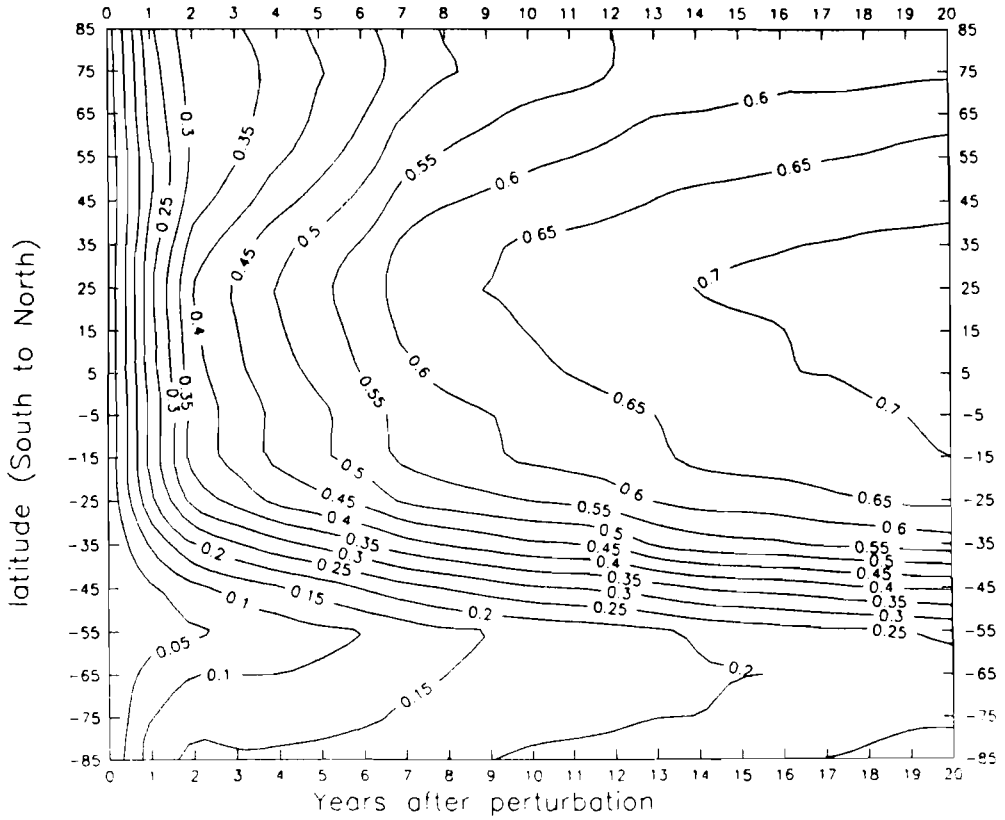

Figure 4.13. Transient relative response of surface air temperature.

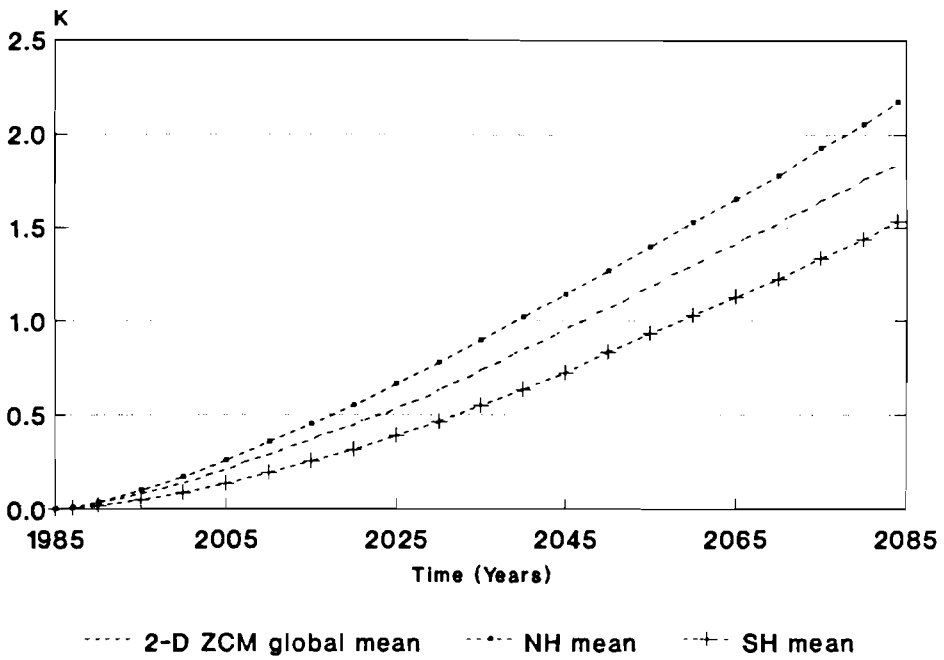

Figure 4.14. Time evolution of hemispheric air temperatures.

In Figure 4.15, the latitudinal distribution of surface air temperature change for Scenarios A (above) and D (below) is shown. The y-axis gives the cumulative change (in K) with respect to the starting year 1985. The background shading indicates the speed of change (K/10y). Three time cuts are shown for the years 2005, 2045 and 2085. In case of Scenario A, the speed of change in high latitudes exceeds 0.4K/10y at the end of the run with no tendency of a stand-still or a decrease. In case of Scenario D, the values are substantially smaller and the maximum does not exceed 0.2K/10y. These values are, of course, connected with the climate sensitivity of the model, which is in the lower part of the IPCC range (see Section 4.2). At the end of the Scenario D, the speed of change does not increase any more and reveals a decreasing tendency. In both scenarios the changes are higher in the northern hemisphere than in the southern, especially near the poles. It shows a lower sensitivity of the Antarctica region in the time-dependent runs.

Profiles of temperature change in the atmosphere (above) and in the ocean (below) at the end of Scenario A are shown in Figure 4.16. In comparison with the equilibrium field (Fig. 4.8), two features can be mentioned with respect to the response of the atmosphere. Firstly, the different behavior between both hemispheres is more pronounced in Scenario A than for the equilibrium response. Secondly, the response of the South Polar region is much less in Scenario A than for the equilibrium response. This indicates that the southern hemisphere as a whole, and the South pole in particular, react with a long response time. As in the case of the equilibrium response, we miss the local maximum of warming beneath the equatorial tropopause due to an oversimplified Hadley circulation.

The distribution of temperature change in the ocean at the end of Scenario A is characterized by two pronounced tongues of positive anomalies, associated with downwelling regions. The penetration depth of the temperature anomalies (see Manabe et al., 1991), which is determined by

$$D_{pen} = \left(\int_0^{H_b} \Delta T \, z \, dz\right) / \left(\int_0^{H_b} \Delta T \, dz\right) , \qquad (4.2)$$

exceeds 1500 m in the subpolar regions. This depth is only about 500 m in the tropical region where upwelling takes place. The positive temperature anomaly is approximately twice

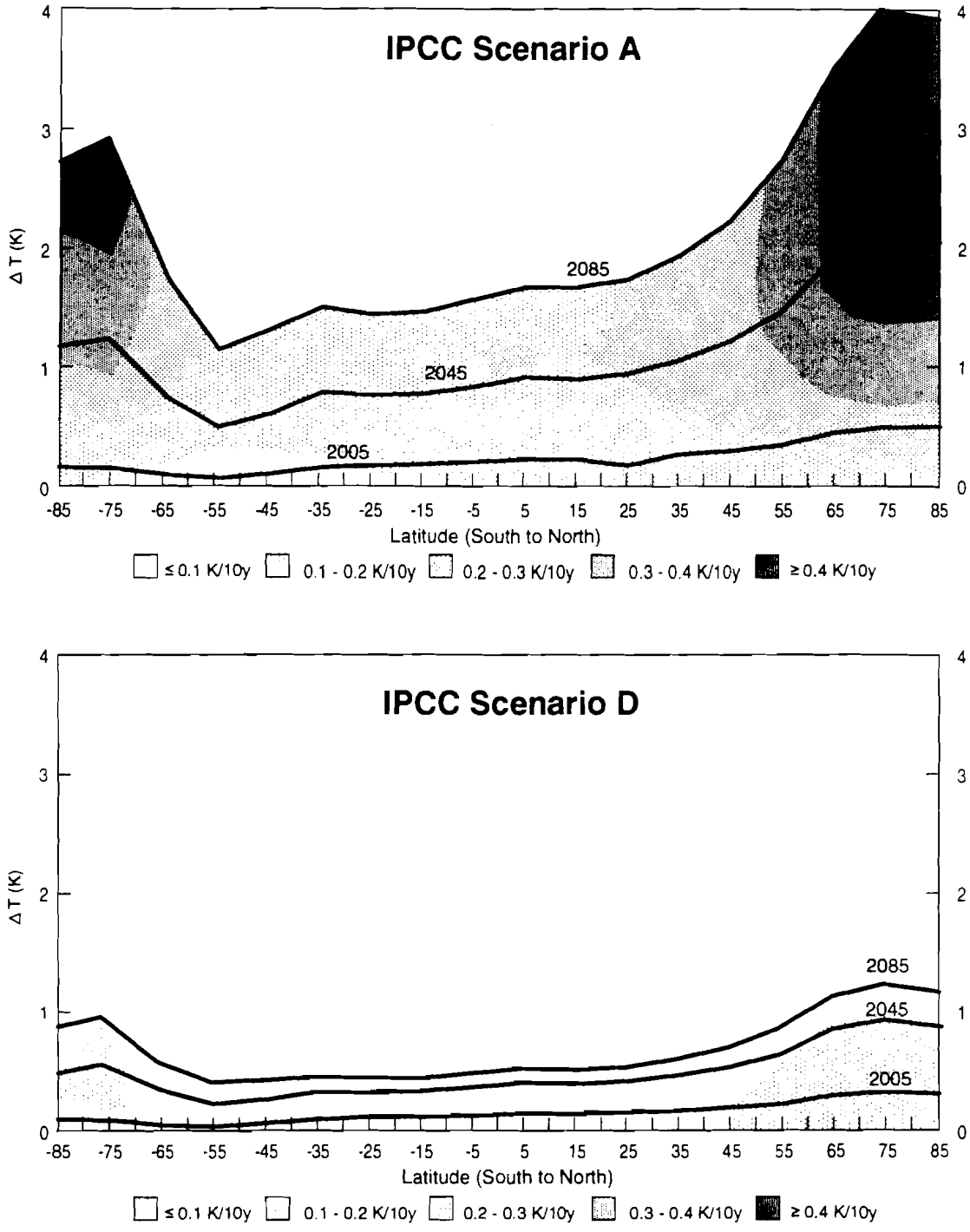

Figure 4.15. Latitudinal distribution of surface air temperature change. The y-axis is the cumulative change while the shading indicates the speed of change per decade.

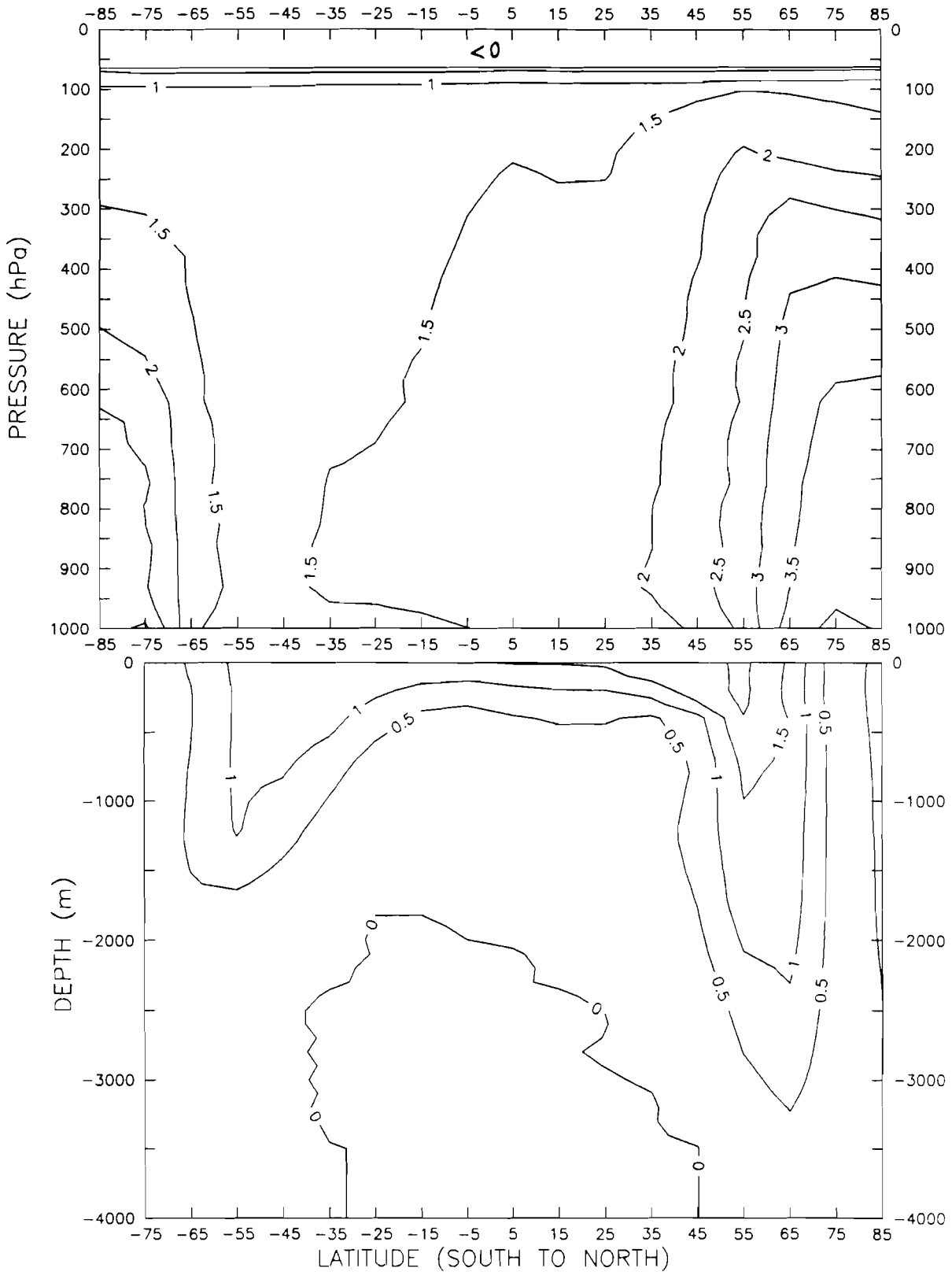

Figure 4.16. Vertical profiles of temperature change at the end of Scenario A.

as great in the northern hemisphere than in the southern hemisphere, which is a typical feature of all models with a realistic distribution of ocean/land fractions. Comparison of our results with Manabe et al. (1991) and Cubasch et al. (1992) shows that the anomaly pattern in our model for the northern hemisphere is more similar to the GCM results of the North Atlantic, while for the southern hemisphere our anomaly pattern is closer to GCM results of the Pacific. As a consequence our results are qualitatively similar to GCM results when zonally averaged, but their anomalies are characterized by a greater rate of downward propagation. In the tropical deep ocean the negative anomaly (but very small in absolute terms) is located. It is connected with the global decay of vertical overturning (see below). The presence of this negative anomaly is typical for many GCM results. For Scenario D (not shown) the results are qualitatively very similar with the absolute values about three times smaller.

In Figure 4.17, the time evolution of the precipitation rate changes with respect to the equilibrium in the year 1985 is shown for Scenarios A and D. The three time cuts again correspond to the years 2005, 2045 and 2085. In case of Scenario D, the changes are much smaller than for Scenario A, but the distribution of local minima and maxima is the same in both scenarios. In comparison with the equilibrium response (Fig. 4.10), the absolute maximum of precipitation change in the latitude belt 60°-70°S is now missing (only a slight local maximum can be seen in Fig. 4.17). This is in agreement with the conclusion drawn with respect to temperature changes, namely that the response of high southern latitudes is very slow in time. On the contrary, the location of local maxima in the equatorial region and in mid northern latitudes agrees well with the location as given by the equilibrium response.

As result of decreasing temperature differences between the equator and the subpolar regions the meridional pressure gradient decreases and the vertical overturning decays (Figure 4.18). The most pronounced decrease of vertical overturning takes place in the northern hemisphere and reaches 10% at the end of Scenario A. This result is qualitatively very similar to the GFDL and MPI GCMs but the last two models demonstrate a more significant decrease of the vertical overturning (up to 30%) for the same time period and a similar forcing. To account for this fact it is necessary to take into consideration that our model does not include two additional mechanisms that are responsible for the change of circulation, namely, the

change in zonal wind stress and salinity. The analysis of GCM results demonstrates that both processes lead to an additional decrease of the vertical overturning. The inclusion of salinity could especially be important in connection with the recently discussed problem of instability of the thermohaline circulation and with the existence of a set of different stable and metastable climate regimes (Bryan, 1986; Marotzke and Willebrand, 1991).

As for the CO_2-equivalent doubling experiment, the change of meridional heat flux in the ocean is very small for Scenario A (a few percent). A careful analysis of the components of the meridional heat transport shows that the small decrease of the horizontal diffusive heat flux is compensated by the increase of the advective heat transport. It may seem that this is in contradiction with the above described decrease of the vertical overturning. But proper allowance must be made for the increase of temperature between surface and bottom layers. The horizontal advective heat transport can be easily estimated by

$$F_{adv}(\varphi) = \int_0^{H_b} \frac{\partial \Psi}{\partial z} T(z)\, dz \approx \Psi_{\max}(\varphi)\, (T_{\max} - T_{\min}) , \qquad (4.3)$$

where T_{max} is the surface ocean layer temperature and T_{min} the temperature of the bottom ocean layer. Since the bottom temperature does not change significantly during a century, the vertical temperature difference increases. The sign of the change of advective heat transport depends on the relation between the change of the intensity of vertical overturning and the change of the vertical temperature difference. In our case the increase of the vertical temperature difference is slightly greater than the decrease of the intensity of vertical overturning in relative terms. As the result, the advective heat transport increases. In case of a more significant decay of overturning, the entire meridional heat transport will decrease as it takes place in the GFDL experiment (Manabe et. al, 1991).

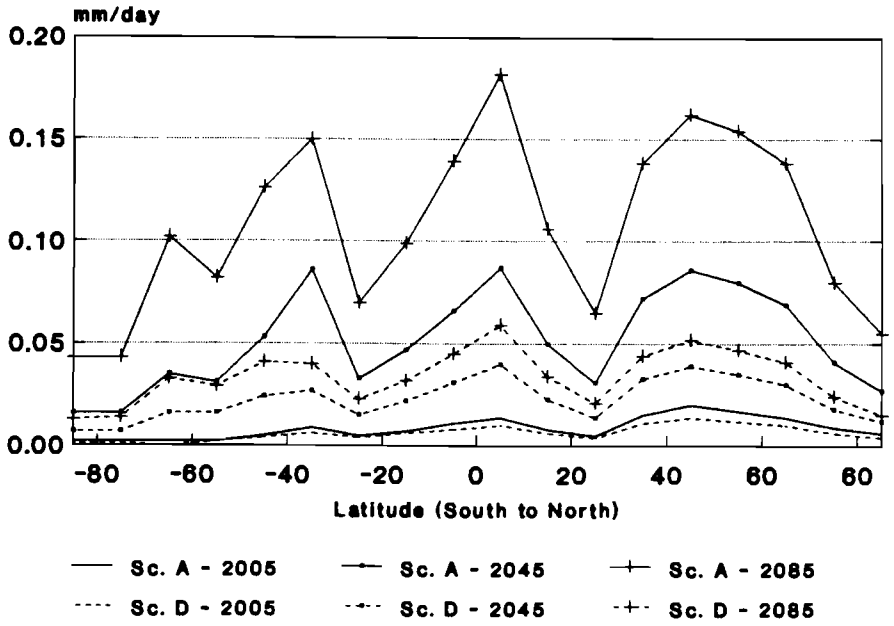

Figure 4.17. Time evolution of precipitation change under Scenarios A and D.

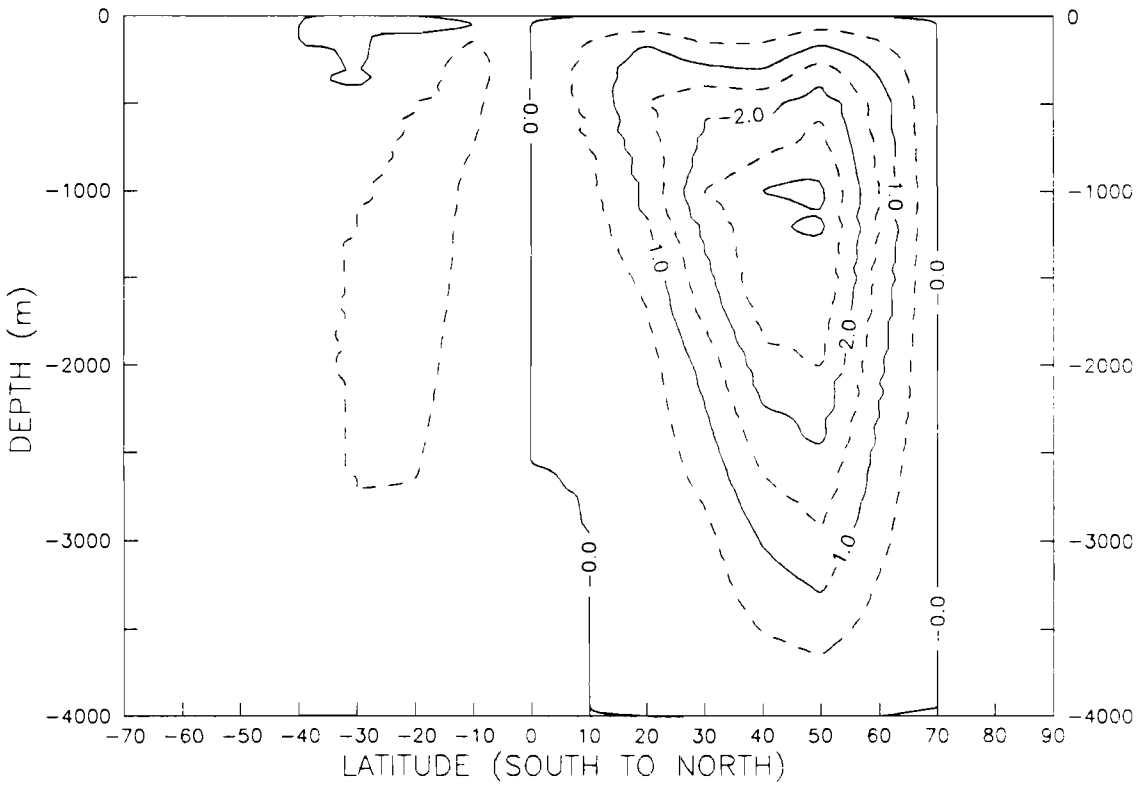

Figure 4.18. Change of the vertical overturning in the ocean at the end of Scenario A in Sv (1 Sv = 10^6 m^3 s^{-1}).

Figure 4.19 demonstrates one of the consequences of global warming, namely sea level rise. There are several factors which contribute to sea level rise, but the thermal expansion of the oceans is the most important one. It strongly depends on the geographical location. In the figure the latitudinal contributions to the global sea level rise due to thermal expansion are shown at the end of the 100 year runs according to Scenarios A and D. It is not surprising that the thermal expansion is maximal in the downwelling region where the oceanic warming penetrates much deeper in comparison with other regions. The globally averaged values of sea level rise are 0.24 m for Scenario A and 0.08 m for Scenario D. These values are only slightly higher than the corresponding values computed by the MPI GCM (0.15 m for Scenario A and 0.05 m for Scenario D, respectively) (Cubasch et al., 1992). However, there is still a great uncertainty in these estimates; the MPI GCM results are approximately 50% lower than the values referred to by the IPCC (1990).

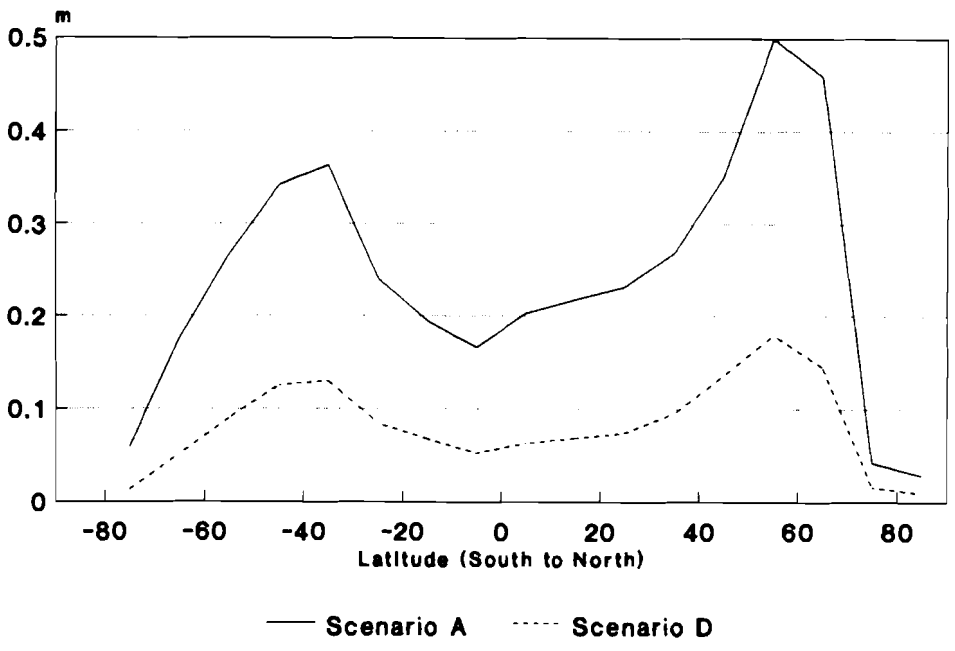

Figure 4.19. Sea level rise due to thermal expansion at the end of Scenarios A and D.

b) A time-dependent experiment based on scenarios of individual greenhouse gases (1900 - 2100)

The radiative code of the model also allows to force the ZCM by a scenario, in which the most important greenhouse gases are taken into account explicitly. In the experiment presented below, a time-dependent run was performed, starting from equilibrium corresponding to the year 1900 and ending in 2100. The model was steered with time-dependent concentrations of CO_2, N_2O, CH_4, CFC-11 and CFC-12 according to 1990 IPCC Scenario A (Business-As-Usual; as generated by IMAGE 1.0). As an example, the concentrations of CO_2 for Scenarios A and D are shown in Figure 4.20. For the other greenhouse gases we give only the initial (referring to 1900) and final values (referring to 2100) used in Scenario A: 0.9 ppm and 5.5 ppm for CH_4, 280 ppb and 406 ppb for N_2O, 0 ppt and 640 ppt for CFC 11, 0 ppt and 1400 ppt for CFC 12. The concentration of ozone remained the same during the whole experiment, corresponding approximately to the year 1990.

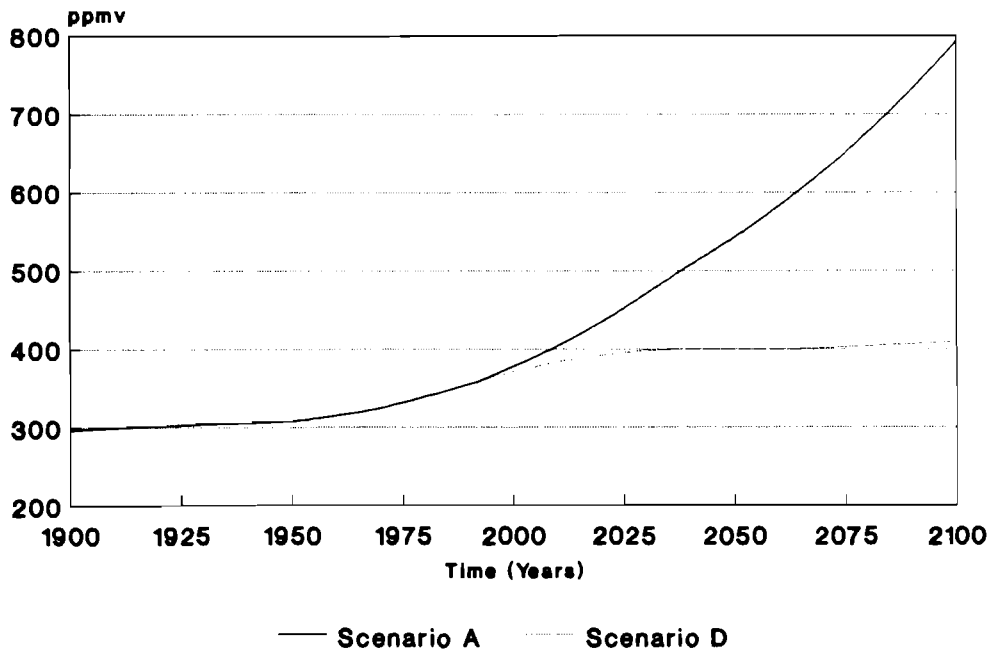

Figure 4.20. 1990 IPCC Scenarios A and D of CO_2 concentration as generated by IMAGE 1.0.

An advantage of such a run starting in the past is that the behavior of the climate model can be validated against climatological records. According to the IPCC (1990), the global mean surface air temperature has increased by 0.3 to 0.6 K over the last 100 years. The ZCM gives 0.4 K for the period 1900 to 1990, which agrees well with the given range.

With respect to estimates of future global warming, the average rate of increase of the global mean temperature during the next century is estimated to be about 0.3 K per decade (with an uncertainty range of 0.2 K to 0.5 K) (IPCC, 1990). The ZCM gives about 0.2 K per decade, which is at the lower limit of the IPCC estimate. It is directly connected with the climate sensitivity of the model (about 1.8 K) which is close to the lower limit of the range estimated by the IPCC.

With respect to this 200 model year run we present only Figure 4.21, which shows the ratio of latitudinal change of surface air temperature to global temperature change versus time. The areas with the ratio greater (less) than one indicate the regions which warm faster (slower) than the globe on the average. In case of the northern hemisphere, the maximal ratio is near the pole and the ratio decreases towards low latitudes. Another interesting feature is that the ratio remains more or less constant during the 200 year simulation. In case of the southern hemisphere, there is a well pronounced minimum between mid and higher latitudes connected with the large ocean extent in this region. Near the South Pole, the ratio increases slowly with time. It supports the conclusion drawn in previous sections that the warming in this region is relatively slow.

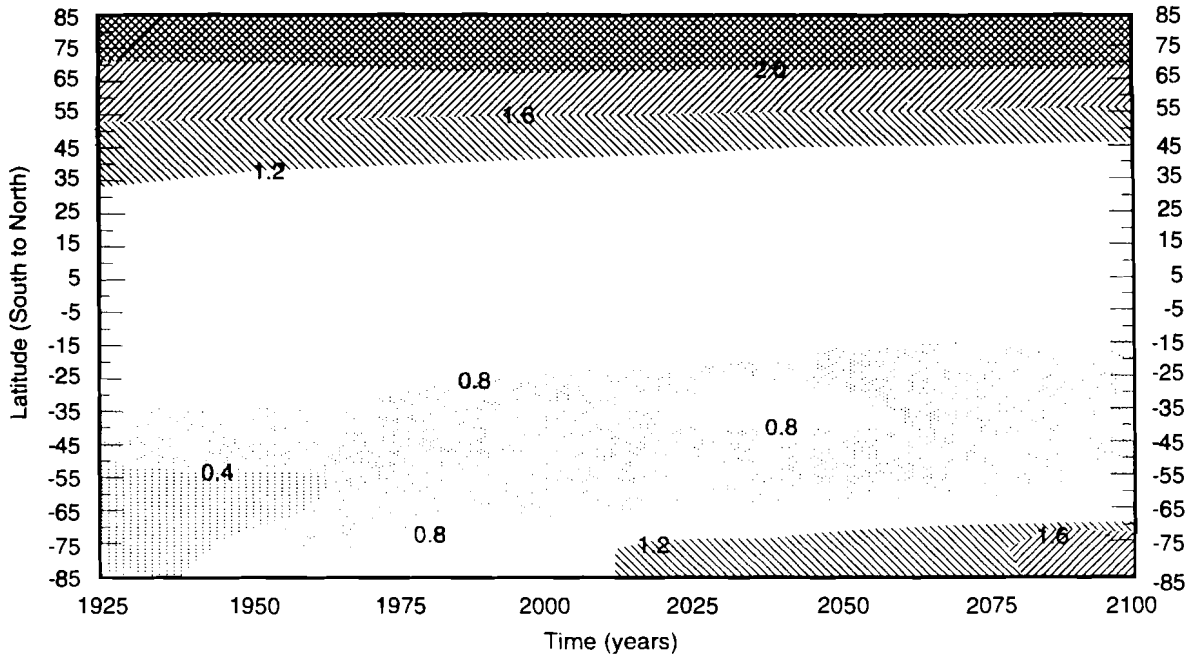

Figure 4.21. Time evolution of the latitudinal response of the surface air temperature.

5. INTEGRATED ASSESSMENT OF CLIMATE CHANGE IMPACTS ON EUROPEAN FORESTS (ICCF) - A PROJECTED APPLICATION TO INTEGRATED MODELLING OF CLIMATE CHANGE IMPACTS

5.1 Description of the Study

The initialization of a study with the above title was the outcome of a 1992 Working Meeting[1] at IIASA. The overall objective of the Study is to carry out an integrated assessment of the impacts of climate change on the European forests for a variety of greenhouse gas emission scenarios. The Study has the following sub-objectives:

- to assess ecophysiological impacts of forests on yields and carbon sequestering due to climate change;
- to identify optimal forest policies for efficient carbon sequestering;
- to assess the overall socioeconomic impacts of climate change on European forest resources;
- to recommend changes required of the forest management; and
- to assess the climate change resulting from changes in regional and European forest cover affecting surface characteristics (feedback).

The ICCF Research Study is a three and a half-year effort (mid 1993-1996) of six research teams from Australia, Finland, Sweden and IIASA. It has been submitted to the GCTE (Global Change Terrestrial Ecosystems) Core Project Office of the IGBP (International Geosphere-Biosphere Programme) for recognition as a GCTE Project. For the realization of the Study a number of models from different disciplines need to be modified and linked in an integrated fashion (Fig. 5.1). The models to be employed are as follows:

- A policy-oriented emission-concentration accounting model framework for natural and man-made greenhouse gases. The front end of IMAGE 1.0 will be used for this

[1] Working Meeting on the Effect of Climate Change and Forest Productivity held at IIASA, 28 November - 4 December 1992.

purpose. It has to be modified to meet the requirements of the other models involved by the Study, possibly in connection with a more advanced atmospheric chemistry model, the Atmospheric Composition Model (ACM) of IMAGE 2.0.

- IIASA's 2-dimensional Zonal Climate Model (2-D ZCM) and 2.5-dimensional Dynamical-Statistical Climate Model (2.5-D DSCM). At the Working Meeting support was given for a step-wise climate model approach. The initial use of the ZCM (employing some superimposing technique in connection with observations) was favored because of its more prompt availability and, also, because of the insufficient spatial resolution of GCMs and their current low confidence in regional predictions. In the next step of the modelling hierarchy the DSCM will be used after various medium-term improvements are introduced (see Section 5.2).

- Detailed ecophysiological models, a forest management model and a Timber Assessment Model (TAM) developed in Australia, Finland and Sweden respectively. These models will be discussed briefly below. Several models are needed to cover the broad spatial and temporal resolution scales involved when dealing with the ecophysiology of a single plant up to aggregated forest ecosystems. The BIOMASS model, e.g., provides a detailed understanding of the mechanisms behind plant responses to CO_2 and temperature changes but it does not account for any long-term changes in nutrient availability (i.e., the feedback through the soil system) when describing the development of a forest stand. Other physiological models, e.g., G'DAY, Q as well as SIMA, can be used to generate appropriate response functions that refer to longer time scales because the detailed physiology in these models is replaced by more phenomenological formulations. G'DAY and Q allow for different levels of temporally aggregated physiological processes, thereby focusing on long-term feedbacks in the plant-soil system, while SIMA is the only model capable to explicitly represent the structure and the regeneration of a forest stand undergoing climate change. The TAM, on the other extreme, can only deal with regional and European-wide equilibrium analyses of the future wood supply. To make it be responsive to changing climatic conditions the TAM needs to be fed with information and knowledge of the ecophysiological models. This transfer of knowledge will be realized via a hybrid model which will aggregate the information generated by the

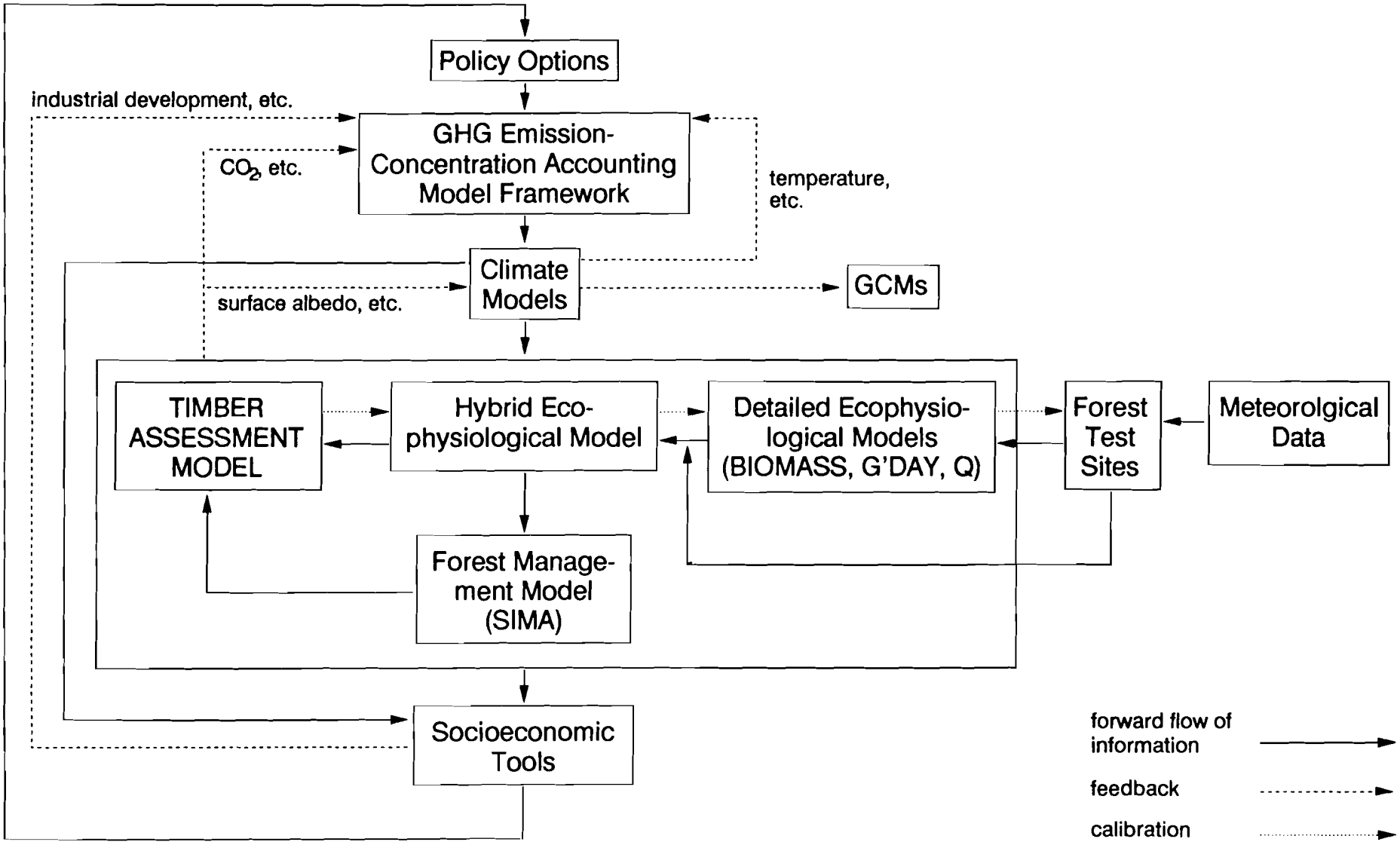

Figure 5.1. Structure of the ICCF Research Study in the perspective of IIASA's climate group.

detailed models and then act as a physiological interface to the TAM and, also, to the supporting SIMA model.

- Tentative impact analyses with available tools indicate that the effects on the European forest resources may be dramatic. It is expected that the future wood-supply distribution may change significantly in Europe due to a changing climate. The overall objective of the socioeconomic analysis is to identify the main socioeconomic impacts. This will help decision makers to determine how to adjust forest policies in different regions of Europe to new conditions. It is important to find a balance between the production of industrial wood, the carbon-sequestering role of forests, and the offsetting of fossil fuels by wood for energy production. Another important part of the socioeconomic analysis is to identify how the non-wood values of European forest resources can be maintained. It is expected that tools available at IIASA can be modified for this purpose.

In the next section we will discuss the different ecophysiological and forest production model requirements for both test sites and climate models and, also, how the requirements for the climate models will be met.

5.2 Ecophysiological and Forest Production Model Requirements for Test Sites and Climate Models

This section reflects the outcome of the 1992 Working Meeting and will experience a continuous update parallel to the progress of the Study.

To link, say, two computer models which originate from different fields of science, is usually a difficult task. Typical problems which arise can be pointed out by referring to the ICCF Study as an example in which a series of ecophysiological and forest production models are being linked to a climate model. Some of the difficulties are as follows:

- the different terminology used by the scientific groups with different backgrounds;
- the need to bridge the gap in regard to the different spatial and temporal resolutions

employed by the different models;

- the agreement on a common set of parameters which is shared by the different models for the exchange of information, i.e. during an integrated run; and
- the transfer of model inherent uncertainties from model to model.

In Table 5.1 we listed the requirements of the ecophysiological models that are involved in the Study for test sites. Test sites are needed for calibrating and testing the detailed ecophysiological models and the hybrid model (see Fig. 5.1). For this Study test sites will be selected from permanent experimental plots throughout Europe. They will be located along a North-South and along a West-East gradient and will cover both poor and good site conditions. Table 5.1 reflects the surroundings, in which the ecophysiological models are typically used, and therefore nicely sheds light on the type of ecophysiological information which needs to be ultimately amalgamated with the information of the climate models at the other end of the involved resolution scales.

In Table 5.2 we try to follow the ecophysiological and forest related information in terms of model input and output from model to model and thus from one set of spatial and temporal resolution to the next down to that of the TAM. As it becomes obvious, the hybrid model will play a crucial role in dovetailing the output information of the more detailed ecophysiological models with the input information of the SIMA model and the TAM. The output of the TAM, finally, will be handed over to a climate model.

Table 5.3 complements Table 5.2 listing the model input and output of the 2-D ZCM and of the 2.5-D DSCM in view of the ecophysiological and forest production models. Obviously still a lot of work is needed, e.g., to let the climate models start from greenhouse gas emissions which are policy-driven and, also, to develop a superimposing technique of lower resolved climate model results over higher resolved results of the TAM and the other models mentioned in Table 5.2. The work schedule for modifying and improving both the ZCM and the DSCM follows three phases which will match the overall work schedule and time horizon of the ICCF Study. The phases are as follows:

Table 5.1. Ecophysiological model requirements for test sites.

Requirements		Remarks
Soil/site properties	soil carbon and nitrogen content; CEC; base saturation; additional information about nutrients if available; soil type and texture or soil water retention function or water storage capacity of the rooting zone; depth of rooting zone	
Stand structure	geographical coordinates and altitude; site index; tree species; diameter distribution by species or stand density and mean diameter; biomass and growth of different tree components; growth and yield tables representing site and tree species; stocking; tree age; leaf area index; projected ground cover (or crown dimensions)	site index needs to be related to soil properties
Forest management/ stand history	type of regeneration: if natural, year of regeneration cut, species of parent trees, density of parent trees, mean diameter of parent trees; if artificial, planting (sowing) density, year of planting (sowing); tending of seedling stand: year and intensity of clearing of other tree species and of thinning of seedling stand; thinning: year, intensity, type; fertilization: year, dosage; additional information if available.	
Meteorological data	daily meteorological data (recorded at site or nearby for a period of at least 3 years, preferably longer) of: maximum and minimum surface air temperatures, precipitation, total shortwave radiation or photosynthetically active radiation; multiannual means of: daily maximum and minimum surface air temperatures, daily precipitation	not clarified which meteorological information should be asked for to characterize snow cover and frozen soil
Species-specific parameters and associated information	maximum stomatal conductance and stomatal response to VPD, light, soil water and overnight frost; photosynthesis: quantum yield, light-saturated photosynthetic rate including its nitrogen dependence, any evidence that photosynthesis is subject to photoinhibition at high light intensities; maintenance respiration rates, their temperature dependence and seasonality; phenological parameters for seasonality of photosynthesis, bud burst and allocation; nitrogen concentration for foliage, stems, branches, roots and litter fractions; specific leaf areas; lignin content of litter components	it is unlikely that these parameters are currently available; in most cases it is expected to obtain estimates from literature or own on-site experiments

Table 5.2. Description of ecophysiological and forest production models and their flow of information in terms of model input and output.

Information / Model	Model description	Input	Output
BIOMASS	process-based model of forest growth incorporating sub-models for radiation absorption, canopy photosynthesis, partitioning of assimilate between plant organs, litterfall, and stand water balance (McMurtrie et al., 1990, 1992a; McMurtrie, 1992; McMurtrie and Landsberg, 1992) spatial resolution: forest stand (gridpoint) temporal resolution: daily	atmospheric CO_2 concentration; daily total shortwave radiation; daily maximum and minimum surface air temperatures; daily precipitation; water holding capacity of the rooting zone; canopy structure; foliar N concentrations; tree physiology; state of the art formulations of physiological responses to ambient CO_2 concentration and temperature	daily canopy photosynthesis; biomass productivity; soil water content; net primary production; light use efficiency (required input to the G'DAY model)
G'DAY	simulates the flow of carbon, water and nutrients through a uniform stand of trees (McMurtrie et al., 1992b; Comins and McMurtrie, 1993); combines a tree-growth model and a decomposition and nutrient-cycling model; can be adapted to a range of different forest tree species spatial resolution: forest stand (gridpoint) temporal resolution: daily or seasonal	atmospheric CO_2 concentration; daily incident shortwave radiation; maximum and minimum surface air temperatures; precipitation; initial soil, litter and plant N and C contents; soil texture; litter lignin content; light use efficiency evaluated using BIOMASS; annual N deposition; N fixation rates	carbon uptake; plant productivity; tissue N concentrations; soil carbon; net ecosystem production
Q	accounts for carbon and nitrogen circulation in forest stands; key processes in the model are carbon fixation and its control by the amount of leaf nitrogen through a nitrogen productivity concept (Ågren, 1983, 1985a,b) and the decomposition of soil carbon and mineralization of nitrogen (Bosatta and Ågren, 1985, 1991a, b; Ågren and Bosatta, 1987) spatial resolution: forest stand (gridpoint) temporal resolution: annual	atmospheric CO_2 concentration; rate of N deposition; soil C and N amounts; stand age	plant and soil C and N stores; plant productivity

Table 5.2. continued:

Hybrid	aggregates the detailed ecophysiological information generated by the detailed models above (BIOMASS, G'DAY, Q) and acts as a physiological interface to the models below (SIMA, TAM); an outline of the conception of the hybrid model exists but will be subject to forthcoming research spatial resolution: forest stand or forest ecosystem temporal resolution: seasonal or annual	atmospheric CO_2 concentration; monthly maximum and minimum surface air temperatures; monthly precipitation; monthly radiation; ecophysiological relationships derived from the models above	input to the models below
SIMA	simulation model developed by Kellomäki et al. (1992) for the succession of the boreal forest ecosystem with subroutines for light availability, water and nitrogen for regeneration, growth and mortality spatial resolution: forest stand (gridpoint) temporal resolution: annual	light conditions in a stand; surface air temperature and precipitation (monthly means and their standard deviations); growth multipliers (for light, temperature, soil water, soil nitrogen, frost damage) for coupling the environment and the dynamics of a tree stand; soil texture; tree species and diameter distribution; management practices (thinning, fertilizing, length of rotation)	as means and partly as distribution functions: rates of forest regeneration, yield, mortality and the overall balance of these processes (the growing stock); totals of regeneration, yield and mortality over the rotation; pulp wood and saw timber; biomass of leaves, stems and roots
TAM	simulates the development of the European forests under different forest management regimes and under current climatic conditions; consists of two parts: a detailed country-by-country database on European forest resources and a matrix-type (volume by age) simulation model (Sallnäs, 1990; Nilsson et al., 1992a, b) spatial resolution: major forest ecosystems in countries or subregions of countries temporal resolution: 5 yearly	parameters describing the forest state (species composition, age classes, etc.), biological dynamics (growth, mortality, etc.), human management activities and effects of external factors like air pollution, etc.	forest yield; reaction of forest to environmental changes; reaction of forest to changes in management; changes in the land-base allocated to forest production

Table 5.3. Climate model description, model input and output in view of the ecophysiological and forest production models listed in Table 5.2.

Information / Model	Model description	Input	Output
2-D ZCM	describes the atmosphere and land and sea ice surfaces following the principles of energy balance modelling, and the ocean in advective-diffusive fashion; temperature is the only prognostic variable of the model (for further details see Table 3.1) spatial resolution: 18 latitude belts of 10° width each and up to 18 layers vertically for radiation transfer processes temporal resolution: annual climate statistics: annual means	greenhouse gas concentrations (H_2O, CO_2, CH_4, N_2O, O_3, CFC-11 and -12); albedo of vegetation covered and bare land; their area fractions; water availability	surface air and surface temperature; solar radiation; precipitation; evaporation; snow cover
2.5-D DSCM	describes the atmospheric, oceanic, sea ice and land components following the concept of dynamical-statistical modelling; temperature and specific humidity are the only prognostic variables of the model (for further details see Table 3.1 in Part II of the Working Paper) spatial resolution: 4.5° latitude x 18° longitude (3 atmospheric, 3 oceanic and 2 soil layers; 8 types of vegetation cover and soil texture) temporal resolution: seasonal climate statistics: seasonal means and synoptic variability parameters	greenhouse gas concentrations (H_2O, CO_2, CH_4, O_3); albedo of vegetation covered and bare land (for dry and saturated conditions, for $\lambda < 0.7$ and $\lambda \geq 0.7$ μm); their area fractions; roughness parameter describing the vegetation covered surface; stomatal resistance; leaf area index; leaf size; stem area index; light sensitivity factor; depth of upper and lower soil layer; rooting depth; porosity; maximum soil suction; saturated hydraulic conductivity; saturated thermal conductivity; moisture content at which evapotranspiration ceases	surface air and surface temperature; specific humidity; solar radiation; precipitation; evaporation and evapotranspiration; run-off; wetness of soil layers

Phase 1: Work on the policy-oriented emission-concentration accounting model framework...

- Modification of some of its geochemical components, e.g., of its global C-cycle module or N_2O module to meet the requirements for the climate models and for the ecophysiological and forest production models. These modifications will be described elsewhere since we did not describe the emission-concentration accounting tool in this Working Paper.

... and on the 2-D ZCM

- Introduction of a seasonal cycle. So far, the ZCM simulates only annual means. Seasonality facilitates to reasonably parameterize ice cover and thickness, and the depth of the mixed layer which vary seasonally. The seasonal changes of the climate variables listed in Table 5.3 (especially of temperature and precipitation) is highly needed by the ecophysiological and forest production models. Among them BIOMASS is the only model (see Table 5.2) which has a higher temporal resolution and will therefore require some superimposing technique (see below) in order to exploit the climate model information temporally.

- Introduction of more land surface types which reflect the distribution of forests. A preliminary test showed that the model is sensitive to changes in surface albedo resulting from changes in forest cover (see below and also Otterman et al., 1984).

- Modification of the radiation code with respect to the treatment of clouds. The effective cloud layer in the radiation code should be replaced by more layers: e.g., low, middle and high clouds. This should lead to a more realistic description of the cloud-temperature feedback.

- Introduction of orography. By taking into account surface heights, more realistic surface temperatures should be simulated, especially over Antarctica where elevations are significant. So far, the lowest level in the atmosphere is 1000 hPa.

- A superimposing technique of climate change model results over local test site data or observations to meet the higher spatial and partly higher temporal resolution of the ecophysiological and forest production models.

  The main idea behind choosing a superimposing techniques is connected with the expectation that the combination "climate change information of lower resolving climate models superimposed over observations" does not exceed the uncertainty of a GCM (the spatial resolution of which is also not sufficient and would therefore entail a similar superimposing or nesting technique). On top of it, it must always be kept in mind that the uncertainties involved in ecophysiological modelling, with which we have to deal in this Study and which are mainly due to missing knowledge, are at least in the same order of magnitude as the uncertainties inherent in climate modelling.

Phase 2: Work related to both the 2-D ZCM and the 2.5 DSCM (transition period)

- Introduction of a water cycle by treating the water vapor mixing ratio as a prognostic variable in connection with a hydrologically sound soil model and, also, a vegetation model. Both the soil model and the vegetation model must meet the requirements for the ecophysiological and the forest production models as well as the requirements for the emission-concentration accounting model framework (e.g., the requirements for its global C-cycle module). In the first instance it is envisaged to review the Biosphere-Atmosphere Transfer Scheme (BATS) of Dickinson et al. (1986), which is implemented in the DSCM.

- Optimization of the radiation transfer calculations with respect to computing time. The radiation codes employed by the ZCM and the DSCM each reveal its own characteristic strengths which can possibly be combined.

- Introduction of a sulfate aerosol layer into the troposphere to account for backscattering of solar radiation under cloud-free conditions, i.e., the direct radiative effect. As it has been shown, the cooling effect of anthropogenic aerosols may offset

the enhanced greenhouse warming in large areas of the globe (Charlson et al., 1991). A simple mass balance equation for SO_4^{2-} could provide a preliminary link between SO_2 emissions and their climate forcing effect.

Phase 3: Work on the 2.5-D DSCM. See Chapter 5 of Part II of the Working Paper.

An important question which still remains to be answered is how to account for regions other than Europe? The present understanding is that a two-step approach will satisfy the overall objective of the Study. In the first step we will only be concerned with European forests and with the global response which they might bring about due to a climate change (i.e., the rest of the world's surface cover will be kept constant). In the second step we will try to also integrate the rest of the globe into the Study and thus put the global response of step one into a proportionate global warming perspective. This has to be done by conducting sensitivity tests because of the geographical restrictions of the TAM to Europe.

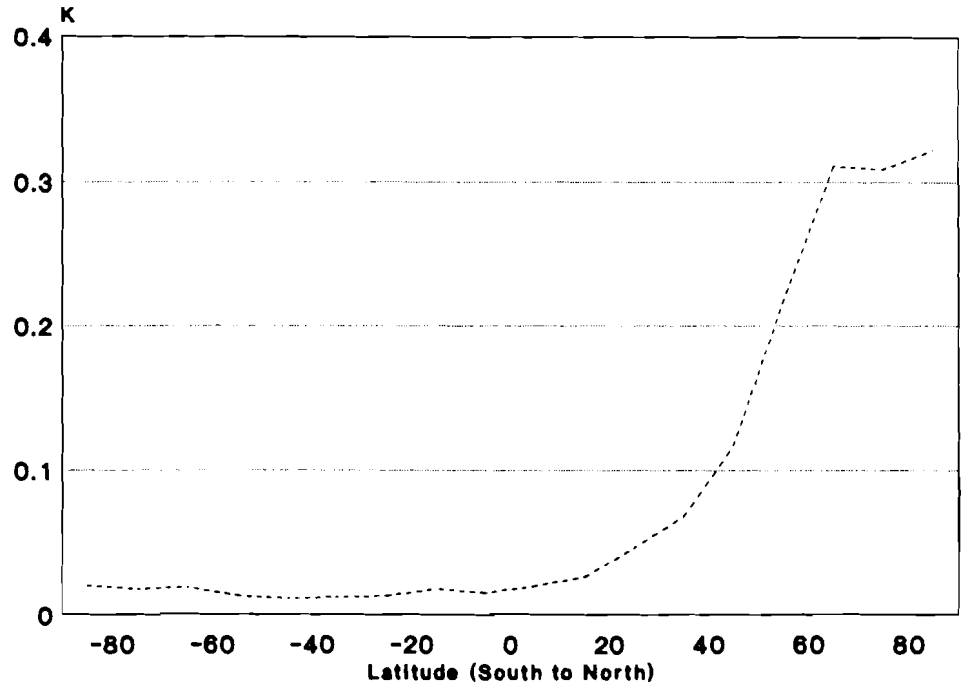

Figure 5.2. Difference in surface air temperature over land between integrations II and I in 2100.
I: reference run (1900-2100), forced by 1990 IPCC Scenario A (IMAGE 1.0);
II: like reference run but with instantaneous 5% increase in forested areas (40° -70°N) in 1900.

Figure 5.2, which shows the results of a preliminary climate model experiment (conducted during the Working Meeting mentioned), gives an example of the sensitivity of the ZCM to surface albedo changes induced by changes in forest cover. For this sensitivity experiment the ZCM was simply modified in such a way that its land parts between 40° to 70°N were additionally subdivided into forests (conifers, deciduous trees, mixed species) and non-forested areas (tundra). These land parts mainly reflected Swedish-Finnish conditions, but applied to the entire latitude belts. For its first run the ZCM was started from equilibrium, which corresponds to 1900, and was then forced by the 1990 IPCC concentration Scenario A (as generated by IMAGE 1.0) for 200 years. In the second run an instantaneous 5% increase in forested areas in 1900 was assumed, and the model was again forced by the same scenario. The increase in forested areas leads to a decrease in effective (zonal) albedo because of the lower albedo of forests compared to that of nonforested area, as an average over the year. This results in an additional warming of the climate system. Figure 5.2 shows the difference in surface air temperature over land between the two integrations in 2100. As expected a significant temperature difference occurs in those latitude zones in which the surface albedo was affected by changes in forest cover but due to meridional heat transport a temperature difference also becomes noticeable outside these latitude belts, especially in the northern polar region.

6. CONCLUSIONS

The objective of Part I of the Working Paper is twofold: first, to summarize the present status of IIASA's 2-D ZCM; and, secondly, to describe the envisaged position of this climate model and that of the 2.5-D DSCM, also available at IIASA and presented in Part II of the Working Paper, in the context of an integrated model of climate change. The latter model aims at a holistic approach that helps policy analysts to rapidly assess time-dependent changes in regional ecology, with feedback, resulting from various greenhouse gas emission policies.

Special attention must be paid to the climate module of an integrated model of climate change,i.a. because it can easily play a dominant role within the integrated model in terms of running time. Attempts were made to facilitate the understanding of the needs of both environmental impact modellers or assessors on the one hand and policy analysts on the other hand. In fact, even among themselves their requirements for an integrated model of climate change can be antagonistic to each other. For example, ecological impact models might require a spatial resolution, which is beyond that of GCMs, and, at the same time, an uncertainty in climate model output that can only be satisfied by GCMs or less sophisticated climate models on a coarser resolution scale, while policy experts are essentially asking for the possibility in assessing the impact of a wide variety of emission strategies, i.e., for a quick turnaround time of the integrated model.

For many applications this problem can be solved by creating a set of climate models of graded complexity that are computer-efficient and suitable for a wide variety of policy and impact analyses. Two independent approaches, the top-down and the bottom-up approach, were identified in regard to the design of the climate module. In our opinion both approaches complement each other and seem to be worthwhile pursuing in parallel. Carefully considering the pros and cons of both approaches, especially the fact that the top-down approach requires frequent access to a GCM, we come to the conclusion that IIASA ought to pursue the bottom-up approach, albeit a somewhat reduced flexibility. The bottom-up approach seems to offer a more restricted choice with respect to diversity of climatic information and its spatial and temporal resolution than the top-down approach. However, this might be compensated for by some advantages of the bottom-up approach, e.g., the

somewhat easier implementation of new feedbacks, if appropriate parameterizations exist or can be derived. The 2-D ZCM and the 2.5-D DSCM are meant for integrated modelling of climate change impacts which makes use of the bottom-up approach. Both climate models are at the upper level of complexity (in terms of spatial and temporal resolutions) out of a set of four climate models that are available or under development at IIASA.

A number of model experiments have been performed which document the present status of the 2-D ZCM. It simulates today's zonal means of the basic climatic characteristics (temperature, precipitation, evaporation, meridional heat transport and others) reasonably well. For a doubling of atmospheric CO_2 the ZCM reveals a climate sensitivity of about 1.8 K and an increase of the globally averaged precipitation rate of about 5%. The climate sensitivity lies within the range estimated by the IPCC (1.5 to 4.5 K) and the ratio of precipitation increase to climate sensitivity agrees well with GCM results (IPCC, 1990).

Two 100 year integrations (1985-2084) employing IPCC's 1990 (CO_2-equivalent) concentration Scenarios A and D and a 200 year integration (1900 - 2100), employing Scenario A (which is generated by IMAGE 1.0 and also accounts for greenhouse gases other than CO_2), were made. In the first case, our results could be compared with the recently published results of the MPI GCM in terms of zonal annual means. The temperature response of the ZCM for Scenario D is close to the respective response of the MPI GCM and somewhat less pronounced for Scenario A. This is because of the lower climate sensitivity of the ZCM. The ZCM reproduces quite well the interhemispheric asymmetry of the temperature response, the zonal speed of temperature change and, also, the depth of temperature anomaly propagation into the deep ocean. The projected sea level rise due to the thermal expansion of the ocean is 0.24 m for Scenario A and 0.08 m for Scenario D, respectively, which is also in good agreement with the latest MPI GCM results and IPCC estimates.

In case of the 200 year integration, the performance of the model in simulating past climate could be verified as well. According to the IPCC, the global mean surface air temperature has increased by 0.3 to 0.6 K over the last 100 years. The ZCM gives 0.4 K for the period 1900 to 1990, which agrees well with the given range.

Finally, Part I of the Working Paper sheds light on an Integrated Assessment of Climate Change Impacts on European Forests, a projected application to integrated modelling of climate change impacts. The integrated model comprises a series of models - from policy-oriented accounting tool for greenhouse gas emissions and concentrations to climate model to sequence of dovetailing ecophysiological and forest production models to socioeconomic tools, with feedback.

An important feature of the integrated assessment is that the ecophysiology of a single plant up to that of aggregated forest ecosystems will be considered. A two-step approach employing both the ZCM and the DSCM, in combination with a suitable superimposing technique aiming at bridging the spatial resolution gap between the climate models on the one hand and the ecophysiological and forest production models on the other hand, was outlined. Such a superimposing technique (or nesting technique in regard to GCMs) will always be necessary if the spatial or temporal resolution of the climate model does not meet the respective resolution needs of an ecological model. In addition, the technique is inherently connected with an uncertainty that adds up to the already existing one of the climate model. However, the combined uncertainty is expected not to exceed the respective uncertainty of a GCM. Also, this problem might turn out to be purely academic in view of the not yet quantifiable uncertainties that are involved in large-scale ecophysiological modelling and are mainly due to missing knowledge. The ICCF Study tries to make a contribution to reducing some of the missing knowledge.

REFERENCES

Ågren, G.I., (1983). Nitrogen Productivity of Some Conifers. *Canadian Journal of Forest Research*, **13**, 494-500.

Ågren, G.I., (1985a). Theory for Growth of Plants Derived from the Nitrogen Productivity Concept. *Physiologia Plantarum*, **64**, 7-28.

Ågren, G.I., (1985b). Limits to Plant Production. *Journal of Theoretical Biology* **113**, 89-92.

Ågren, G.I. and E. Bosatta, (1987). Theoretical Analysis of the Long Term Dynamics of Carbon and Nitrogen in Soils. *Ecology*, **68**, 1181-1189.

Baskin, Y., (1993). Ecologists Put Some Life Into Models of a Changing World. Could Plants Help Tame the Greenhouse? *Science*, **259**, 1694-1696.

Baumgartner, A., and E. Reichel, (1975). *Die Weltwasserbilanz.* Munich and Vienna, Oldenbourg.

Boer, G.J., K. Arpe, M. Blackburn, M. Déqué, W.L. Gates, T.L. Hart, H. le Treut, E. Roeckner, D.A. Sheinin, I. Simmonds, R.N.B. Smith, T. Tokioka, R.T. Wetherald and D. Williamson (1991). CAS/JSC Working Group on Numerical Experimentation: An Intercomparison of the Climates Simulated by 14 Atmospheric General Circulation Models. Report No. 15, WMO/ICSU World Climate Research Programmme.

Boer, G.J., N.A. McFarlane, and M. Lazare, (1992). Greenhouse Gas-induced Climate Change Simulated with the CCC Second-Generation General Circulation Model. *Journal of Climate*, October 1992, 1045-1077.

Bosatta, E. and G.I. Ågren, (1985). Theoretical Analysis of Decomposition of Heterogeneous Substrates. *Soil Biology and Biochemistry*, **17**, 601-610.

Bosatta, E. and G.I. Ågren, (1991a). Dynamics of Carbon and Nitrogen in the Organic Matter of the Soil: A Generic Theory. *The American Naturalist*, **138**, 227-245.

Bosatta, E. and G.I. Ågren, (1991b). Theoretical Analysis of Carbon and Nutrient Interactions in Soils under Energy Limited Conditions. *Soil Science Society of America Journal*, **55**, 728-733.

Bryan, F., (1986). High-Latitude Salinity Effects and Interhemispheric Thermohaline Circulations. *Nature*, **323**, 301-304.

Budyko, M.I., (1969). The Effect of Solar Radiation Variations on the Climate of the Earth. *Tellus* **21**(5), 611-619.

Budyko, M.I., (1974). Climate and Life. *Wiley and Sons*, 588 pp.

Carissimo, B.C., A.H. Oort and T.H. Vonder Haar, (1985). Estimating the meridional Energy Transports in the Atmosphere and the Ocean. *J. Phys. Oceanogr.* **15**, 82-91.

Cess, R.D. and V. Ramanathan, (1972). Radiative Transfer in the Atmosphere of Mars and that of Venus above the Cloud Deck. *J. Quantitative Sepctroscopy and Radiative Transfer*, **12**, 933-945.

Charlson, R., J. Langner, H. Rodhe, C.B. Leovy, and S.G. Warren, (1991). Perturbation of the Northern Hemisphere Radiative Balance by Backscattering from Anthropogenic Sulfate Aerosols. *Tellus*, **43AB**, 152-163.

Comins, H.N. and R.E. McMurtrie, (1993). Long-Term Biotic Response of Nutrient--Limited Forest Ecosystems to CO_2-Enrichment: Equilibrium Behaviour of Integrated Plant-Soil Models. *Ecological Applications*. (In press.)

Crafoord, C. and E. Källén, (1978). A Note on the Condition for Existence of More than One Steady-State Solution in Budyko-Sellers Type Models. *J. Atmos. Sci.*, **35**, 1123-1125.

Cubasch, U., K. Hasselmann, H. Höck, E. Maier-Reimer, U. Mikolajewicz, B.D. Santer and R. Sausen (1992). Time-Dependent Greenhouse Warming Computations with a Coupled Ocean-Atmosphere Model. *Climate Dynamics*. **8**, 55-69.

Curran, R.J., R. Wexler, M.L. Nack (1978). Albedo Climatology Analysis and the Determination of Fractional Cloud Cover. NASA, Technical Memorandum 79576 (NASA-TM-79576), 52 pp.

Dickinson, R.E. (1986). How will Climate Change? Pages 206-270 *in:* B. Bolin, B.R. Döös, J. Jäger, and R.A. Warrick (eds.), *The Greenhouse Effect, Climatic Change, and Ecosystems*. SCOPE **29**, John Wiley and Sons, Chichester, U.K.

Dickinson, R.E., A. Henderson-Sellers, P.J. Kennedy and M.F. Wilson, (1986). Biosphere-Atmosphere Transfer Scheme (BATS) for the NCAR Community Climate Model. *NCAR Technical Note*, NCAR/TN-275+STR, 63 pp.

Dushkin, P.K., E.G. Lomonosov, Yu. N. Lunin, (1960). A Test of Numerical Humidity, Cloudiness and Precipitation Forecasting Method using a Computer. *Meteorology and Hydrology*, **12**, 5-12. (In Russian.)

Ellis, J.S. and T.H. Vonder Haar, (1976). Zonal Average Earth Radiation Budget Measurements from Satellites for Climate Studies. *Atmos. Sci.* Paper 240. Colorado State University, Fort Collins, Colorado, U.S.A.

Esbensen, S.K. and Y. Kushnir, (1981). The Heat Budget of the Global Ocean: An Atlas Based on Estimates from Surface Marine Observations. Climate Research Institute, Oregon State University, Report No. 29.

FAO, (1991). Wood and Wood Products, 1961-1989. *Food and Agriculture Organization of the United Nations*, Rome.

Flannery, B.P., A.J. Callegari and M.I. Hoffert, (1984). Energy Balance Models Incorporating Evaporative Buffering of Equatorial Thermal Response. In: Climate Processes and Climate Sensitivity, J.E. Hansen and T. Takahashi (eds.), *Geophys. Monogr.*,**29**, *Maurice Ewing*, **5**, 108-117.

Fraedrich, K., (1978). Structural and Stochastic Analysis of a Zero-Dimensional Climate System. *Quart. J. R. Met. Soc.*, **104**, 461-474.

Ganopolski, A., (1991). A Multilayer Model for the Ocean Seasonal Variability. *Oceanology*, **31**, 892-897. (In Russian.)

Gates, W.L., (1992). AMIP: The Atmospheric Model Intercomparison Project. *PCMDI*, **7**.

Gill, A.E., (1982). Atmosphere-Ocean Dynamics, *Int. Geophys. Ser.*, **Vol. 30,** Academic Press, 662 pp.

Gutowski, W.J., D.S. Gutzler, D. Portman, W.-C. Wang, (1988). Surface Energy Balance of Three General Circulation Models: Current Climate and Response to Increasing Atmospheric CO_2. Atmospheric and Environmental Research Inc., Cambridge MA 02129. Under contract No. DE-FG02-86ER60422 prepared for U.S.D.E.

Han, Y.-J. and S.-W. Lee, (1983). An Analysis of Monthly Mean Wind Stress over the Global Ocean. *Mon. Wea. Rev.*, **111**, 1554-1566.

Hasselmann, K. and H. von Storch, (1992). Concept of a Global-Environment-and Man (GEM) Model. Presentation at Second International Conference on Modelling of Global Climate Change and Variability, Sept. 7-11, 1992, Max-Planck-Institut für Meteorologie, Hamburg, Germany.

Harvey, L.D.D. (1988). A Semianalytic Energy Balance Climate Model with Explicit Sea Ice and Snow Physics. *J. Climate* **1**, 1065-1085.

Henderson-Sellers, A and K. McGuffie, (1987). *A Climate Modelling Primer.* John Wiley and Sons, Chichester, U.K.

Hsiung, J., (1985). Estimates of Global Oceanic Meridional Heat Transport. *J. Phys. Oceanogr.*, **15**, 1405-1413.

Intergovernmental Panel on Climate Change, (1990). *Climate Change 1990: The IPCC Scientific Assessment.* Working Group I, Cambridge University Press, Cambridge, U.K.

Intergovernmental Panel on Climate Change, (1991). *Climate Change. The IPCC Response Strategies.* Island Press, Washington, D.C., U.S.A., 272 pp.

Intergovernmental Panel on Climate Change, (1992). *Climate Change 1992, The supplementary report to the IPCC Scientific Assessment*, Working Group I, Cambridge University Press, Cambridge, U.K.

Jaeger, L. (1976). Monatskarten des Niederschlags für die ganze Erde. *Ber. d. Dt. Wetterdienstes* **139** (18).

Jonas, M., M. den Elzen and K. Olendrzyński (1991). A Time Dependent Zonally Averaged Energy Balance Model to be Incorporated into IMAGE (Integrated Model to Assess the Greenhouse Effect). CP-91-16. IIASA, Laxenburg, Austria.

Jonas, M., K. Olendrzyński, J. Krabec and R. Shaw (1992). IIASA's Work on Climate Change: Assessing Environmental Impacts. SR-92-9. IIASA, Laxenburg, Austria.

Karol, I.L. and V.A. Frolkis, (1984). Energy Balance Radiative-Convective Model of Global Climate. *Meteorology and Hydrology*, **8**, 59-67 (in Russian).

Kellomäki, S., H. Väisänen, H. Hänninen, T. Kolström, R. Lauhanen, U. Mattila, and B. Pajari, (1992). A Simulation Model for the Succession of the Boreal Forest Ecosystem. *Silva Fennica*, **26**, 1-18.

Kuo, H.L., (1965). On Formation and Intensification of Tropical Cyclones through Latent Heat Release by Cumulus Convection. *J. Atmos. Sci.*, **22**, 40-63.

Lacis, A.A. and J.E. Hansen, (1974). A Parameterization for the Absorption of Solar Radiation in the Earth's Atmosphere. *J. Atmos. Sci.* **31**, 118-133.

Lee, P.S., and F.M. Snell, (1977). An Annual Zonally Averaged Global Climatic Model With Diffuse Cloudiness Feedback. *J. Atmos. Sci.*, **34**, 847-853.

Levitus, S. (1982). Climatological Atlas of the World Ocean. NOAA Prof. Pap. No. 13, US Government Printing Office, Washington, D.C.

McKay, R.M. and M.A.K. Khalil, (1991). Theory and Development of a One Dimensional Time Dependent Radiative Convective Climate Model. *Chemosphere*, **22**, 383-417.

McMurtrie, R.E., M.L. Benson, S. Linder, S.W. Running, T. Talsma, W.J.B. Crane and B.J. Myers, (1990). Water-Nutrient Interactions Affecting the Productivity of Stands of Pinus radiata. *Forest Ecology and Management*, **30**, 415-423.

McMurtrie, R.E., (1992). Modelling Canopy Carbon and Water Balance. In: D.O. Hall, J.M.O. Scurlock, H. Bolar, R.C. Leegood and S.P. Long (eds), *Photosynthesis and Production in a Changing Environment: a Field and Laboratory Manual*, Chapman and Hall. (in press).

McMurtrie, R.E. and J.J. Landsberg, (1992). Using a Simulation Model to Evaluate the Effects of Water and Nutrients on Growth and Carbon Partitioning of Pinus Radiata. *Forest Ecology and Management* **52**, 243-260.

McMurtrie, R.E., H.N. Comins, M.U.F. Kirschbaum and Y.-P. Wang, (1992a). Modifying Existing Forest Growth Models to Take Account of Direct Effects of Elevated CO_2. *Australian Journal of Botany*, (Submitted).

McMurtrie, R.E., R. Leuning, W.A. Thompson and A.M. Wheeler, (1992b). A Model of Canopy Photosynthesis and Water Use Incorporating a Mechanistic Formulation of Leaf CO_2 Exchange. *Forest Ecology and Management*, **52**, 261-278.

Manabe, S., K. Bryan and M.J. Spelman, (1990). Transient Response of a Global Ocean-Atmosphere Model to a Doubling of Atmospheric Carbon Dioxide. *J. Phys. Oceanogr.*, **20**, 722-749.

Manabe, S., R.J. Stouffer, M.J. Spelman and K. Bryan, (1991). Transient Responses of a Coupled Ocean-Atmosphere Model to Gradual Changes of Atmospheric CO_2. Part I: Annual Mean Response. *J. Climate.* **4**, 785-818.

Manabe, S., M.J. Spelman and R.J. Stouffer, (1992). Transient Responses of a Coupled Ocean-Atmosphere Model to Gradual Changes of Atmospheric CO_2. Part II: Seasonal Response. *J. Climate*, **5**, 105-126.

Marotzke, J. and J. Willebrand, (1991). Multiple Equilibria of the Global Thermohaline Circulation. *J. Phys. Oceanogr.*, **21**, 1372-1385.

Mearns, L.O., S.H. Schneider, S.L. Thompson and L.R. McDaniel, (1990). Analysis of Climate Variability in General Circulation Models: Comparison with Observations and Changes in Variability in $2xCO_2$ Experiments. *J. Geophys. Res.*, **95**(D12), 20, 469-20, 490.

Meadows, D., (1992). The Role of Global and Dynamic Computer Simulation Models for Sustainable Development. Presentation at Workshop on Integrated Models of Global Change: Coupling Social and Natural Sciences. Potsdam, Germany.

Mokhov, I.I., O.I. Mokhov, V.K. Petoukhov, R.R. Khairullin, (1992). On Trends of Atmospheric Cyclogenetic Activity under Global Climate Changes. Izv. Acad. of Sciences of Russia, FAO, **28**(1), 11-26.

Nilsson, S., O. Sallnäs and P. Duinker, (1992a). Future Forest Resources of Western and Eastern Europe. Parthenon Publishing Group Ltd., Casterton Hall, Carnforth, Lancs., U.K. ISBN 1-85070-424-4. 496 pp.

Nilsson, S., O. Sallnäs, M. Hugosson, and A. Shvidenko, (1992b). *The Forest Resources of the Former European USSR.* Parthenon Publishing Group Ltd., Casterton Hall, Carnforth, Lancs., U.K.

North, G.R. and J.A. Coakley, (1979). Differences between Seasonal and Mean Annual Energy Balance Model Calculations of Climate and Climate Sensitivity. *J. Atmos. Sci.* **36**, 1189-1204.

North, G.R., R.F. Cahalan and J.A. Coakley, (1981). Energy Balance Climate Models. *Rev. Geophys. Space Phys.* **19**, 91-121.

North, G.R., D.A. Short, J.G. Mengel, (1983). Simple Energy Balance Model Resolving the Seasons and the Continents: Application to the Astronomical Theory of the Ice Ages. *J. Geophys. Res.*, **88**, 6576-6586.

Oerlemans, J. and H.M. Van Den Dool, (1978). Energy-Balance Climate Models: Stability Experiments with a Refined Albedo and Updated Coefficients for Infrared Emission. *J. Atmos. Sci.*, **35**, 371-381.

Ohring, G. and S. Adler, (1978). Some Experiments with a Zonally Averaged Climate Model. *J. Atmos. Sci.*, **35**, 186-205.

Oort, A.H. and T.H. Vonder Haar, (1976). On the Observed Annual Cycle in the Ocean-Atmosphere Heat Balance Over the Northern Hemisphere. *J. Phys. Oceanogr.*, **6**(6), 781-800.

Oort, A.H. (1983). Global Atmospheric Circulation Statistics, 1958-1973. NOAA Prof. Pap. 14., U.S. Dept. of Commerce, Rockville, Md. U.S.A.

Otterman, J., M.D. Chou and A. Arking, (1984). Effects of Non-Tropical Forest Cover on Climate. *Journal of Climate and Applied Meteorology*, **23**, 762-767.

Peng, L., M.-D. Chou and A. Arking (1982). Climate Studies with a Multi-Layer Energy Balance Model: I. Model Description and Sensitivity to the Solar Constant. *J. Atmos. Sci.* **39**(12), 2639-2656.

Peng, L., M.-D. Chou and A. Arking (1987). Climate Warming due to Increasing Atmospheric CO_2: Simulations with a Multilayer Coupled Atmosphere-Ocean Seasonal Energy Balance Model. *J. Geophys. Res.* **92**(D5), 5505-5521.

Petoukhov, V.K., (1976). Zonally Averaged Model of Heat and Moisture Exchange in Atmosphere Underlying Ocean Layer System, Izvestia Acad. Sciences USSR, *FAO*, **12**(11), 1130-1142 (in Russian).

Petoukhov, V.K., and N.I. Manuilova, (1984). Estimation of Some Climate-Forming Factors in a Simple Thermodynamical Climate Model. *Meteorology and Hydrology*, No. 10, 31-37. (in Russian).

Petoukhov, V.K., (1991). *Dynamical-Statistical Modeling of Large-Scale Climatic Processes.* Leningrad Hydrometeorological Institute, St. Petersburg, Russia. (in Russian).

Ramanathan, V., (1976). Radiative Transfer within the Earth's Troposphere and Stratosphere: A Simplified Radiative-Convective Model. *J. Atmos. Sci.*, **33**, 1330-1346.

Roberts, R.E., J.E.A. Selby and L.M. Biberman, (1976). Infrared Continuum Absorption by Atmospheric Water Vapor in the 8-12 μm Window. *Applied Optics*, **9**, 2085-2090.

Rotmans, J., 1990. *IMAGE: An Integrated Model to Assess the Greenhouse Effect*, Kluwer Academic Publishers, Dordrecht, The Netherlands.

Robinson, P.J. and P.L. Finkelstein (1991). The Development of Impact-Oriented Climate Scenarios. *Bulletin American Meteorological Society*, **72**, 4, 481-490

Robock, A., (1978). Internally and Externally Caused Climate Change. *J. Atmos. Sci.*, **35**, 1111-1122.

Robock, A., (1980). The Seasonal Cycle of Snow Cover, Sea Ice, and Surface Albedo. *Mon. Wea. Rev.*, **108**, 267-285.

Sallnäs, O., (1990). A Matrix Growth Model of the Swedish Forest. *Studia Forestatia Suecica*, **183**, Uppsala, Sweden.

Saltzman, B. and A.D. Vernekar, (1971). An Equilibrium Solution to the Axially Symmetric Component of the Earth's Macroclimate). *J. Geophys. Res.*, **76**, 1498-1527.

Sasamori, T., J. London and D.V. Hoyt, (1972). Radiation Budget of the Southern Hemisphere. *Meteor. Monogr.* **13**(35), 9-23.

Sellers, W.D. (1965). Physical Climatology. The University of Chicago Press, 272 pp.

Sellers, W.D., (1969). A Global Climatic Model Based on the Energy Balance of the Earth-Atmosphere System. *J. Appl. Meteor.* **8**, 392-400.

Sellers, W.D., (1973). A New Global Climatic Model. *J. Appl. Meteor.*, **12**, 241-254.

Sellers, W.D., (1976). A Two-dimensional Global Climatic Model. *Mon. Wea. Rev.*, **104**, 233-248.

Sellers, W.D., (1983). A Quasi-three-dimensional Climate Model. *J. Climate Appl. Meteor.*, **22**, 1557-1574.

Shuleykin, V.V., (1978). Calculations of Development, Movement and Fading of the Tropical Hurricanes and of the Basic Waves generated by Hurricanes. *L. Hydrometeoizdat.*, 96 p.

Smagorinsky, J., (1960). On the Dynamical Prediction of Large-Scale Condensation by Numerical Methods. *Physics of Precipitation.* Monograph No. 5, American Geophysical Union. 71-78.

Smith, E.A. and M.R. Smith, (1987). Interannual Variability of the Tropical Radiation Balance and the Role of Extended Cloud Systems. *J. Atmos. Sci.*, **44**, 3210-3224.

Stocker, T.F. and D.G. Wright, (1991). A Zonally Averaged Ocean Model for the Thermohaline Circulation. Part II: Interocean Circulation in the Pacific-Atlantic Basin System. *J. Phys. Oceanogr.*, **21**, 1725-1739.

Stone, P.H., (1978). Baroclinic Adjustment. *J. Atmos. Sci.*, **35**, 561-571.

Stouffer, R.J., S. Manabe and K. Bryan, (1989). Interhemispheric Asymmetry in Climate Response to a Gradual Increase of Atmospheric CO_2. *Nature*, **342**, 660-662.

Sunders, F., A.L. Adams, N.I.B. Gordon, W.D. Jensen, (1980). Further Development of a barotropic Operational Model for Predicting the Paths of Tropical Storms. *Mon. Wea. Rev.*, **108**,(5), 642-654.

Talley, L.D., (1984). Meridional Heat Transport in the Pacific Ocean. *J. Phys. Oceanogr.*, **14**, 231-241.

Thompson, S.L. and S.H. Schneider, (1979). A Seasonal Zonal Energy Balance Climate Model with an Interactive Lower Layer. *J. Geophys. Res.*, **84**, 2401-2414.

Trenberth, K.E., (1979). Mean Annual Poleward Energy Transports by the Oceans in the Southern Hemisphere. *Dyn. Atmos. Oceans*, **4**, 57-64.

Walsh, J.E. and R. G. Crane, (1992). A Comparison of GCM Simulations of Artic Climate. *Geophys. Res. Letters*, **19**, 29-32.

Wang, W.-C. and P.H. Stone, (1980). Effect of Ice-Albedo Feedback on Global Sensitivity in a One-Dimensional Radiative-Convective Climate Model. *J. Atmos. Sci.*, **37**, 545-552.

Washington, W.M. and G.A. Meehl, (1989). Climate Sensitivity due to Increased CO_2: Experiments with a Coupled Atmosphere and Ocean General Circulation Model. *Climate Dynamics* **4**, 1-38.

Weaver, A.J. and E.S. Sarachik, (1991). The Role of Mixed Boundary Conditions in Numerical Models of the Ocean's Climate. *J. Phys. Oceanogr.*, **21**, 1470-1493.

Wigley, T.M.L. and M.E. Schlesinger, (1985). Analytical Solution for the Effect of Increasing CO_2 on Global Mean Temperature. *Nature* **315**, 649-652.

Wigley, T.M.L. and S.C.B. Raper, 1990. Natural variabilitity of the climate system and detection of the greenhouse effect. *Nature*, **344**, 324-327.

Wright, D.G. and T.F. Stocker, (1991). A Zonally Averaged Ocean Model for the Thermohaline Circulation. Part I: Model Development and Flow Dynamics. *J. Phys. Oceanogr.*, **21**, 1713-1724.